



Pacific Northwest
NATIONAL LABORATORY

Proudly Operated by Battelle Since 1965

FY16 Status of Immersion Phased Array Ultrasonic Probe Development and Performance Demonstration Results for Under Sodium Viewing

M3AT-16PN2301025 Technical Letter Report

August 2016

AA Diaz
CE Chamberlin
MK Edwards
TJ Hagge
MS Hughes

MR Larche
RA Mathews
KJ Neill
MS Prowant

DISCLAIMER

This report was prepared as an account of work sponsored by an agency of the United States Government. Neither the United States Government nor any agency thereof, nor Battelle Memorial Institute, nor any of their employees, makes **any warranty, express or implied, or assumes any legal liability or responsibility for the accuracy, completeness, or usefulness of any information, apparatus, product, or process disclosed, or represents that its use would not infringe privately owned rights.** Reference herein to any specific commercial product, process, or service by trade name, trademark, manufacturer, or otherwise does not necessarily constitute or imply its endorsement, recommendation, or favoring by the United States Government or any agency thereof, or Battelle Memorial Institute. The views and opinions of authors expressed herein do not necessarily state or reflect those of the United States Government or any agency thereof.

PACIFIC NORTHWEST NATIONAL LABORATORY

operated by

BATTELLE

for the

UNITED STATES DEPARTMENT OF ENERGY

under Contract DE-AC05-76RL01830

Printed in the United States of America

Available to DOE and DOE contractors from the
Office of Scientific and Technical Information,

P.O. Box 62, Oak Ridge, TN 37831-0062;

ph: (865) 576-8401

fax: (865) 576-5728

email: reports@adonis.osti.gov

Available to the public from the National Technical Information Service,
U.S. Department of Commerce, 5285 Port Royal Rd., Springfield, VA 22161

ph: (800) 553-6847

fax: (703) 605-6900

email: orders@ntis.fedworld.gov

online ordering: <http://www.ntis.gov/ordering.htm>



This document was printed on recycled paper.

(9/2003)

FY16 Status of Immersion Phased Array Ultrasonic Probe Development and Performance Demonstration Results for Under Sodium Viewing

M3AT-16PN2301025 Technical Letter Report

AA Diaz	MR Larche
CE Chamberlin	RA Mathews
MK Edwards	KJ Neill
TJ Hagge	MS Prowant
MS Hughes	

August 2016

Prepared for
the U.S. Department of Energy
under Contract DE-AC05-76RL01830

Pacific Northwest National Laboratory
Richland, Washington 99352

Acknowledgments

The work reported here is sponsored by the U.S. Department of Energy (DOE), Office of Nuclear Energy (NE), under DOE Contract DE-AC05-76RL01830; Pacific Northwest National Laboratory (PNNL) Project No. 58745. Dr. David Holcomb is the ART-I&C Research Program Manager, Mr. Chris Grandy is the Technical Area Lead (TAL), and Mr. Bob Hill is the National Technical Director. Additionally, PNNL recognizes Mr. Tom Sowinski as the DOE Technical Manager and Mr. Carl Sink as the HQ Program Director.

PNNL would like to thank Dr. Holcomb for his guidance and technical direction throughout the course of this effort. At PNNL, the authors would like to extend their gratitude to Ms. Lori Bisping for all of her hard work in providing administrative and financial reporting support to this project. Lori's attention to detail, expertise, and efficiency are second to none. In addition, the authors would like to recognize Crystal Mullen for her support in generating design schematics and technical drawings for the probe design modifications, and A. Mark Jones for his support of EM modeling efforts. Finally, the PNNL technical team would like to extend their thanks to Ms. Kay Hass for her ongoing support and technical editing expertise in preparing and finalizing this technical letter report.

PNNL is operated by Battelle for the U.S. Department of Energy under Contract DE-AC05-76RL01830.

Acronyms and Abbreviations

1D	one-dimensional
2D	two-dimensional
ANL	Argonne National Laboratory
ASTM	American Society for Testing and Materials
dB	decibel
BW	bandwidth
DOE	U.S. Department of Energy
DOE-NE	U.S. Department of Energy, Office of Nuclear Energy
ETU	engineering test unit
FFT	fast Fourier transform
FY	fiscal year
ISI&R	inservice inspection and repair
λ	wavelength
MARICO-2	Material Testing Rig with Temperature Control (version 2)
MHz	megahertz
NDE	nondestructive examination (or nondestructive evaluation)
Ni	nickel
PA	phased array
PA-UT	phased-array ultrasonic testing
PD	performance demonstration
PNNL	Pacific Northwest National Laboratory
PSF	point spread function
rf	radio frequency
SFR	sodium-cooled fast reactor
SNR	signal-to-noise ratio
SN2	22×1 linear array prototype probe serial number 2
SN3	10×3(×2) transmit-receive longitudinal array prototype probe serial number 3
SN4	32×1 linear array or 32×1(×2) matrix array prototype probe serial number 4
SS	stainless steel
TLR	technical letter report
USV	under-sodium viewing
UT	ultrasonic testing
PZT	lead zirconate titanate

Contents

Acknowledgments.....	iii
Acronyms and Abbreviations	v
1.0 PNNL Technical Progress	1.1
1.1 Introduction	1.1
1.2 Objective and Scope.....	1.2
1.3 Key Performance Parameters	1.4
1.4 SN4 1D and 2D Array Probe Design and Fabrication Differences.....	1.6
1.4.1 General 1D Linear and 2D Matrix-Array, ETU Design Considerations	1.1
1.5 Pre-Fabrication Evaluation of Individual PA-UT Probe Elements for the SN4 ETUs	1.15
1.6 Post-Fabrication Evaluation of Housed PA-UT SN4 ETU	1.26
1.6.1 Post-Fabrication Pulse-Echo Testing on Individual Array Elements (in Water)	1.27
1.6.2 Post-Fabrication Testing Using Elements in Concert (in Water)	1.37
1.6.3 Sound Field Dimensional Characterization Analysis for SN4 Prototype Probes.....	1.41
1.6.4 Spatial Resolution and SNR Analysis for SN4 Prototype Probes.....	1.41
1.7 Primary Inspection Parameters for 3D Imaging Assessment	1.47
1.8 Imaging Assessment in Water for SN4 Prototype Probes and Post Processing Method for Noise Reduction in UT Data	1.48
1.9 Imaging Assessments in Sodium for SN4 Prototype Probes.....	1.55
1.9.1 Probe Face, Sodium Preparations, and Scanning Configuration for In-Sodium Scanning	1.55
1.9.2 In-Sodium Testing Results	1.59
1.10 Discussion and Conclusions.....	1.69
2.0 References	2.1

Figures

1.1	Side-view Schematic, Illustrating the Japanese Joyo Reactor Fuel Sub-assembly and the Associated Cross-Sectional Dimensions of an Isolated Pin (simulated here), within the MARICO-2 Test Sub-assembly	1.4
1.2	(left) Photograph of the FY14 ETU Showing the Internal Positions of the Embedded Thermocouples Inside the Transducer Shaft. (right) Data Acquisition and Measurement Configuration within the Fume-Hood.....	1.2
1.3	Temperature Profile Data Obtained as a Function of Vertical Position up the Probe Shaft and Plotted as Temperature versus Time	1.2
1.4	Phased-Array Directivity Calculator Results for a Probe Steered at 20°, with Proper Element Pitch (left) and Improper Element Pitch (right).....	1.3
1.5	(a) and (b) Simulated Sound Fields (main and grating lobes) Emanating from SN4 Matrix Array Design Scenario for 0° and 10° Steering, Respectively.....	1.5
1.6	(a) and (b) Simulated Sound Fields (main and grating lobes) Emanating from SN4 Linear Array Design Scenario for 0° and 10° Steering, Respectively.....	1.7
1.7	Laser Machined Ni-Cup Assembly for the SN4 64-Element Matrix Array PA-UT ETU (right) and the SN4 32-Element Linear Array PA-UT ETU (left).....	1.8
1.8	Illustration of Concept for Increasing Effective Aperture by Doubling Excitation Contact Points on Individual Piezo-Elements	1.9
1.9	Illustration of the High-Frequency Ultrasonic Imaging Approach for Evaluation of the Bonding Process for the SN4 ETUs.....	1.9
1.10	Illustration of the High Frequency Ultrasonic Imaging Approach for Evaluation of the Bonding Process for the SN4 ETUs.....	1.10
1.11	Example of an Inspection of a Nickel Faceplate-to-Piezo-Element Solder Bond to Assess Joint Integrity (SN4)	1.10
1.12	Two Pathways for Assessing Cabling Improvements for the SN4 Probe Design.....	1.11
1.13	(left) Insulated Copper Magnet Wires Soldered to a 32×1 Linear SN4 Array in Preparation for Use of the Zetec Cable. (right) Direct Soldering of HSI Cable to the individual 32×1 Element Linear SN4 Array.....	1.12
1.14	Addition of High-Temperature Ceramic Adhesive/Epoxy Potting Material in SN4 Matrix Array ETU Probe	1.12
1.15	Digital Photographs of the SN4 Linear-Array (top) and Matrix-Array (bottom) ETU Probes, Showing the Probe Housings, Connectors, and Cabling, Prior to the Initiation of Post-Fabrication Testing and Evaluation.....	1.14
1.16	Digital Photographs of the SN4 Cabling Configurations (top) and View of the Hypertronics Connector (bottom) used in Fabrication of the SN4 PA-UT Probes.....	1.15
1.17	Pulse-Echo Evaluation of Individual Elements Using a Quartz Reflector 50.8 mm (2 in.) from the Ni-cup Faceplate.....	1.16
1.18	Plot of the Signal Response and associated FFT from Individual Elements 7–9 in the SN4 Linear Array ETU during Preliminary Pre-Fabrication (housing) Tests Using Manually Applied Measurement Techniques.....	1.17

1.19	Plot of the Signal Response and Associated FFT from Individual Backed Elements 7–9 in the SN4 Linear Array ETU during Preliminary Pre-Fabrication (housing) Tests Using Manually Applied Measurement Techniques	1.19
1.20	Pre- and Post-Backed Element-by-Element –6 dB BW Variation for the SN4 Linear Array ETU Probe.....	1.21
1.21	Pre- and Post-Backed Element-by-Element Center Frequency Variation for the SN4 Linear Array ETU Probe	1.21
1.22	Photo of SN4 Matrix Array ETU Ni-cup During Pre-fabrication Element Evaluation Testing.....	1.22
1.23	Plot of the Signal Response and Associated FFT from Individual Backed Elements 52–54 in the SN4 Matrix Array ETU during Preliminary Pre-fabrication (housing) Tests Using Manually Applied Measurement Techniques	1.22
1.24	Plot of the Signal Response and Associated FFT from Individual Backed Elements 52–54 in the SN4 Matrix Array ETU during Preliminary Pre-fabrication (housing) Tests Using Manually Applied Measurement Techniques	1.24
1.25	Pre- and Post-Backed Element-by-Element –6 dB BW Variation for the SN4 Matrix Array ETU Probe.....	1.26
1.26	Pre- and Post-Backed Element-by-Element Center Frequency Variation for the SN4 Matrix Array ETU Probe	1.26
1.27	Facemap Assessment of Individual SN4 Linear Array Elements in Water Using a Broadband Pinducer	1.27
1.28	Raster Scan of Element #1 for the SN4 Linear Array Prototype Probe	1.28
1.29	Raster Scan of Element #10 for the SN4 Linear Array Prototype Probe	1.29
1.30	Raster Scan of Element #33 from the SN4 Matrix Array Prototype Probe.....	1.29
1.31	C-scan Linear Array of Element #12 Showing No Detection of Adjacent Element Excitation	1.33
1.32	C-scan Matrix Array of Element #57 Showing No Detection of Adjacent Element Excitation	1.33
1.33	Linear Array Element #1 Analysis Window for Frequency Response and Bandwidth Evaluation	1.34
1.34	0° Depth Focus at 76.2 mm (3 in.) for the SN4 Linear Array Prototype Probe. The top left C-scan shows the sound field clipped at –6 dB.	1.38
1.35	0° Depth Focus at 76.2 mm (3 in.) for the SN4 Matrix Array Prototype Probe. The top left C-scan shows the sound field clipped at –6 dB.	1.38
1.36	Linear Array Sound Field for 20° Azimuthal at a Depth of 76.2 mm (3 in.) Clipped to –6 dB	1.40
1.37	Matrix Array Sound Field for 20° Azimuthal at a Depth of 76.2 mm (3 in.) Clipped to –6 dB.....	1.40
1.38	Photograph of the Resolution Target Used to Assess Imaging Resolution Characteristics	1.42
1.39	PA-UT Image of the Resolution Target Using the SN4 Linear Array Probe in Water at a Focal Distance of 76.2 mm (3.0 in.) and a Probe Skew of 270°	1.43
1.40	PA-UT Image of the Resolution Target Using the SN4 Matrix Array Probe in Water at a Focal Distance of 76.2 mm (3.0 in.) and a Probe Skew of 90°	1.43

1.41	Image of the SN4 Matrix Array Probe Being Raster Scanned Across the PNNL Resolution Target at a Distance of 76.2 mm (3.0 in.)	1.44
1.42	PA-UT Image of the PNNL Resolution Target Using the SN4 Linear Array Probe in Water at a Focal Distance of 76.2 mm (3.0 in.) and a Probe Skew of 0°	1.45
1.43	PA-UT Image of the PNNL Resolution Target Using the SN4 Linear Array Probe in Water at a Focal Distance of 76.2 mm (3.0 in.) and a Probe Skew of 90°	1.46
1.44	PA-UT Image of the PNNL Resolution Target Using the SN4 Matrix Array Probe in Water at a Focal Distance of 76.2 mm (3.0 in.) and a Probe Skew of 0°	1.46
1.45	PA-UT Image of the PNNL Resolution Target Using the SN4 matrix Array Probe in Water at a Focal Distance of 76.2 mm (3.0 in.) and a Probe Skew of 90°	1.47
1.46	Design Drawing for the FY16 PNNL Resolution Target.....	1.49
1.47	Photo of FY16 PNNL Resolution Target.....	1.49
1.48	FY15 Post-Processed Data Illustrating (a) Raw RF Waveform (A-scan); (b) Processed RF Waveform after Subtraction	1.50
1.49	Evaluation and Categorization of Various Ultrasonic Signals from Data Acquired in FY 15, for In-sodium Tests at 260°C from Target Reflectors.....	1.51
1.50	Illustration Showing the Mean Frequency Response (x axis in MHz) and Filtered FFT Results of FY 15 Ultrasonic Data. Boxed area indicates the application of a low-pass filter eliminating noise components above approximately 2.3 MHz.	1.52
1.51	B-scan and D-scan Image Views of Specific Targets in Sodium from FY 15 Data. Top row shows original data with noise bands; bottom row shows post-processed data using the high-pass filtering approach.	1.52
1.52	<i>Right:</i> Raw PA-UT Data with No Processing. <i>Left:</i> Time-Gated and Frequency Filtered Data (post-processed).....	1.53
1.53	Stainless Steel Target Drawing (<i>left</i>) and Ultrasonic Image (<i>right</i>) Reconstructed Using Analytic Signal Magnitude Processing	1.54
1.54	<i>Left:</i> Rack Mounted Scanning Controller Instrumentation and Motor Drivers. <i>Middle:</i> Top View of 3-Axis Raster Scan Platform. <i>Right:</i> Side View of 3-Axis Raster Scan Platform.	1.57
1.55	Rack-Mounted Scanning Controller System, Configured for Use Near the Sodium Glovebox	1.57
1.56.	Scanning Platform, Configured over the Sodium Containment Vessel within the Sodium Glovebox	1.58
1.57	(a) SN2 Probe after Scanning has been Completed, Just Prior to Removal from Sodium Containment Vessel; (b) Target after Sodium has been Emptied from Containment Vessel	1.58
1.58	Stainless Steel Imaging Reflector Target Used for Performance Demonstration in Sodium at PNNL	1.59
1.59	Illustration of the Point Source Diffraction Pattern (Airy Pattern)	1.60
1.60	Illustration of the Rayleigh Resolution Criterion Defining Spatial Resolution for Two Closely Spaced Reflectors.....	1.61
1.61	Processed Ultrasonic Image (C-scan view) Showing the Shadowing Effect, or Lack-of-Backwall Echo Response (a) Corresponding to the Various Features on the Target (b) for FY15 data. 1.62	

1.62	Unprocessed (Raw) Ultrasonic Image (C-scan view) Showing the Shadowing Effect, or Lack-of-Backwall Echo Response (a) Corresponding to the Various Features on the Target (b) for FY16 data.....	1.63
1.63	(a) C-scan View Showing the Lack of Backwall Shadowing Effect from all Three Vertical and all Four Horizontal Pins; (b) B-scan View and (c) D-scan View Showing Reflected Energy Signal Responses from All Horizontal and Vertical Pins.....	1.64
1.64	D-scan View Illustrating the Four Horizontal Pins of Different Diameters.....	1.64
1.65	C-scan (top-down) Views	1.65
1.66	D-scan (end-view) Depicting Signal Responses from all Three Vertical Pins	1.65
1.67	D-scan (end-view) Depicting Magnified Signal Responses from all Three Vertical Pins, Identified by Green Arrows	1.66
1.68	C-scan (top-view) (<i>left</i>); D-scan (end-view) (<i>right</i>), Depicting Signal Responses from 9 mm Diameter Horizontal Pin	1.66
1.69	A-, B-, C-, and D-scan Views Illustrating the Detection and Localization of the Four Step Reflectors on the Target in Sodium, at 260°C from Raw Unprocessed Ultrasonic Data.....	1.67

Tables

1.1	Modeling Scenarios and Simulation Results for FY16 SN4 PA-UT Probe Designs	1.7
1.2	Array Design Parameter Considerations for Theoretical Assessments	1.4
1.3	Compiled Pre-Backing Frequency Response Information for Each Element of the SN4 Linear Array ETU Showing Peak, Center, -6 dB Low and High Frequency Values for Each Element as well as the Computed Bandwidth.....	1.18
1.4	Compiled Frequency Response Information for Each Element of the SN4 Linear Array with Acoustic Backing Material.....	1.20
1.5	Compiled Frequency Response Information for Each Element of the SN4 Matrix Array without Acoustic Backing Material.....	1.23
1.6	Compiled Frequency Response Information for Each Element of the SN4 Matrix Array with Acoustic Backing Material.....	1.25
1.7	Individual Linear Array Element Sizing Results from Face Mapping Assessment at -6 dB	1.30
1.8	Individual Matrix Array Element Sizing Results from Face Mapping Assessment at -6 dB.....	1.31
1.9	Element-by-Element Data and Calculations Resulting from the Frequency Response Analysis of Signal Responses from the SN4 Linear Array Prototype Probe, Captured from Immersion Testing in Water Using a Pinducer as the Receiver.....	1.35
1.10	Element-by-Element Data and Calculations Resulting from the Frequency Response Analysis of Signal Responses from the SN4 Matrix Array Prototype Probe, Captured from Immersion Testing in Water Using a Pinducer as the Receiver.....	1.36
1.11	Passive and Active (length and width) Sound Field Dimensions as a Function of the Focal Depth, at -6 dB Points, for the SN2 22-Element Linear Probe and both SN4 Prototype Probes.....	1.39
1.12	Sound Field Dimensions for Linear and Matrix Arrays at 50.8 and 76.2 mm Focal Depth at -6 dB.....	1.41
1.13	True-State Dimensions of the Resolution Target Reflectors and Ultrasonically Measured Separation Dimensions from the PA-UT Data Obtained from SN2 and SN4 Probes.....	1.44
1.14	Vertical and Horizontal Pin Sizing Results for FY15	1.68
1.15	Vertical and Horizontal Pin Sizing Results for FY16 Unprocessed (Raw) UT Data.....	1.68
1.16	FY16 -6 dB Sizing and SNR Data for Target Step Reflectors in Sodium at 260°C	1.69

1.0 PNNL Technical Progress

1.1 Introduction

This section of the Joint summary technical letter report (TLR) describes work conducted at the Pacific Northwest National Laboratory (PNNL) during FY 2016 (FY16) on the under-sodium viewing (USV) PNNL project 58745, work package AT-16PN230102. This section of the TLR satisfies PNNL's M3AT-16PN2301025 milestone and is focused on summarizing the design, development, and evaluation of two different phased-array ultrasonic testing (PA-UT) probe designs—a two-dimensional (2D) matrix phased-array probe, and two one-dimensional (1D) linear array probes, referred to as serial number 4 (SN4) engineering test units (ETUs). The 2D probe is a pulse-echo (PE), 32×2, 64-element matrix phased-array ETU. The 1D probes are 32×1 element linear array ETUs. This TLR also provides the results from a performance demonstration (PD) of in-sodium target detection trials at 260°C using both probe designs. This effort continues the iterative evolution supporting the longer term goal of producing and demonstrating a pre-manufacturing prototype ultrasonic probe that possesses the fundamental performance characteristics necessary to enable the development of a high-temperature sodium-cooled fast reactor (SFR) inspection system for in-sodium detection and imaging.

Sodium-cooled fast reactors are a technology of choice for advanced recycle reactors to be developed as part of the Generation IV (Gen IV) Program. There is a need to re-establish the domestic technology infrastructure in order to support deployment of SFR technology. One key enabling technology is ultrasonic testing for under-sodium viewing that would be employed to 1) monitor operations in optically opaque sodium and 2) inspect structures, systems, and components within the reactor. PNNL's efforts are focused on demonstrating the use of immersible, linear and matrix phased-array ultrasonic probes to meet the needs of ranging and imaging in liquid SFRs. PNNL is currently developing a variety of PA-UT probes that are considered ETUs that couple ultrasonic energy to the submerged structures of interest through liquid sodium. These probes provide the capability to image and conduct nondestructive examination (NDE) of critical components in high-temperature SFRs. The conceptual advantage of this approach is that the liquid sodium provides a medium that can directly couple the ultrasonic energy to the reactor components for imaging and inspection, if the liquid sodium is prepared, managed, and maintained appropriately (with regard to impurities and oxygen levels). The challenge is that the probe must withstand extended exposure to high temperatures and overcome wetting issues that can preclude the transmission of ultrasonic energy from coupling into the medium. PNNL demonstrated good success with the SN2 PA-UT probe in FY15, and the signal-to-noise ratio (SNR) was better for in-sodium testing trials than at any time for any previously designed PNNL probe over the life of the project. In FY15, PNNL developed the capability to invoke raster scanning of the probes in sodium, and the results showed significant improvements for detection/resolution, localization, and characterization of targets in sodium at 260°C (Diaz et al. 2015a). These improvements were incremental in nature and more work was required to reduce noise, improve signal fidelity, and continue to enhance overall probe performance in sodium, at temperature. The aim of the FY16 work was to demonstrate a probe design that would be more robust and provide improved UT performance capabilities and attributes for advanced, high-temperature imaging applications, which are anticipated to be applicable to a variety of inservice inspection and repair (ISI&R) procedures and/or component inspections as they mature.

Sodium-cooled fast reactors present some unique requirements in terms of technologies needed to support operations and maintenance. ISI&R methods must be developed to support deployment of advanced SFRs. Such reactors will require high plant availability (capacity factor) and long lifetimes, and will require advanced ISI&R technologies to ensure the integrity and safety of structures and components submerged in sodium, operating at elevated temperatures (~260°C). Key enabling technologies will allow operators to “see” through optically opaque sodium to support effective operations and maintenance

activities. At the heart of the capability to image in sodium is the development of reliable probes to collect the basis data (justification for proof-of-concept) for reconstructing images of structures submerged in liquid sodium. This project is focused on developing, demonstrating, and optimizing probe platforms capable of supporting anticipated ISI&R requirements. The baseline detection requirement, established during the first year (FY09) of the project, was derived from the need to detect a specific prototypic component (cross section of an isolated pin used within the MARICO-2 test subassembly). This benchmark has driven the prototype probe designs and performance evaluation methodologies. This report provides data, analyses, and the results of a performance characterization of the latest SN4 prototype, linear and matrix array ETUs. In addition, this TLR provides results from in-sodium target detection trials using both of these advanced array ETU designs.

This section of the Joint TLR provides a technical introduction to PNNL's USV research efforts, and in Section 1.2, the objectives and scope of the work are provided. Section 1.3 describes the key performance parameters that define the criteria for assessing probe characterization and performance attributes. Section 1.4 provides a summary of the design specifications and fabrication processes employed for development of the SN4 PA-UT probe designs. It also presents PNNL's initial modeling and simulation results associated with the design of the probes. Section 1.5 provides the results of pre-fabrication evaluations (prior to enclosure of the elements within the housings) of the 1D and 2D probe elements. Section 1.6 provides an assessment and discussion of the post-fabrication evaluations (after seal-welding of the probe housings) conducted on the SN4 probes. This section includes results from immersion water testing. Section 1.7 defines the primary inspection parameters and critical attributes that provide the criteria for assessing the 3D image performance, functionality, and effectiveness of the SN4 PA-UT ETUs. Section 1.8 provides the imaging tests and data obtained from these probes in water (at room temperature), to provide a baseline for future target detection trials in sodium and to help define where future improvements can be made. Additionally, this section includes a description of work to assess signal processing algorithms and advanced image reconstruction approaches for improving raw UT data to enhance detection and characterization capabilities. Section 1.9 describes the sodium wetting challenges, the solution to mitigate those issues, and imaging tests and data obtained from the SN2 prototype probe in sodium, to compare and contrast with results from FY16 SN4 performance characterization results. Lastly, Section 1.10 provides the findings and discusses the conclusions and next steps from this work. References cited in this report are listed in Section 2.0.

1.2 Objective and Scope

An under-sodium viewing system will be an essential instrument for in-situ inspection of components in sodium-cooled fast reactors. The USV system must be able to sustain operation and effective performance under the high temperatures and corrosive environment of liquid sodium. At PNNL technical efforts are focusing on the development and demonstration of an effective and robust PA-UT imaging approach to address the inherent inservice inspection challenges associated with imaging and resolving the specified MARICO-2 pin cross section within the Joyo reactor fuel sub-assembly geometry.

From FY10 through FY12, work at PNNL focused on identification and testing of commercially available phased-array probes; designing, fabricating, and testing single-element ultrasonic probes; designing a 24-element linear PA probe; and building/testing a 9-element linear PA probe that was successfully demonstrated in sodium at 260°C. From FY13 through FY15, PNNL further refined design criteria using modeling and simulation tools and lessons learned from previous work, and subsequently developed methodologies for characterization of two 22-element, ETU linear PA probes, SN1 and SN2, respectively, and a third 2D matrix array design identified as SN3. Over this time period, the probe evaluation process included:

- Radiographic testing – X-ray imaging and analysis
- Ultrasonic testing – Acoustic microscopy imaging and analysis
- Pre-fabrication assessments in water (after potting)
- Post-fabrication assessments (after housing the elements)
 - Immersion testing and characterization (in water)
 - Immersion testing and characterization (in hot oil)
 - Immersion testing and characterization (in sodium).

In addition, PNNL developed fixtures and specialized tooling to hold, position, and rotate the ETU probes under test. The 9-element linear PA-UT probe was fully characterized and shown to function and perform at a consistent level after 9 hours of immersion in sodium. The design and assembly process was captured and documented for this 9-element probe, and used as a basis for the design, fabrication, and testing of the first-generation, 22-element, linear PA-UT ETU design (SN1). This probe was assembled and tested in FY13 in sodium up to the maximum temperature of 260°C; however, the majority of data were obtained at a constant temperature of 200°C, because of identified thermally induced performance limitations. The results of these tests indicated poor SNR in sodium, which translated into marginal image quality and probe resolution, at best (Watkins et al. 2012). PNNL theorized possible root causes of the performance challenges and the analysis identified both thermo-mechanically induced issues coupled with poor sodium wetting. The former would be addressed with fabrication process enhancements, while the latter would be addressed with applying the appropriate level of sodium purification/regeneration, reduction of impurities and oxygen levels, and suitable probe faceplate polishing and surface conditioning to enhance wetting (Braatz et al. 2013). In FY14, the SN2 design was operated in sodium without the implementation of raster scanning (Diaz et al. 2014a). Results were marginal at best; however, in FY15, the SN2 probe was again tested in sodium with the use of full raster scanning and improved signal conditioning. The results for detection, resolution, and sizing were significantly improved, and this work was the foundation for the efforts in FY16 (Diaz et al. 2015a). The SN3 probe design did not pass the performance criteria established for in-lab water testing in FY15, and therefore was not tested in sodium last year. It was shown that the SNR in water for the SN3 probe design was quite low, and noise within the probe coupled with signal losses from cabling and connector matching issues were having a significant impact on the probe's ability to effectively transmit sufficient energy into the medium. In addition, the low SNR made it very difficult to detect targets, discriminate relevant signals, and subsequently characterize detected target features in water.

The objective of the work conducted at PNNL and reported here is to demonstrate the ability to detect a target feature, equivalent to the largest cross section of an isolated pin used within the MARICO-2 test sub-assembly, submersed in 260°C liquid sodium. Figure 1.1 illustrates the Japanese Joyo reactor fuel sub-assembly and the cross sectional dimensions of a simulated pin. In the present fiscal year (FY16), emphasis was focused on design, fabrication, and assessment of two 1D linear array (32×1) probes and a 2D matrix array probe, operated in pulse-echo mode, and comprised of 32×1(×2) arrays. A performance characterization activity was conducted and testing of these immersible PA-UT probes was performed in water. In addition, the performance demonstration protocol, developed and implemented for in-sodium target detection trials in FY14, was again used for the evaluation phase of these probes in sodium. These tests were conducted at 260°C, and the results are documented in this report.

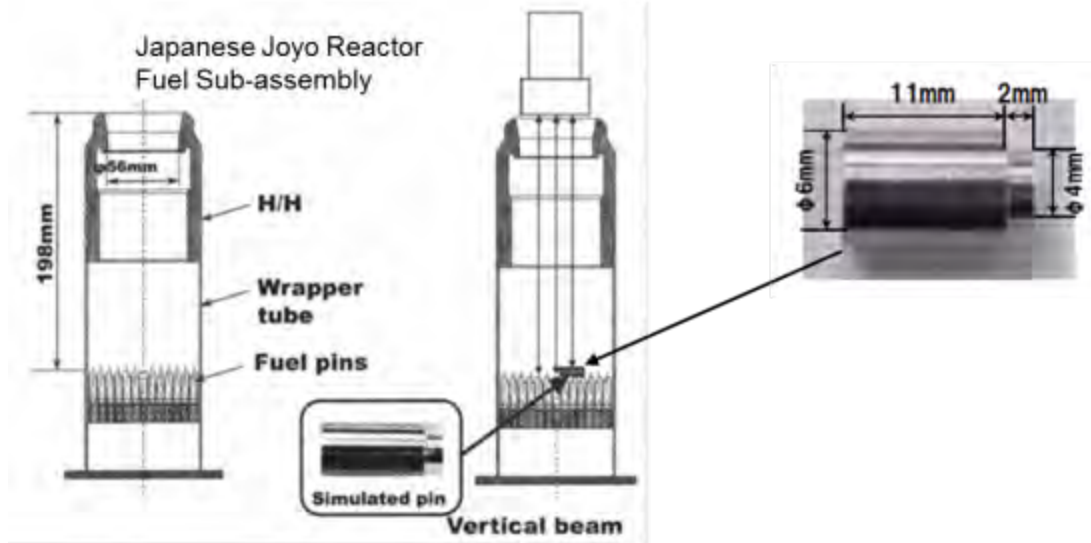


Figure 1.1. Side-view Schematic, Illustrating the Japanese Joyo Reactor Fuel Sub-assembly and the Associated Cross-Sectional Dimensions of an Isolated Pin (simulated here), within the MARICO-2 Test Sub-assembly

The scope of the PNNL efforts conducted in FY16 includes performing an evaluation and assessment of the performance characteristics of the SN4 PA-UT ETUs manufactured at PNNL. This assessment is based on probe performance in water (at room temperature). In addition, PNNL’s FY16 scope included an assessment of the 3D image quality resulting from in-sodium PD tests of the probes as a function of primary inspection parameters. The PD protocol employed for these tests was documented and provided in Diaz et al. (2015b). These primary inspection parameters include such factors as inspection time, spatial sampling frequency, sensor-to-target distance, sodium temperature, thermal cycling, etc. The work described here, associated with the SN4 ETU probes, is based on technical evaluations and tests obtained at two different stages of fabrication: pre-fabrication—before the SN4 arrays were permanently enclosed within the sensor housing, and post-fabrication—after the SN4 arrays were permanently welded and enclosed within their respective housings.

1.3 Key Performance Parameters

This section of the report defines the key performance parameters and critical attributes that provide the criteria for assessing the performance, functionality, and effectiveness of a phased-array ultrasonic testing probe. The effort reported here is focused on analysis of data and performance metrics obtained from both the 1D linear and 2D matrix arrays, PA-UT SN4 probes. These data are used to discuss the performance characteristics of the probes. In this section, the evaluation will not include performance of the probes in sodium, but will instead focus on the performance characteristics via direct measurements obtained prior to housing the elements, after housing the elements, and in water, at room temperature.

American Society for Testing and Materials (ASTM) E2491-13 is a standard guide for evaluating performance characteristics of phased-array ultrasonic probes (ASTM E2491-13). In addition, for PA-UT probes where single focal laws essentially fix the beam and electronic or sectorial scan modes are not employed, ASTM E1065 offers standard guidance using a ball target in an immersion test setting (ASTM E1065/E1065M-14). In FY13, PNNL reported some work in the joint technical report on USV progress with Argonne National Laboratory (ANL) that focused on obtaining data for characterization of the SN1 PA-UT probe (Braatz et al. 2013). PNNL used the key performance parameters outlined in this report,

and also acquired data supporting the use of additional metrics and attributes for the prototype probes that were developed, to effectively compare performance of these ETUs. From the efforts conducted in previous years, the following characterization tests are listed for review. Not all of these tests were conducted on the SN4 probes. The list of tests includes:

1. Pre-fabrication pulse-echo testing on individual array elements (in water)
2. Post-fabrication pulse-echo testing on individual array elements (in water)
 - a. Validation of array pin connections
 - b. Evaluation of transmit uniformity per element (using a pinducer as the receiving probe in raster scan mode)
 - c. Evaluation of element-to-element cross talk (to assess inter-element coupling between neighboring elements)
 - d. Evaluation of selected depth focus points
 - e. Evaluation of selected angles (to assess how effectively the probe can skew the sound field off its 0° primary axis)
3. Post-fabrication assessment of temperature resistance and thermal cycling effects (in hot oil).

In addition to these tests, PNNL conducted post-fabrication characterization assessments aimed at quantifying a suite of additional critical attributes, including:

4. Individual voltage responses from each element after employing a standard excitation pulse, and reflected from a polished, fused silica reflector plate (conducted in pulse-echo mode, without the use of a separate pinducer for receiving signal responses)
5. Center and peak frequency responses from the fast Fourier transforms (FFTs) of individual element responses in #4 above
6. -6 dB (decibels) bandwidths (BWs) of each element, calculated from #5 above
7. Sensitivity variations (in normalized % amplitude) from element-to-element
8. Sound field dimensions (focal spot size) at -6 dB and -12 dB points at a nominal distance from the face of the probe in water, using a pinducer receiving probe
9. Spatial resolution testing using raster scanning of the probe and employing flat reflectors with various spacings to evaluate array resolution performance in water
10. Evaluation of SNR from both pre-fabrication testing of the individual elements and post-fabrication tests.

With the analyses of the data obtained from many of these performance characterization tests, PNNL was able to quantify key performance parameters used to assess the viability of implementing the SN4 ETUs in sodium. In particular, sound field dimensions (spot size), resolution capabilities, SNR, frequency response, and BW characteristics constitute the suite of critical attributes used to evaluate these probes and to support any future decisions regarding viability for continued optimization in FY17. Examples of test data and results from these performance assessments are provided in Sections 1.5, 1.6, and 1.9, and the conclusions obtained from the performance evaluations of both ETU probes are discussed in Section 1.10.

1.4 SN4 1D and 2D Array Probe Design and Fabrication Differences

This section of the report summarizes the key design and fabrication aspects and differences between the SN4 32-element linear PA-UT probe design and the SN4 2D matrix array probe design, built at PNNL during FY16, which to some degree, play a role in probe performance. The processes and methods to design, fabricate, and compare probe performance variation have been documented previously (Diaz et al. 2014b). From this work, PNNL developed a test methodology, test targets, and a probe positioner for characterizing next-generation PA prototypes by acoustic microscopy, and UT in water, hot oil, and eventually in sodium. In FY16, two distinct versions of the SN4 probe design were developed and tested. These designs were based on improved linear array and matrix array designs, and included modifications to the design and fabrication process protocols to accommodate lessons learned, theoretically improve SNR and signal fidelity, and enhance overall probe capabilities and performance.

As the project work unfolded in FY16, primary challenges that were identified included: 1) maximizing the excitation of the active element area; 2) maintaining a suitable sound field spot size, depth of field, and steering capability; 3) improving the PA-UT data acquisition instrumentation system; and 4) addressing noise reduction and enhancing signal fidelity via improved cabling and connectors coupled with advanced post-processing/signal conditioning of UT data. This included improvements and modifications to wiring and cabling protocols and specifications, performing X-Y raster scan data acquisition over the targets in sodium, and applying the use of advanced signal processing algorithms for noise reduction and signal fidelity enhancement. This also included the use of modeling and simulation tools to optimize the design of both array probes. The 2D matrix array design was considered here to essentially isolate individual sections of the array to reduce noise and improve SNR, and to better assess the impact of piezo-element area on sound transmission effectiveness using the pulse echo modality. The detailed description of the probe design and performance characteristics is provided in further detail in Sections 1.5 and 1.6.

In FY16, PNNL completed a modeling and simulation assessment to determine the design specifications and better understand the key characteristics for the FY16 PA-UT probe design, known as SN4 or serial number 4. In order to continue improving ultrasonic detection and characterization capability for in-sodium ISI examinations (within some set of known constraints and limitations), primary attributes were identified and investigated, which included resolution capability, penetration power, steering capability, sound field dimensions, active piezo-element area, active aperture size, and many other parameters. Based on lessons learned over the past few years, and in particular from FY14 and FY15, it was determined that the SN4 probe design would include two similar design approaches. One design would be a linear array using 32 elements (essentially an extension of the SN2 design that worked particularly well in FY15), and the second design would be a matrixed array employing 32×2 elements both operating in a pulse-echo modality. These new SN4 probes would incorporate improved cabling and connectivity to reduce noise and increase signal fidelity. Table 1.1 provides a list of the various scenarios assessed using modeling and simulation tools. Simulated sound fields focused at a particular depth in sodium to better understand sound field and propagation aspects as a function of the various design parameters are provided in Section 1.4.1.1. While the individual element sizes are 50% smaller for the 32×2 matrixed array than for the 32×1 linear array, both sections of the array are employed for transmission using the pulse-echo modality. However, all of these elements are much larger than the elements of the SN3 10×3(×2) matrix array probe assessed in FY15. PNNL believes that element size (area) is a key factor for providing enough sonic energy to effectively propagate in sodium and provide suitable SNR and penetration capabilities at depths of 50 to 100 mm.

Table 1.1. Modeling Scenarios and Simulation Results for FY16 SN4 PA-UT Probe Designs

Case	Array Config.	Sound Field Dimensions																
		Primary Axis					Secondary Axis											
		Number of Elements	Element Size (mm)	E-E Gap (mm)	Pitch (mm)	Aperture (mm)	Near Field Length (mm)	Number of Elements	Element Size (mm)	E-E Gap (mm)	Pitch (mm)	Aperture (mm)	Near Field Length (mm)	Focal Depth (mm)	Reflected Angle (deg.)	Primary Axis Spot Size (mm) @ 6 dB	Secondary Axis Spot Size (mm) @ 6 dB	Depth of Field @ 6 dB
1	24×2	24	2	0.25	2.25	53.75	590	2	7.00	0.25	7.25	14.25	41	50.8	0	1.9	11.3	18.7
																2.1	10.9	25.7
																2.4	9.8	32.6
																2.6	9.9	40
																3.0	11.7	55.2
																3.2	11.8	66.3
																1.9	11.4	18.5
																2.1	11.1	25.6
2	24 Linear	24	2	0.25	2.25	53.75	590	1	14.25	-	-	14.25	41	76.2	0	2.4	9.9	32.5
																2.6	10	39.7
																3.0	11.9	55.2
																3.2	12	66.1
																2.8	12.3	39.4
																3.0	12.1	43.6
3	24 Linear	24	1	0.20	1.20	28.60	167	1	15.00	-	-	15.00	46	76.2	0	4.1	10	81.5
																4.2	10	90
																5.3	11.5	111.5
																5.5	11.5	119.5
																1.9	6.2	18.2
																2.1	6	25.5
4	24×3	24	2	0.25	2.25	53.75	590	3	5.00	0.25	5.25	15.50	49	76.2	0	2.4	8	32.7
																2.4	8.1	41.5
																3.0	10.2	56.2
																3.2	10.4	67.7

Case	Array Config.	Sound Field Dimensions																	
		Primary Axis					Secondary Axis												
		Number of Elements	Element Size (mm)	E-E Gap (mm)	Pitch (mm)	Aperture (mm)	Near Field Length (mm)	Number of Elements	Element Size (mm)	E-E Gap (mm)	Pitch (mm)	Aperture (mm)	Near Field Length (mm)	Focal Depth (mm)	Refracted Angle (deg.)	Primary Axis Spot Size (mm) @ 6 dB	Secondary Axis Spot Size (mm) @ 6 dB	Depth of Field @ 6 dB	
5	22 Linear	22	1	0.25	1.25	27.25	152	1	15.00	-	-	15.00	46	76.2	0	4.2	10	10	86.5
														50.8	0	2.9	10	10	42.5
														101.6	1	5.6	10	10	128.5
														50.8	0	2.1	10	10	25.7
														76.2	0	3.1	10	10	34.3
6	32x2	32	1	0.20	1.2	38.20	298	2	7.40	0.20	7.60	15.00	46	76.2	10	3.2	10	10	54.9
														101.6	1	4.0	10	10	60.8
														101.6	10	4.2	10	10	91.5
														50.8	0	2.1	10	10	104
														50.8	10	2.4	10	10	25.5
														76.2	0	3.1	10	10	34.3
7	32 Linear	32	1	0.20	1.20	38.20	298	1	15.00	-	-	15.00	46	76.2	0	3.1	10	10	54.7
														101.6	1	4.0	10	10	60.6
														101.6	10	4.2	10	10	96
														101.6	10	4.2	10	10	110.5

1.4.1 General 1D Linear and 2D Matrix-Array, ETU Design Considerations

The simulation-based design activity conducted in FY16 and discussed in the previous section was used to develop the SN4 linear and matrix array PA-UT ETUs. The design of the SN4 probes incorporate specifications requiring the capability to raster scan the probe over the targets in sodium. The array housings would be submerged approximately 25 mm below the sodium fill level, and the array face would be pointed towards the bottom of the tank during data collection. Both linear and matrix array probes were designed using identical materials for the probe housing, piezo-element backing, Ni-200 faceplate, and seam welds as previously used and proven out in FY14 and FY15 for SN2 and SN3 probe designs. In FY15, PNNL worked to improve the probe design in order to enhance sound field propagation and ultimately increase image resolution in sodium. The key array design parameters included evaluating both a 1D linear-array configuration and a 2D matrix-array, configuration. This change in design and technical direction was aimed at improving resolution and sensitivity, increasing the volume of examination (via enhanced beam control and steering in primary and secondary axes), and improving signal fidelity and SNR through isolation of transmit and receive array elements with the 2D probe. In addition, the ability to improve sound field focal dimensions and the capability of invoking a raster-scan modality for data acquisition were viewed as positive enhancements that would lead to improved target detection and characterization performance in sodium. While these design modifications and process improvements did indeed result in significantly enhanced results from previous years' efforts, the 2D array SN3 design did not provide enough energy to be tested in sodium. This led to FY16 design considerations aimed at increasing individual piezo-element size in order to provide sufficient sonic energy for propagation and imaging in sodium. Additionally, PNNL began to evaluate potential improvements to signal fidelity by modifying the cables and connectors used for transmission of electrical excitation signals and receiving of ultrasonic energy between the probe and data acquisition instrumentation. In order to properly develop the cable and connector specifications, it was critical to accurately quantify the temperature profile (gradient) from the immersion bath of 260°C up the probe shaft to the primary connector that leads to the ultrasonic data acquisition system.

PNNL employed an older probe ETU from FY14 and conducted laboratory tests to determine the temperature profile (gradient) along the probe shaft at various distances from the lead zirconate titanate (PZT) to determine the viability of using commercially designed PA-UT cables and to quantify the required distance from the PZT to enable cable use without being affected by temperature. These temperature tests were performed in a fume-hood using avocado oil as the hot-liquid medium for probe immersion (see Figure 1.2). The housing had four embedded thermocouples positioned at varying distances from the faceplate, also shown in Figure 1.2. The probe was partially immersed in oil (to a level between T1 and T2) and all thermocouple readings were monitored as the oil was heated to 260°C and the system reached thermal equilibrium. These data are plotted and provided in Figure 1.3.

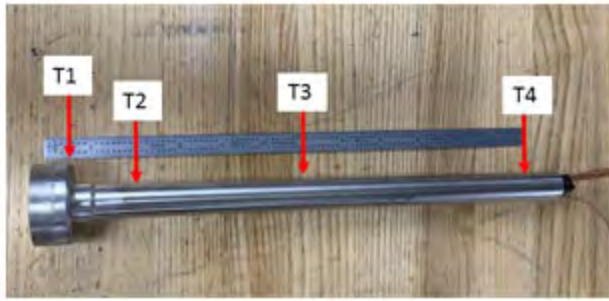


Figure 1.2. (left) Photograph of the FY14 ETU Showing the Internal Positions of the Embedded Thermocouples Inside the Transducer Shaft. (right) Data Acquisition and Measurement Configuration within the Fume-Hood.

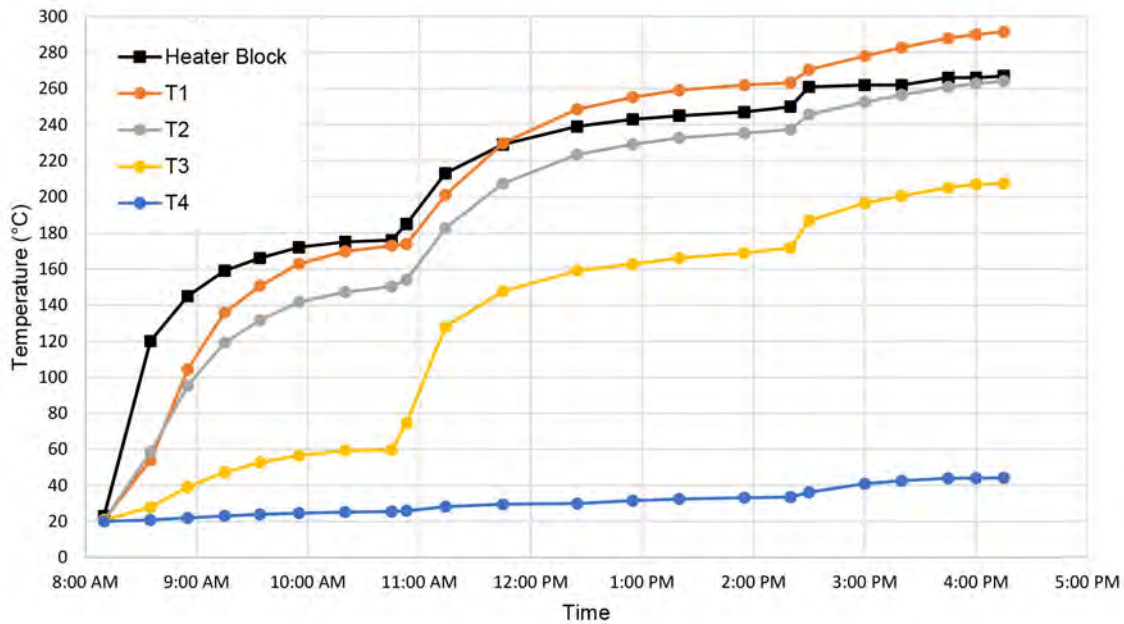


Figure 1.3. Temperature Profile Data Obtained as a Function of Vertical Position up the Probe Shaft and Plotted as Temperature versus Time

Once this information was obtained, PNNL focused on obtaining quotes for custom-designed high-temperature, high-fidelity cabling (standalone bundled micro-coaxial cables as well as cable assemblies) for wiring of the PZT elements to the Hypertronics connectors for the PA-UT prototype probes. Several potential vendors were identified who stated they could provide bundled, shielded, micro-coaxial cable assemblies with operating temperatures up to 260°C. PNNL also conducted ANSYS modeling of signal transmission/noise from PZT elements through magnet wires and through procured Zetec cables. In addition, PNNL also conducted ANSYS modeling of signal transmission/noise from PZT elements directly to the specified Zetec cables (without magnet wires). These simulation studies were conducted to evaluate the potential for electromagnetic coupling between unshielded magnet wires used as the first level interconnect to the array elements. Predicted results for a series of wire placements demonstrated that the current and electric field levels on parasitically coupled neighboring array elements were very

small compared to a directly excited array element. Based on these results, there was a very low probability for undesired coupling between magnet wires inside the array housing as long as the magnet wires were not intentionally bundled together. These data were used to generate specifications for high-fidelity, high-temperature cabling. Two vendors were identified for manufacturing the required lengths of cabling for use in probe fabrication and testing in FY16. These vendors were Zetec and HSI.

1.4.1.1 1D Linear and 2D Matrix Array ETU Mechanical Design Differences

The materials used for design specifications are identical to those documented for the SN2 22-element linear-array. The relevant specifications for this probe are found in previous TLRs (Braatz et al. 2013; Watkins et al. 2012). In FY16, as in past years, PNNL employed modeling and simulation tools to better understand the impacts of various design changes between probe ETU designs. PNNL employed normalized acoustic pressure calculations using Huygen’s Principle for modeling ultrasonic sound field propagation in media (Wooh and Shi 1999; Wooh and Shi 1998; Wooh et al. 2000). A PA directivity calculator was used to predict grating lobe and side lobe energy losses that detract from overall probe performance. The Huygen’s Principle calculation demonstrates the PA directivity capability of a probe to azimuthally steer angles in a medium. When the array is designed with proper individual element sizes and configurations for a particular material, a single peak with maximum acoustic pressure will result at the desired sweep angle. Additional peaks that are present near the primary lobe represent unwanted off-axis energy (known as grating lobes). These grating lobes provide an indication of how efficient and effective the probe is at concentrating acoustic energy along the primary axis of the main lobe. If the grating lobes are significant, they can detract from the ability of the probe to focus energy along the primary angle ofinsonification. The generation of grating lobes can create undesired noise in the data. These calculations are critical in understanding the impacts of various design features for PA-UT probes. Figure 1.4 illustrates an example of the PA directivity calculator output showing normalized sound field pressure (essentially amplitude) as a function of the steered angle from two arrays being steered at a 20° angle. The array on the left has been designed with proper element pitch, while the array on the right has been designed with an improper element pitch as indicated by an off-axis grating lobe (denoted by a red arrow in the figure).

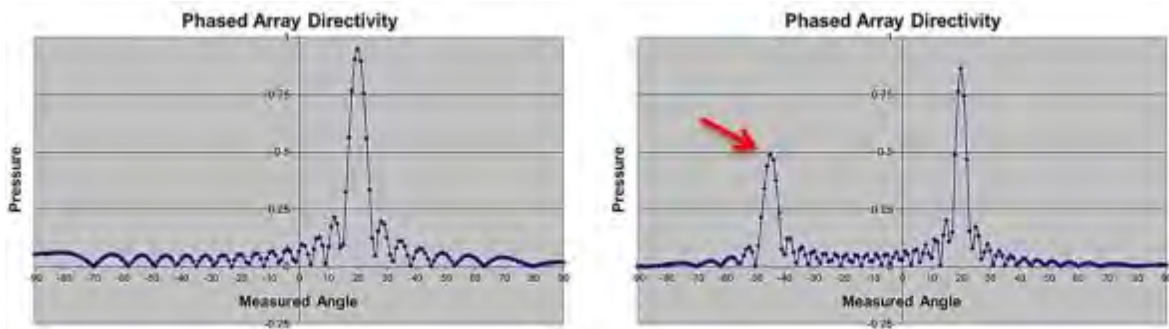


Figure 1.4. Phased-Array Directivity Calculator Results for a Probe Steered at 20°, with Proper Element Pitch (*left*) and Improper Element Pitch (*right*)

In addition to this tool, PNNL also employed CIVA and Zetec’s UltraVision software version 3, for simulating the sound fields from various PA-UT probe designs. In order to theoretically evaluate various probe design specifications and assess the impacts of these design parameters on the resultant simulated sound fields, the following design features were considered:

1. The 1D probes would be an enhanced version of the 22×1 linear array probe that performed quite well in sodium testing in FY15.
2. The 2D probe would be a modified version of the PE 1D linear array probe, however, this probe would have two rows of elements for better electrical excitation across the length of each element.
3. A decision was made to design a planar array configuration where no roof angle would be applied. This requires electronic skewing of the planar arrays, but significantly reduces the level of complexity required for fabrication and fixturing, and provides a longer depth of field.
4. A minimum element size is needed to minimize laser dicing limitations and hand-soldering issues, including the potential for shorting adjacent elements and increasing mechanical cross talk with a reduced gap size.
5. It was decided to maintain the frequency requirement for this probe design. Thus, the specification for the nominal operating frequency of the probe was maintained at 2.0 MHz to be consistent with previous designs and retain a wavelength in liquid sodium of 1.23 mm. This wavelength is compatible for meeting the required resolution to detect an 11 × 6 mm Joyo fuel pin.
6. A desired working distance of 76.2 mm was identified as optimal, but 50.8 mm distance was also considered. This has impact to the array length for effective scan performance in the active axis.
7. An assumption of a 50% –6 dB BW was used as an initial design consideration for these simulations. This was consistent with other probe designs in FY13, FY14, and FY15.

The PA directivity calculator was used to assess both the 32×2 linear and 32×1(×2) configurations. For each array configuration, various specifications were evaluated, and these included focal distance, steering angle, probe separation, primary and secondary pitch, element dimensions and, of course, total aperture dimensions. Table 1.2 provides the various values for these design parameters for each of the array configuration scenarios that were simulated. True-depth focusing was applied at 50.8, 76.2, and 101.6 mm and steering angles were incremented in 1° steps. The spatial resolution for these sodium simulations was set to 0.3 × 0.3 mm.

Table 1.2. Array Design Parameter Considerations for Theoretical Assessments

Design	Sound Field Dimensions					Separation/Pitch/Element			
	Focal Depth (mm)	Refracted Angle	Primary Axis Spot (mm) @ –6 dB	Secondary Axis Spot (mm) @ –6 dB	–6 dB Depth of Field (mm)	Array Separation (mm)	Primary Pitch/ Element (mm / mm)	Secondary Pitch/ Element (mm / mm)	Total Aperture (mm)
32×2 Matrix Array	50.8	0	2.1	12.3	25.7	0.2	1.2 / 1.0	7.6 / 7.4	38.2×15
		10	2.4	12.3	34.3				
	76.2	0	3.1	9.8	54.9				
		10	3.2	9.8	60.8				
101.6	0	4.0	11.1	91.5					
	10	4.2	11.4	104.0					
32×1 Linear Array	50.8	0	2.1	12.3	25.5	--	1.2 / 1.0	-- / 15.0	38.2×15
		10	2.4	12.4	34.3				
	76.2	0	3.1	10.0	54.7				
		10	3.2	10.1	60.6				
101.6	0	4.0	11.3	96.0					
	10	4.2	11.6	110.5					

Simulations conducted for SN4 matrix array design are illustrated in Figure 1.5 and show that the working distance of 76.2 mm, or even greater focal distances, are achievable in sodium, but the advent of a grating lobe limits the primary beam steering performance to approximately $\pm 10^\circ$ for this design. However, in practice, empirical measurements showed that $\pm 20^\circ$ could be achieved without negative impacts from a grating lobe, and indeed data were acquired using this larger range of angles.

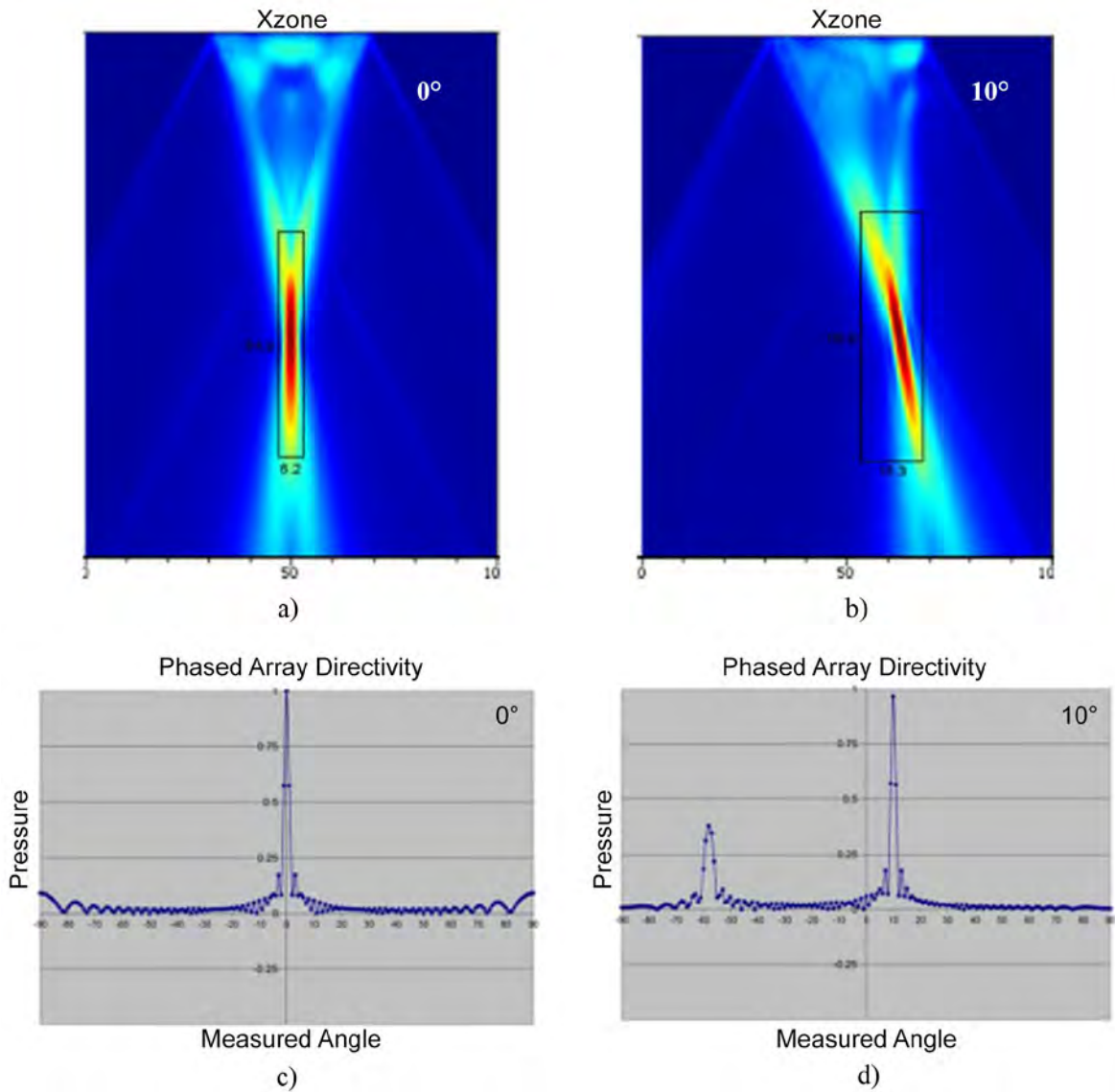


Figure 1.5. (a) and (b) Simulated Sound Fields (main and grating lobes) Emanating from SN4 Matrix Array Design Scenario for 0° and 10° Steering, Respectively. Phased Array Directivity Calculator Results for SN4 Matrix PA-UT Probe Steered at (c) 0° and (d) 10° in the Active Axis.

Simulated results for the scenarios representing both the linear array and matrix array designs exhibited similar performance at the focal depths evaluated in this study. The scenarios in both cases yielded similar sound field dimensions (spot sizes) across the spectrum of focal depths and steering angles, and grating lobes were generally well below -20 dB for both cases. Because of similarities in theoretical performance, PNNL was able to assess and compare probe performance between linear and matrix array designs to better understand the effects of piezo-element size on sound field formation, propagation and detection capabilities. The active axis scan range of $\pm 20^\circ$ corresponds to ± 18.5 mm of target coverage at 50.8 mm focal distance, while at 76.2 mm focal distance this target coverage region expands to ± 27.7 mm. With only 2 rows of elements in this matrix array design, it is not possible to steer the beam in the passive (secondary) axis, so passive axis plots are not presented here. Simulations conducted for SN4 linear array design are illustrated in Figure 1.5 and again show that the working distance of 76.2 mm, or even greater focal distances are achievable in sodium, but the advent of a grating lobe limits the primary beam steering performance to approximately $\pm 10^\circ$ for this design as well. Once again, measurements showed that $\pm 20^\circ$ could be achieved without negative impacts from a grating lobe with the linear array as well, and indeed data were acquired using this larger range of angles. The PA directivity plots for the linear array design cases are also provided in Figure 1.6 for a range of active axis scan angles between 0° and 10° . The CIVA-generated beam simulations for this case are provided at a 76.2 mm focal depth. These results were, as anticipated, very similar to the previous results for the matrix array design due to nearly identical array dimensions.

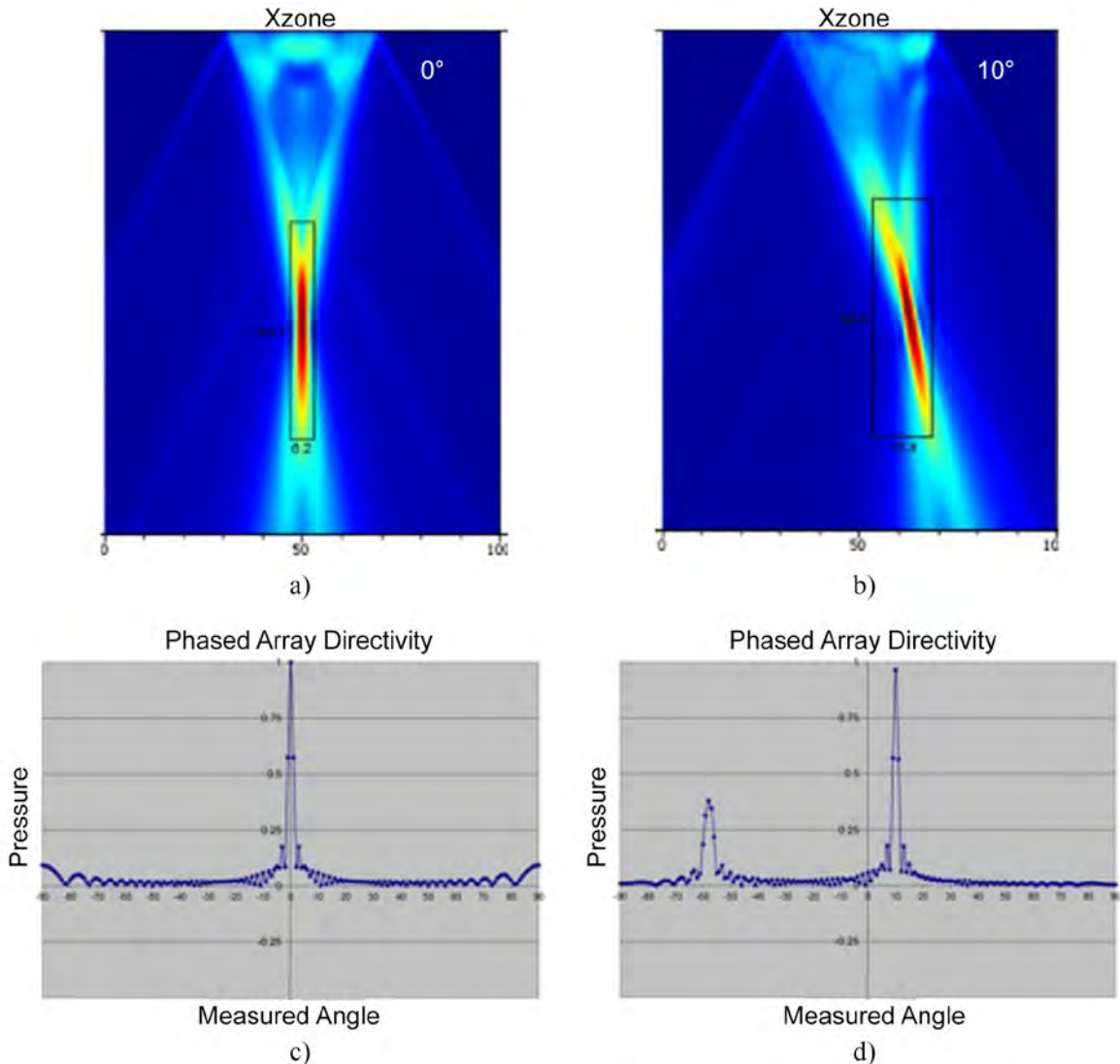


Figure 1.6. (a) and (b) Simulated Sound Fields (main and grating lobes) Emanating from SN4 Linear Array Design Scenario for 0° and 10° Steering, Respectively. Phased Array Directivity Calculator Results for SN4 Linear PA-UT Probe Steered at (c) 0° and (d) 10° in the Active Axis.

1.4.1.2 1D Linear and 2D Matrix Array ETU Fabrication Process Enhancements

The fabrication process outlined previously in the FY15 Joint TLR for the SN2 22-element linear array was essentially followed for development of the SN4 ETUs. However, a few critical process modifications were introduced during FY16. In particular, element isolation via an improved laser dicing process was implemented for physically separating each element from one another. Figure 1.7 shows the laser machined cup assemblies for both SN4 probe designs. Process improvements conducted by the vendor included improved solder materials, enhanced control of solder pooling, and employed a higher process temperature. As a result of this improved process, re-poling of the elements was not required for the SN4 probe, as it was for the SN1 probe in FY13.



Figure 1.7. Laser Machined Ni-Cup Assembly for the SN4 64-Element Matrix Array PA-UT ETU (*right*) and the SN4 32-Element Linear Array PA-UT ETU (*left*)

The SN4 piezo-elements were bonded to the cup assembly using a solder strip in an industrial oven at a temperature of 340°C. A copper weight and associated fixture were placed on top of the piezo-element to ensure centering of the element and maintain even pressure for bonding between the element and the Ni faceplate. With the SN4 prototypes, the Ni cups and faceplates were designed and fabricated as a single assembly. The faceplate thickness increased to 0.100 in. and was then subsequently machined to approximately 0.060 in. after completing the piezo-element solder/bonding process. The matrix array design piezo-element was then laser diced to the specifications for a 32×2 array with a 0.2 mm separation (edge-to-edge) between rows of elements and a nominal operating frequency of 2.0 MHz. The entire PZT-5A element measured 15.0 mm × 38.2 mm (passive axis-x-active axis, respectively). For the linear array design, each individual rectangular element was 1.0 mm × 15.0 mm, and each channel was laser machined to a width of 0.2 mm. The SN4 piezo-elements were then evaluated for any depoling of the piezo-element after the oven-baking process.

These two array designs were chosen based on successes from FY15 in-sodium tests, and the concept of more effectively increasing individual piezo-element excitation was identified from sound field mapping exercises performed in FY14 and FY15. It was anticipated that the 64-element matrix array probe variant of the SN4 design would outperform the 32-element linear array due to improved element excitation along the secondary (passive) axis by exploiting more element area via excitation. Figure 1.8 illustrates the concept.

As in previous years, PNNL employed high-frequency acoustic microscopy to assess the quality and homogeneity of the high-temperature solder bond between the PZT-5A element and the Ni-200 faceplate. Figure 1.9 illustrates the technique employed to assess these bonds.

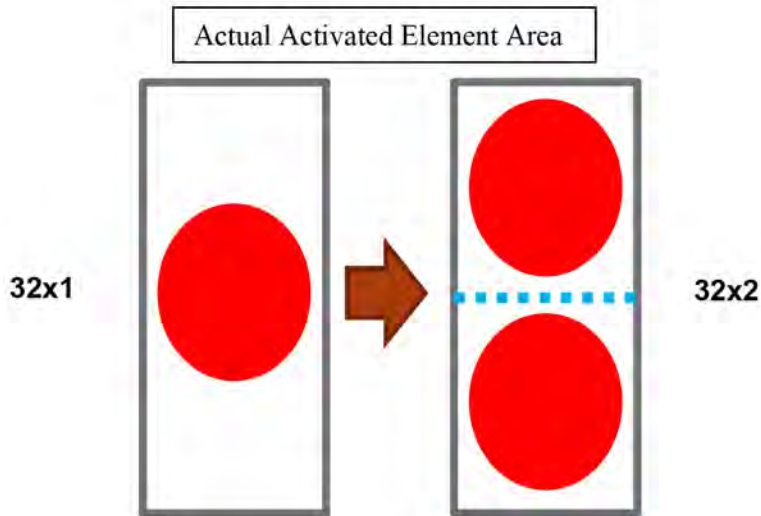


Figure 1.8. Illustration of Concept for Increasing Effective Aperture by Doubling Excitation Contact Points on Individual Piezo-Elements

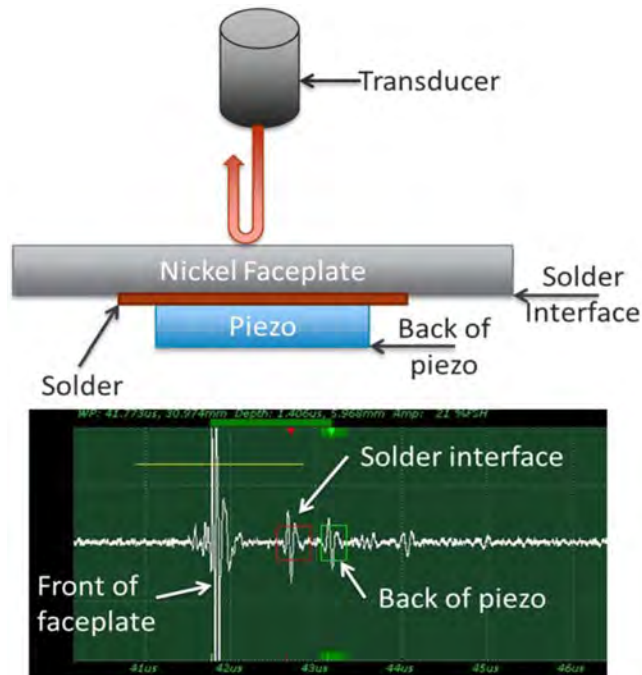


Figure 1.9. Illustration of the High-Frequency Ultrasonic Imaging Approach for Evaluation of the Bonding Process for the SN4 ETUs

The data acquisition system used for this assessment included a 50 MHz focused immersion probe in a water bath. The pulse-echo mode was employed, and a $50 \times 50 \mu\text{m}$ scan resolution was used. Time gates in software were used to collect data (C-scan images) at the piezo-solder interface and at the back of the piezo-element. The photographs in Figure 1.10 show the laboratory system used for this effort.

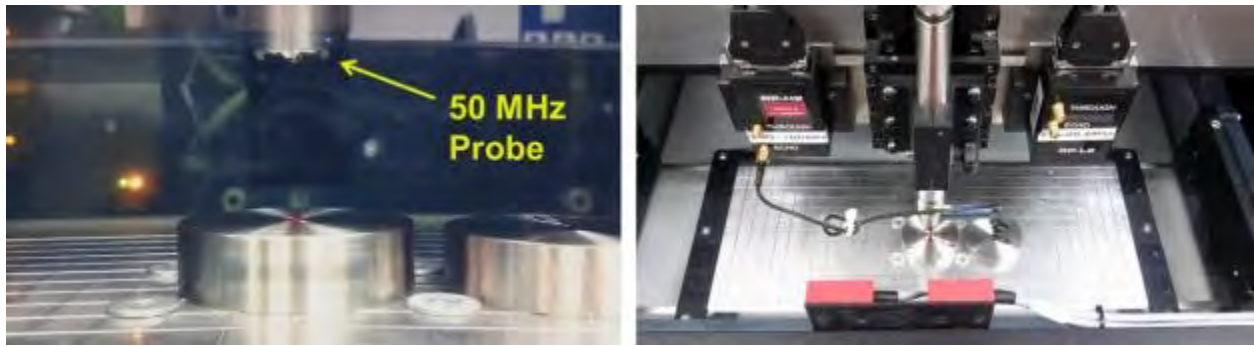


Figure 1.10. Illustration of the High Frequency Ultrasonic Imaging Approach for Evaluation of the Bonding Process for the SN4 ETUs

The primary characteristics of a quality bond can be assessed by evaluating the ultrasonic signal responses at the interface of the solder-bond and the Ni faceplate interface. The sound field of the acoustic microscope was focused to insonify the inside surface of the nickel cup faceplate and the back surface of the piezo-element. These signals were gated in time and the assemblies were raster scanned. In this manner, properly soldered areas (that represent a strong bond) would allow the ultrasonic energy to penetrate through, while areas that were not soldered correctly would present a de-bonded area, essentially reflecting ultrasonic energy back to the focused probe. Low-amplitude (black) signal responses from the solder-nickel interface indicate good transmission of sound through the interface into the piezo-element. Figure 1.11 shows the result of inspecting the SN4 solder joints beneath the square piezoelectric elements with a 50 MHz focused probe. This process was repeated for all six Ni cups.

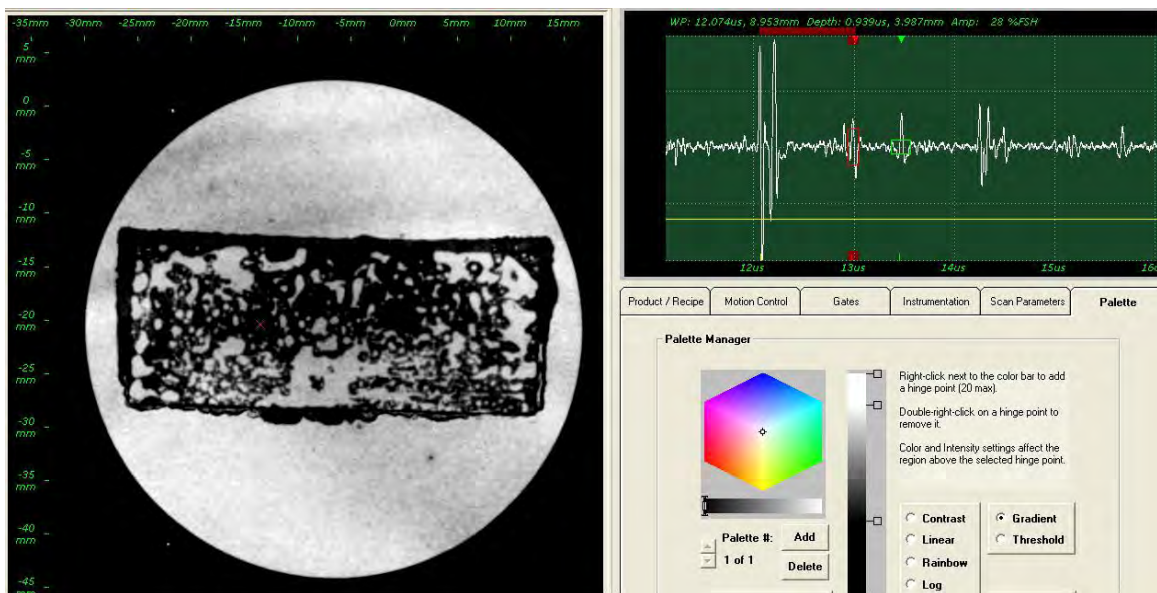


Figure 1.11. Example of an Inspection of a Nickel Faceplate-to-Piezo-Element Solder Bond to Assess Joint Integrity (SN4)

For connectivity in the SN2 and SN3 prototype designs, insulated magnet wire was soldered to each individual piezo-element. The processes employed for wiring, soldering, and backing the SN4 prototype probes has been refined due primarily to experience in the laboratory, but the processes employed have also been modified. These modifications have been documented in great detail in the FY13 Joint TLR (Braatz et al. 2013). The magnet wires used in FY15 were identical to the wires used in FY14, with the exception of having a higher heat resistance. However, in FY16, new high-temperature, high-fidelity cabling from Zetec and HSI were evaluated for viability in sodium and to increase SNR. Figure 1.12 illustrates the two cabling configurations.

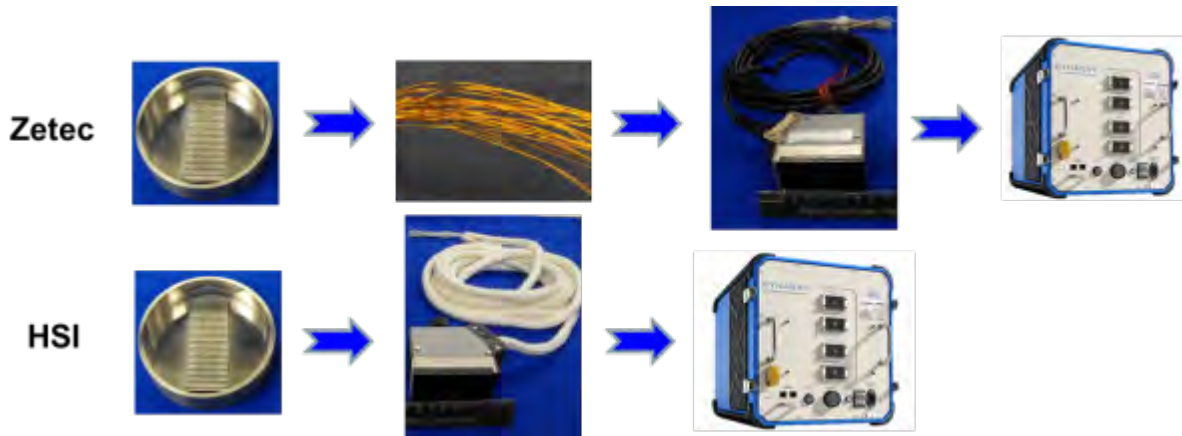


Figure 1.12. Two Pathways for Assessing Cabling Improvements for the SN4 Probe Design

A plan was devised to fabricate one of the 32×1 linear array probes using magnet wire soldered directly to the piezo-element, and then connected to a Zetec PA-UT high-fidelity cable via a second solder joint. This cable would then be connected to the Dynaray ultrasonic data acquisition system via a Hypertronics connector. Simultaneously, a second (but identical) 32×1 linear array probe would be fabricated whereby the HSI high-temperature cable would be directly soldered to the individual piezo-elements and connected at the instrument end via Hypertronics connection, eliminating a solder joint.

Figure 1.13 shows the soldered assemblies for the SN4 prototype probes. This soldering process was performed manually using a high-temperature solder and soldering iron. Not only are there opportunities for electrical shorts to occur, there is also the potential of locally overheating (exceeding 350°C) the piezo-element and causing the piezoelectric material to depole. The next step was to apply a high-temperature (1315°C) Resbond ceramic adhesive/epoxy potting material over the piezoelectric and magnet wires to a depth of ~7–8 mm as shown in Figure 1.14. This material serves as an acoustic backing to the piezoelectric elements and also as a strain relief for the magnet wires. This material controls the damping of the piezoelectric elements and also impacts the frequency response of the elements as well. In FY16, the soldering processes continued to improve, but the application process for the backing material was identical. This process was completed for both 32×1 linear arrays and for the 32×1(×2) matrixed array probes.

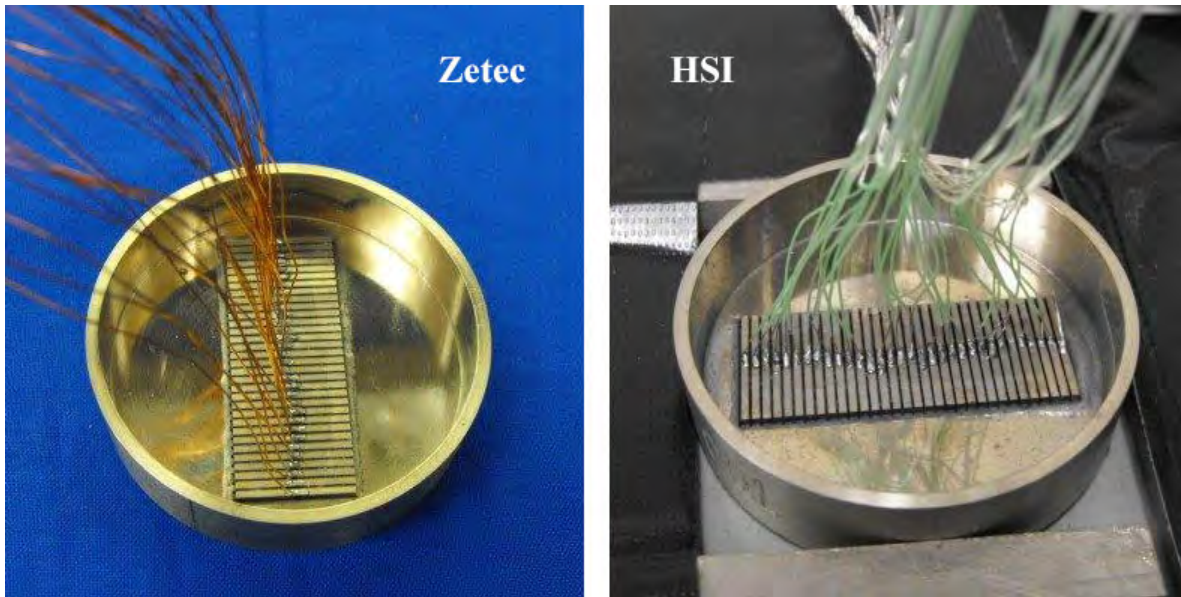


Figure 1.13. (left) Insulated Copper Magnet Wires Soldered to a 32×1 Linear SN4 Array in Preparation for Use of the Zetec Cable. (right) Direct Soldering of HSI Cable to the individual 32×1 Element Linear SN4 Array.



Figure 1.14. Addition of High-Temperature Ceramic Adhesive/Epoxy Potting Material in SN4 Matrix Array ETU Probe

The objective of this assessment was to evaluate the probe performance as a function of cabling to determine which configuration provides the most improvement to signal fidelity and SNR. During application of the seam weld on the 32×1 HIS-configured probe housing, many of the wired connections were melted due to higher than anticipated weld temperatures. This process damaged the probe, thereby requiring PNNL to use the Zetec cable configuration for fabrication of the SN4 matrix array (64-element) PA-UT probe.

In FY16, refinements to the manual soldering technique were applied to the fabrication process of the SN4 probes. In addition, great care was taken to physically isolate each of the individual magnet wires, by separating them during the curing process of the backing material. The design and fabrication process differences described in this section underpin some significant (anticipated) performance improvements embodied in the SN4 prototype probes; and during the pre-fabrication assessment, these improvements have been discussed here. The 32×1 linear array probe using the Zetec cabling configuration was fabricated from a shaft of the same dimensions as used in previous probe fabrication efforts for SN2 and SN3 designs, with the exception of introducing a branched channel strain relief for cabling. This additional “Y” branch is shown in Figure 1.15, and was added to improve strain relief for cabling and to allow for more effective channeling of cable bundles and grounding wires to the data acquisition system connectors. In addition, the 64-element matrix array probe also included this feature; however, the shaft diameter was also increased to accommodate the larger number of wires required for the additional 32 elements in this probe design. After probe housings were assembled and seam welds were completed, the probe wiring bundles were then soldered to the Zetec cables and readied for testing. Both SN4 linear and matrix array ETU probes are illustrated in Figure 1.15.

The magnet wire used on both SN4 arrays was slightly different from the SN1 and SN2 arrays designed in previous years, to better withstand potential heating effects from the liquid sodium. The backing material used in the array cup insulated the piezo-element connections from these potential heating effects, but a decision was made to be more conservative and further protect these connections by employing a magnet wire with higher heat resistance. The only difference between the original and new magnet wire was the coating used to insulate the wire and the length of the wires. The wire gauge was identical (MWS 30 ga). The original magnet wire was rated at 140°C and the new magnet wire was rated at 240°C. Lengths were increased from 200 mm to 355 mm. The Zetec cables were ordered with Hypertronics connectors already installed on one end, for direct connection to the Zetec Dynaray data acquisition system. In this manner, individual cable impedances and soldered connection joints were all fabricated by a proven/commercial PA-UT vendor. This vendor has the necessary expertise and skills to provide high-quality, high-fidelity PA probe cabling that is optimally matched (electrically) to the data acquisition system instrument.

Digital photographs of the final cabling configurations and Hypertronics connector used on the SN4 ETUs are provided in Figure 1.16.



Figure 1.15. Digital Photographs of the SN4 Linear-Array (*top*) and Matrix-Array (*bottom*) ETU Probes, Showing the Probe Housings, Connectors, and Cabling, Prior to the Initiation of Post-Fabrication Testing and Evaluation.



Figure 1.16. Digital Photographs of the SN4 Cabling Configurations (*top*) and View of the Hypertronics Connector (*bottom*) used in Fabrication of the SN4 PA-UT Probes

1.5 Pre-Fabrication Evaluation of Individual PA-UT Probe Elements for the SN4 ETUs

This section describes the measurements and data obtained during the fabrication of the SN4 linear and matrix array ETU probes prior to housing the elements. A set of pulse-echo tests were conducted on the pre- and post-potted assemblies to 1) ensure that each individual array element provides an acoustic response to a narrow square-wave electrical input signal, 2) to make a relative comparison of the amplitude responses of each element to determine if any are “weak” or “unresponsive,” and 3) to establish a baseline for the expected response. Weak or unresponsive elements would provide a qualitative indication of depoling occurring as a result of exceeding the piezoelectric Curie temperature of 350°C during the soldering processes. Depoling could be localized to a heat-affected zone in the vicinity of the magnet wire-to-piezoelectric solder joint, permitting the element to continue functioning, but with a weaker response. Unresponsive elements would indicate total depoling or alternatively an electrical disconnect of the magnet wire from the piezoelectric element. The tests were conducted by placing only the external, sodium-facing side of the cup assembly into a water bath with a 50 mm spacing from a

quartz reflector to obtain signal responses for these measurements. Each individual element was driven with a short-duration 180V square-wave pulse at a suitable repetition rate for data acquisition. This pulse length was chosen to optimally excite the piezoelectric elements at their fundamental design frequency of 2.0 MHz.

Initial laboratory work employed the use of a digital oscilloscope, UTEX pulser/receiver, and a PC for capturing pulse-echo waveforms reflected off of a quartz reflector in an immersion tank. All elements of the array were evaluated using this method. The testing setup for evaluation of pre- and post-backed Ni-cup configurations is illustrated in Figure 1.17.

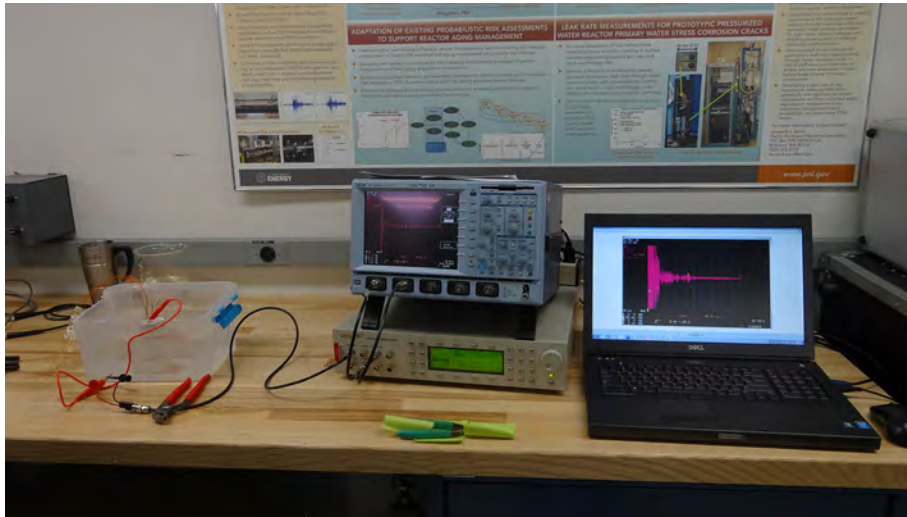


Figure 1.17. Pulse-Echo Evaluation of Individual Elements Using a Quartz Reflector 50.8 mm (2 in.) from the Ni-cup Faceplate

Figure 1.18 shows the captured radio frequency (RF) waveforms from the oscilloscope and the corresponding fast Fourier transforms (FFTs) for linear array elements #7–10. The red highlighted region on the A-scan plot represents the portion of the RF waveform used to compute the FFT. The compiled frequency response information for each element of the SN4 linear array without acoustic backing material is shown in Table 1.3.

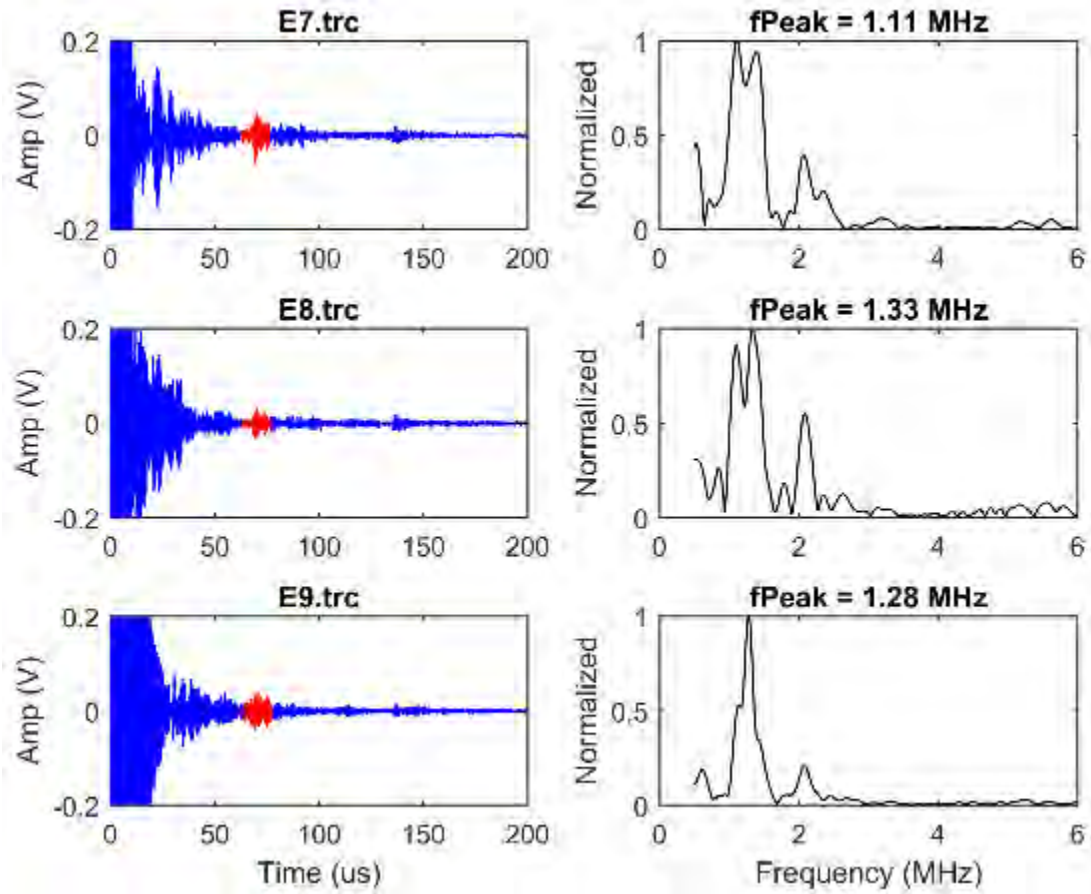


Figure 1.18. Plot of the Signal Response and associated FFT from Individual Elements 7–9 in the SN4 Linear Array ETU during Preliminary Pre-Fabrication (housing) Tests Using Manually Applied Measurement Techniques

Table 1.3. Compiled Pre-Backing Frequency Response Information for Each Element of the SN4 Linear Array ETU Showing Peak, Center, -6 dB Low and High Frequency Values for Each Element as well as the Computed Bandwidth

Element	FPeak (MHz)	FCenter (MHz)	BW%	FLow (MHz)	FHigh (MHz)
1	1.25	1.24	17	1.14	1.34
2	1.21	1.21	22	1.08	1.35
3	1.14	1.21	38	0.98	1.44
4	1.20	1.17	26	1.01	1.32
5	1.15	1.14	14	1.06	1.22
6	1.08	1.09	22	0.96	1.21
7	1.11	1.25	42	0.98	1.51
8	1.33	1.25	38	1.01	1.48
9	1.28	1.23	21	1.10	1.36
10	1.15	1.15	23	1.01	1.28
11	1.14	1.17	24	1.03	1.32
12	1.12	1.13	23	0.99	1.26
13	1.09	1.11	21	0.99	1.23
14	1.28	1.28	13	1.19	1.36
15	1.20	1.25	25	1.09	1.40
16	1.28	1.17	33	0.98	1.37
17	1.10	1.17	30	0.99	1.35
18	1.12	1.22	33	1.02	1.42
19	1.28	1.21	30	1.03	1.39
20	1.15	1.26	32	1.06	1.46
21	1.18	1.25	30	1.06	1.43
22	1.09	1.10	19	0.99	1.20
23	1.17	1.16	19	1.05	1.27
24	1.16	1.18	21	1.06	1.31
25	1.18	1.19	21	1.07	1.31
26	1.17	1.18	22	1.05	1.31
27	1.10	1.27	42	1.00	1.54
28	1.12	1.12	17	1.02	1.21
29	1.13	1.13	19	1.03	1.24
30	1.26	1.25	22	1.12	1.39
31	1.30	1.19	37	0.97	1.40
32	1.23	1.22	20	1.10	1.34

The individual element performance evaluation was repeated after the backing material was applied. Figure 1.19 shows the A-scan and FFT results from this evaluation for array elements #7–9. Table 1.4 shows the compiled frequency response information for each element of the array after the acoustic backing material was applied.

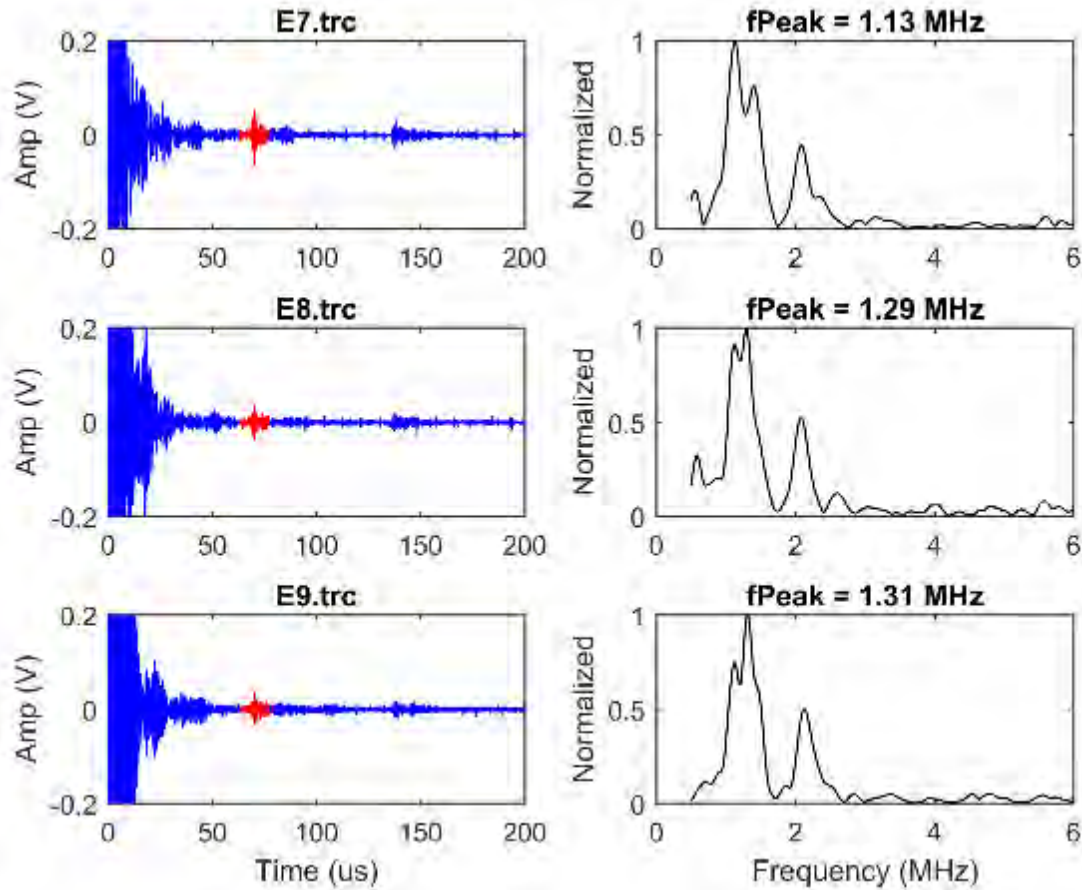


Figure 1.19. Plot of the Signal Response and Associated FFT from Individual Backed Elements 7–9 in the SN4 Linear Array ETU during Preliminary Pre-Fabrication (housing) Tests Using Manually Applied Measurement Techniques

Table 1.4. Compiled Frequency Response Information for Each Element of the SN4 Linear Array with Acoustic Backing Material

Element	FPeak (MHz)	FCenter (MHz)	BW%	FLow (MHz)	FHigh (MHz)
1	1.27	1.27	16	1.17	1.37
2	1.15	1.17	18	1.07	1.28
3	1.12	1.13	23	1.00	1.26
4	1.09	1.11	24	0.98	1.24
5	1.14	1.14	20	1.02	1.25
6	1.14	1.14	29	0.98	1.31
7	1.13	1.25	41	0.99	1.51
8	1.29	1.22	33	1.02	1.43
9	1.31	1.27	38	1.03	1.51
10	1.14	1.18	28	1.01	1.35
11	1.12	1.14	26	0.99	1.29
12	1.10	1.11	20	1.00	1.22
13	1.12	1.13	21	1.01	1.25
14	1.30	1.21	31	1.02	1.40
15	1.15	1.14	17	1.05	1.24
16	1.20	1.15	26	1.00	1.31
17	1.10	1.10	17	1.01	1.20
18	1.12	1.20	34	1.00	1.40
19	1.09	1.18	32	0.99	1.37
20	1.10	1.17	27	1.01	1.32
21	1.14	1.23	34	1.02	1.44
22	1.12	1.23	36	1.01	1.45
23	1.11	1.21	36	0.99	1.42
24	1.10	1.25	39	1.01	1.50
25	1.11	1.13	23	1.00	1.26
26	1.26	1.23	22	1.09	1.37
27	1.14	1.20	30	1.02	1.38
28	1.12	1.23	38	0.99	1.46
29	1.10	1.20	33	1.00	1.39
30	1.21	1.21	20	1.09	1.34
31	1.28	1.27	16	1.17	1.37
32	1.24	1.24	15	1.14	1.33

From a review of the data obtained from all 32 elements (within the time-gated window as shown in Figures 1.18 and 1.19), the individual pulse-echo signal responses from the elements of the SN4 Linear Array probe (with backing) were generally reduced in amplitude (dampened) and slightly cleaner (less noisy) than those collected prior to backing. For each element, at a nominal gain setting that was not changed during data acquisition, the maximum peak-to-peak signal amplitude response was recorded. These data were analyzed and the FFT results were calculated to generate bandwidth for each element. From an analysis of these signal responses (see Figures 1.20 and 1.21), it was clearly evident that both

probes had very similar individual BW and center frequency values at this same stage of the testing and evaluation process. While raw signal amplitudes were slightly lower with the SN4 matrix array, 64-element probe, this was anticipated because of the smaller element sizes between the linear and matrixed array designs.

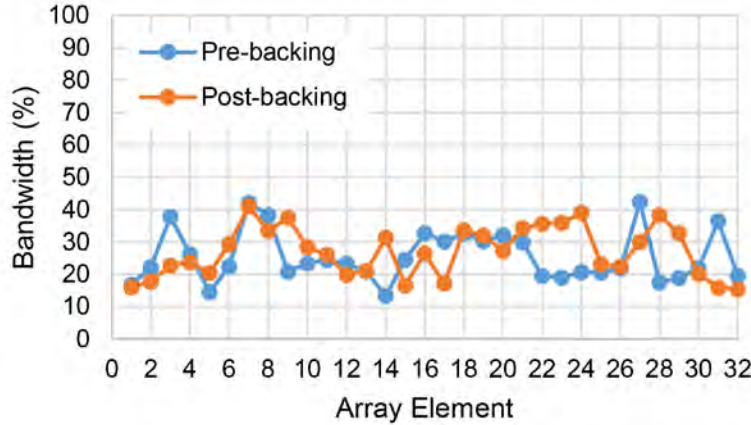


Figure 1.20. Pre- and Post-Backed Element-by-Element -6 dB BW Variation for the SN4 Linear Array ETU Probe

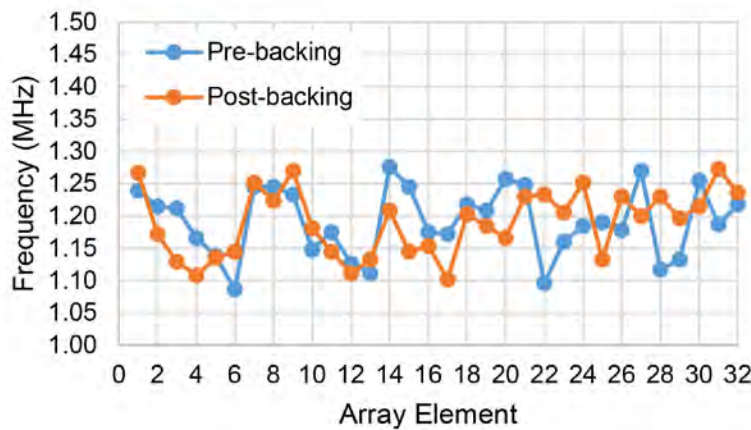


Figure 1.21. Pre- and Post-Backed Element-by-Element Center Frequency Variation for the SN4 Linear Array ETU Probe

From this initial assessment, prior to completion of the probe housing and wiring activities, these data showed that the backing had a minimal effect on average BW. The average center frequency of the probe across all 32 elements stayed constant at 1.19 MHz. The downshift in frequency is likely attributed to the inappropriate matching layer thickness of the Ni-cup faceplate. The thickness of the layer is decreased, and consequently matched correctly, when the faceplate of the transducer is polished for performance evaluation trials in sodium.

The pre-fabrication evaluation process was also applied to the SN4 matrix array ETU using the same testing configuration described earlier. Figure 1.22 shows the 64-element array and Ni-cup during testing. Example RF responses and computed FFTs are provided for elements #52–54 in Figure 1.23. The compiled frequency response information for each array element without acoustic backing is provided in Table 1.5.

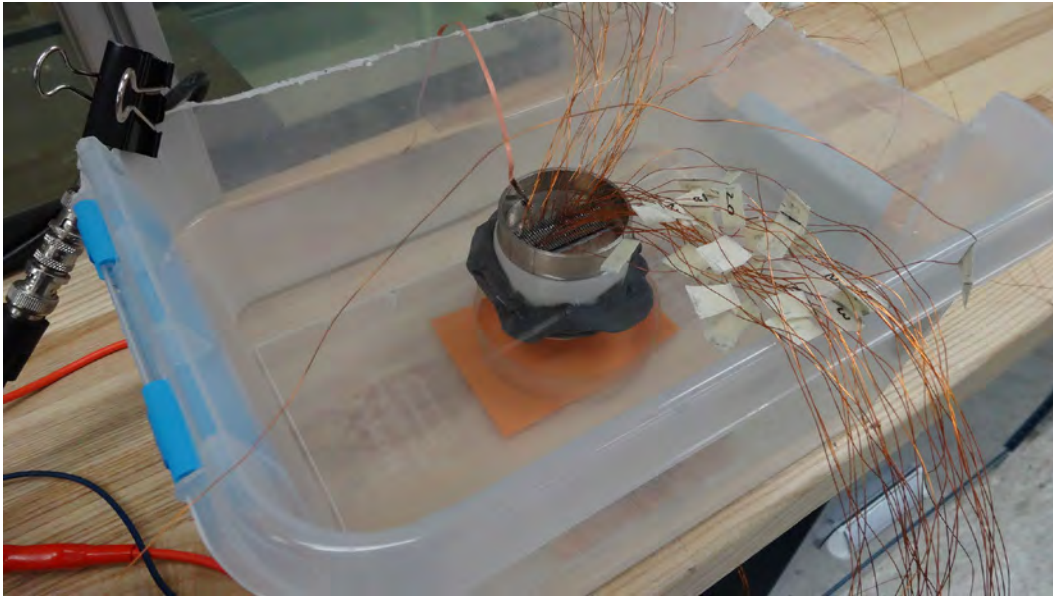


Figure 1.22. Photo of SN4 Matrix Array ETU Ni-cup During Pre-fabrication Element Evaluation Testing

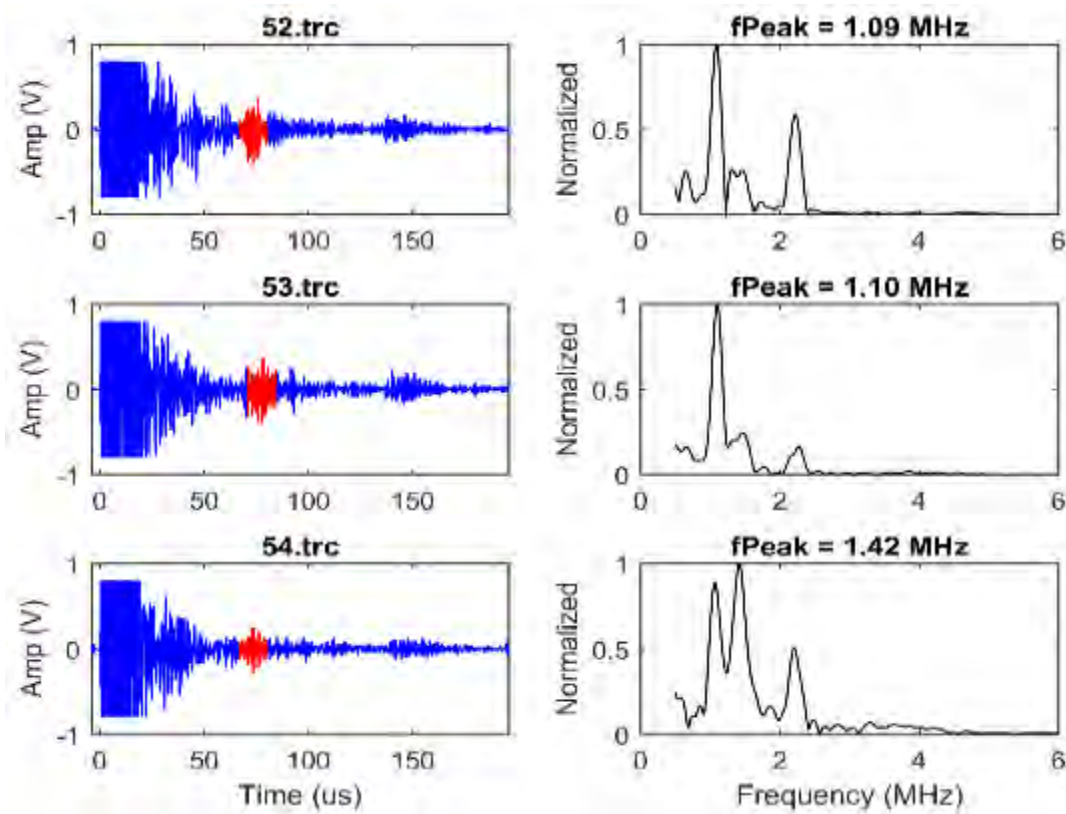


Figure 1.23. Plot of the Signal Response and Associated FFT from Individual Backed Elements 52–54 in the SN4 Matrix Array ETU during Preliminary Pre-fabrication (housing) Tests Using Manually Applied Measurement Techniques

Table 1.5. Compiled Frequency Response Information for Each Element of the SN4 Matrix Array without Acoustic Backing Material

Element	FPeak (MHz)	FCenter (MHz)	BW %	FLow (MHz)	FHigh (MHz)	Element	FPeak (MHz)	FCenter (MHz)	BW %	FLow (MHz)	FHigh (MHz)
1	1.29	1.28	14	1.19	1.37	33	1.32	1.33	16	1.23	1.43
2	1.26	1.25	16	1.15	1.35	34	1.09	1.10	16	1.01	1.18
3	1.41	1.37	19	1.24	1.50	35	1.11	1.21	37	0.99	1.43
4	1.18	1.30	33	1.09	1.52	36	1.14	1.10	24	0.97	1.23
5	1.30	1.20	48	0.91	1.49	37	1.09	1.10	21	0.98	1.21
6	1.29	1.31	19	1.19	1.43	38	2.22	2.23	10	2.11	2.34
7	1.31	1.31	15	1.21	1.40	39	1.09	1.10	16	1.01	1.19
8	1.35	1.35	15	1.25	1.46	40	2.23	2.24	10	2.12	2.36
9	1.43	1.43	13	1.34	1.52	41	1.10	1.10	13	1.03	1.17
10	1.04	1.17	43	0.92	1.42	42	1.09	1.09	16	1.00	1.18
11	1.07	1.07	15	0.99	1.15	43	1.39	1.38	13	1.29	1.47
12	1.28	1.17	32	0.98	1.35	44	1.09	1.08	15	1.00	1.17
13	1.29	1.21	39	0.98	1.45	45	1.38	1.37	14	1.28	1.47
14	1.29	1.29	23	1.15	1.44	46	1.36	1.36	17	1.25	1.48
15	1.05	1.14	34	0.94	1.33	47	1.45	1.43	18	1.30	1.56
16	1.38	1.33	22	1.18	1.48	48	1.42	1.43	15	1.32	1.54
17	1.04	1.09	30	0.93	1.25	49	1.34	1.34	16	1.23	1.45
18	1.32	1.22	41	0.97	1.46	50	1.10	1.30	48	0.99	1.61
19	1.26	1.21	29	1.04	1.39	51	2.23	2.25	11	2.12	2.37
20	2.24	2.25	10	2.14	2.36	52	1.09	1.08	16	0.99	1.17
21	1.25	1.13	37	0.92	1.34	53	1.10	1.10	17	1.01	1.19
22	1.41	1.42	14	1.32	1.52	54	1.42	1.41	18	1.29	1.54
23	1.07	1.16	35	0.95	1.36	55	1.12	1.12	22	0.99	1.24
24	1.14	1.23	31	1.04	1.42	56	2.21	2.24	13	2.10	2.38
25	1.30	1.32	27	1.14	1.50	57	1.25	1.25	43	0.98	1.51
26	1.17	1.15	29	0.98	1.32	58	2.25	2.25	9	2.15	2.36
27	1.06	1.07	21	0.95	1.18	59	1.27	1.27	14	1.18	1.36
28	2.21	2.21	8	2.12	2.30	60	2.21	2.21	10	2.10	2.32
29	2.23	2.23	9	2.13	2.33	61	1.34	1.30	30	1.11	1.50
30	1.31	1.32	17	1.20	1.43	62	1.35	1.36	16	1.26	1.47
31	1.29	1.29	15	1.20	1.39	63	1.12	1.11	19	1.01	1.21
32	1.26	1.25	18	1.14	1.35	64	2.18	2.19	13	2.05	2.33

This series of individual element measurements were repeated once the acoustic backing material was applied to the Ni-cup. The acquired A-scans and FFTs for elements 52–54 are provided as reference in Figure 1.24. The compiled frequency response information from the acoustically backed elements is provided in Table 1.6.

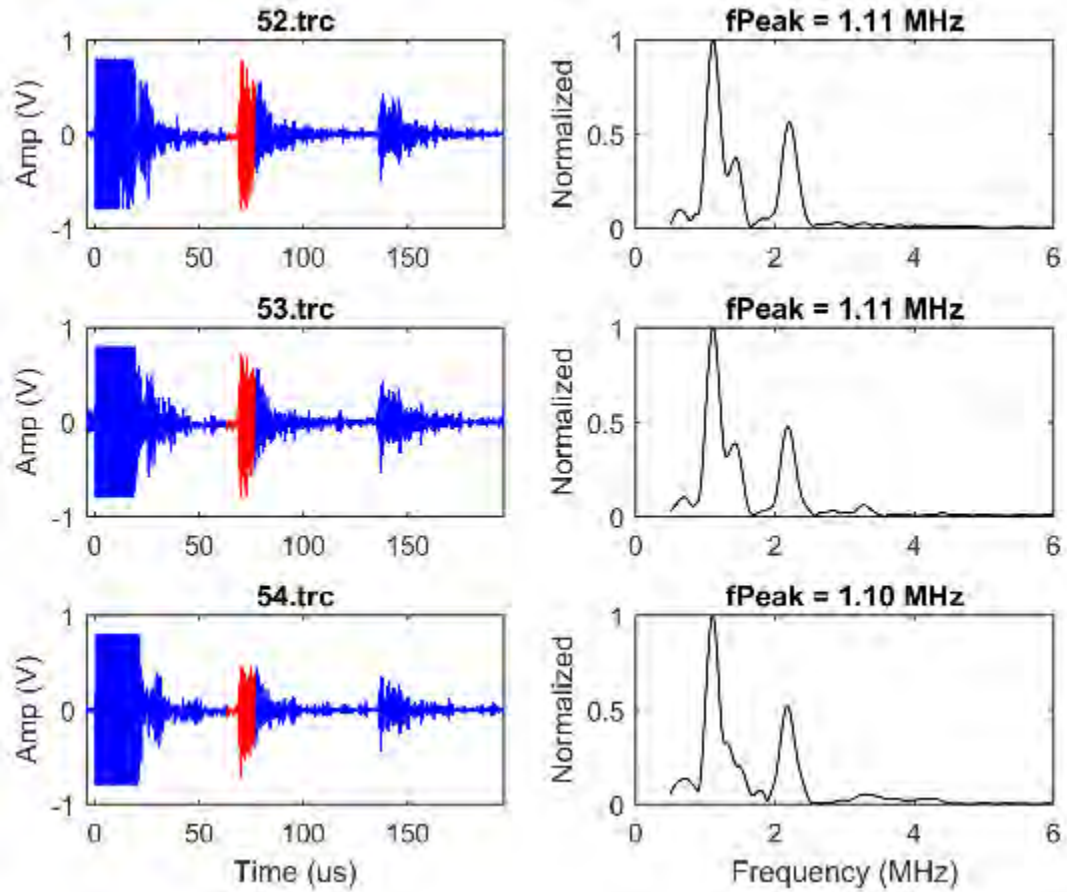


Figure 1.24. Plot of the Signal Response and Associated FFT from Individual Backed Elements 52–54 in the SN4 Matrix Array ETU during Preliminary Pre-fabrication (housing) Tests Using Manually Applied Measurement Techniques

Table 1.6. Compiled Frequency Response Information for Each Element of the SN4 Matrix Array with Acoustic Backing Material

Element	FPeak (MHz)	FCenter (MHz)	BW %	FLow (MHz)	FHigh (MHz)	Element	FPeak (MHz)	FCenter (MHz)	BW %	FLow (MHz)	FHigh (MHz)
1	1.08	1.08	18	0.98	1.18	33	1.10	1.10	21	0.99	1.22
2	1.36	1.37	16	1.26	1.48	34	1.09	1.09	17	0.99	1.18
3	1.38	1.38	15	1.28	1.48	35	1.10	1.09	20	0.98	1.20
4	2.23	2.22	10	2.12	2.33	36	1.09	1.09	21	0.98	1.20
5	1.07	1.07	17	0.98	1.16	37	1.09	1.08	20	0.98	1.19
6	1.08	1.08	16	0.99	1.17	38	1.09	1.09	20	0.98	1.20
7	1.09	1.09	16	1.00	1.17	39	1.09	1.09	20	0.98	1.20
8	1.07	1.08	16	0.99	1.17	40	1.10	1.11	21	0.99	1.23
9	2.21	2.21	9	2.11	2.31	41	1.09	1.09	16	1.01	1.18
10	3.54	3.77	27	3.26	4.28	42	1.10	1.10	15	1.01	1.18
11	1.83	1.89	19	1.70	2.07	43	1.09	1.09	16	1.00	1.17
12	3.55	3.76	26	3.27	4.25	44	1.10	1.10	15	1.01	1.18
13	3.80	3.86	31	3.27	4.46	45	1.09	1.10	15	1.01	1.18
14	3.52	3.76	24	3.30	4.22	46	1.09	1.09	16	1.01	1.18
15	3.57	3.81	27	3.30	4.32	47	1.10	1.10	20	0.99	1.21
16	1.43	1.43	14	1.33	1.53	48	1.11	1.11	21	0.99	1.23
17	1.07	1.07	15	0.99	1.15	49	1.12	1.11	22	0.99	1.23
18	1.43	1.42	16	1.31	1.53	50	1.12	1.12	23	0.99	1.25
19	1.09	1.08	15	1.00	1.16	51	1.11	1.11	19	1.01	1.22
20	1.12	1.20	30	1.02	1.38	52	1.11	1.12	22	0.99	1.24
21	1.10	1.10	14	1.03	1.18	53	1.11	1.12	22	0.99	1.24
22	1.09	1.09	15	1.01	1.17	54	1.10	1.11	20	0.99	1.22
23	1.10	1.10	15	1.02	1.19	55	1.12	1.14	24	1.00	1.28
24	1.11	1.11	14	1.03	1.19	56	1.11	1.11	18	1.01	1.21
25	1.12	1.23	35	1.01	1.45	57	1.10	1.24	40	0.99	1.49
26	1.10	1.11	22	0.99	1.23	58	1.10	1.24	43	0.97	1.50
27	1.09	1.20	38	0.97	1.42	59	2.22	2.22	9	2.12	2.32
28	1.10	1.09	21	0.98	1.20	60	1.10	1.25	41	0.99	1.50
29	1.10	1.10	20	0.99	1.21	61	2.20	2.21	12	2.08	2.34
30	2.20	2.21	11	2.09	2.33	62	2.25	2.25	11	2.13	2.37
31	1.09	1.09	16	1.01	1.18	63	1.10	1.10	15	1.02	1.18
32	1.25	1.24	16	1.14	1.34	64	1.34	1.34	10	1.27	1.40

Figures 1.25 and 1.26 show the pre- and post-backing comparison of bandwidth and center frequency for each element. This comparison is in good agreement with the linear array data, and shows that the backing process has a minimal effect on the center frequency of the probe. The backing process did increase the average center frequency from 1.39 MHz to 1.46 MHz.

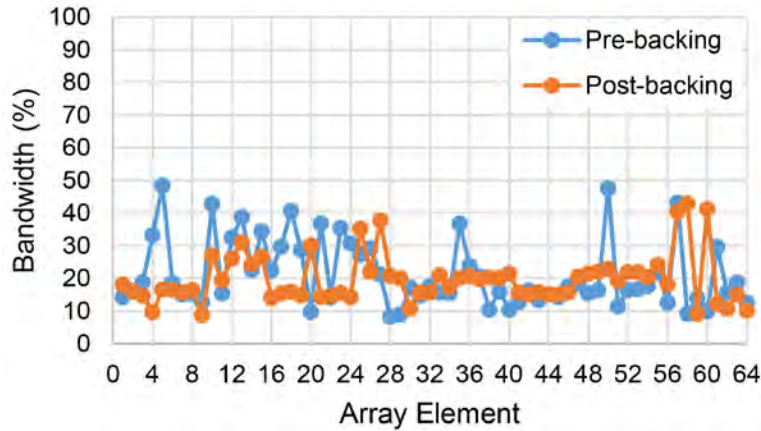


Figure 1.25. Pre- and Post-Backed Element-by-Element -6 dB BW Variation for the SN4 Matrix Array ETU Probe

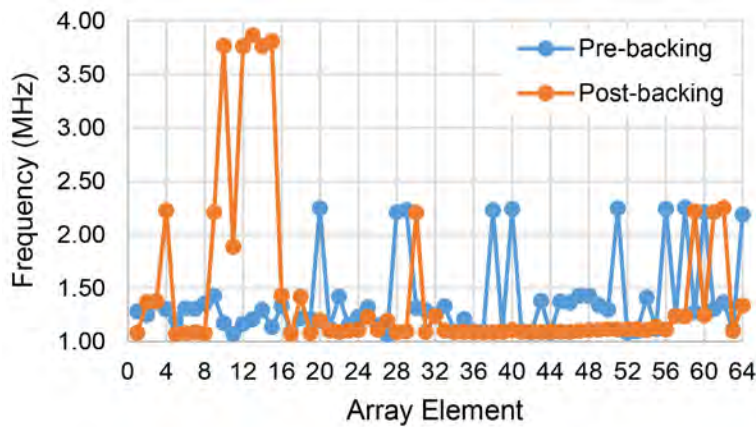


Figure 1.26. Pre- and Post-Backed Element-by-Element Center Frequency Variation for the SN4 Matrix Array ETU Probe

1.6 Post-Fabrication Evaluation of Housed PA-UT SN4 ETU

This section describes the details of performance characterization assessments and functional testing for the SN4 32-element linear and 64-element matrix array prototype probes, after housing had been completed. This section includes the results of post-fabrication pulse-echo testing on individual array elements (in water), for validation of array pin connections; evaluation of transmit uniformity per element (using a pinducer as the receiving probe in raster-scan mode); evaluation of element-to-element cross talk (to assess inter-element coupling between neighboring elements); evaluation of frequency response per element; evaluation of selected depth focus points; and evaluation of selected angles (to assess how effectively the probe can skew the sound field off its 0° primary axis). The sound field dimensions (focal spot size) at -6 dB points at a nominal distance from the face of the probe in water, using a pinducer receiving probe, will be evaluated and contrasted. Results from spatial resolution testing using raster scanning of the probe (in pulse-echo mode) and employing elevated, flat reflectors with various spacing to evaluate array resolution performance in water, will be provided and assessed. Finally, an evaluation of SNR from both pre-fabrication testing of the individual elements and post-fabrication tests will be addressed.

1.6.1 Post-Fabrication Pulse-Echo Testing on Individual Array Elements (in Water)

This subsection describes post-fabrication, performance testing, and functional validation of individual array elements (in water) for the SN4 linear and matrix array probes. This evaluation of individual elements is performed by exciting a particular element while raster scanning the array over a receiver pinducer. The pinducer is oriented normal to the faceplate of the array and is mounted 4.5 mm from the faceplate. Another pinducer is attached to the array, and is oriented toward the receiver to provide a spatial reference point in each data set. This configuration is used to evaluate pin connections of elements, transmit uniformity, inter-element cross talk, and assess frequency response of individual elements. The configuration used for this facemap testing is shown in Figure 1.27. In this figure, the receiver pinducer is indicated by the red arrow and the spatial reference pinducer is indicated by the yellow arrow.

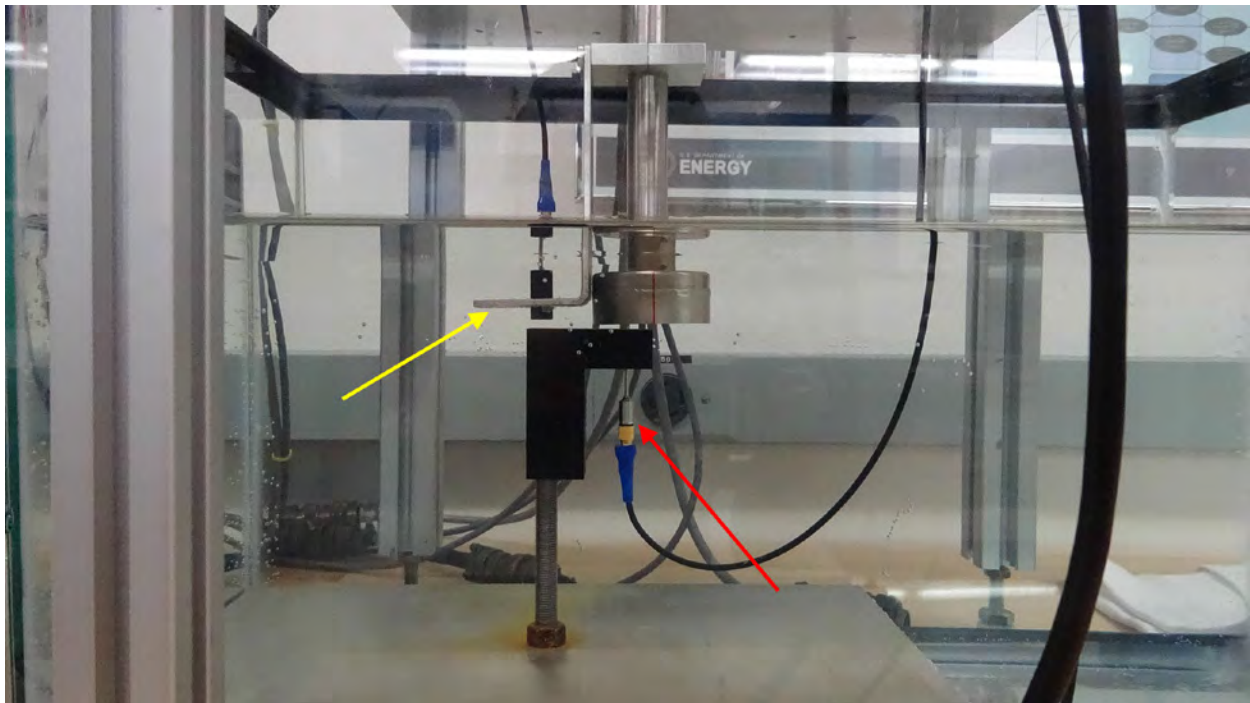


Figure 1.27. Facemap Assessment of Individual SN4 Linear Array Elements in Water Using a Broadband Pinducer

1.6.1.1 Validation of Array Pin Connections

Centering over the fiducial pinducer (0 point) with a standoff of 4.5 mm (0.17 in.), raster scans were executed along the primary and secondary axis of the array where only a single element was active (0 ns delay) during a given scan. The raster scans of the linear array were spatially encoded with a resolution of 0.5 mm (0.02 in.) for a scan length of 85 mm (3.34 in.) and an index length of 50 mm (1.96 in.). The raster scans of the matrix array were spatially encoded with a resolution of 0.5 mm (0.02 in.) for a scan length of 80 mm (3.14 in.) and an index length of 50 mm (1.96 in.).

Each element was individually assessed for position location in the array. Figure 1.28 shows the UltraVision reconstruction of the raster scan of element #1 from the SN4 linear array prototype probe. The B-scan side view (left) is along the primary axis (blue axis) and the time-gated C-scan (top) view is

on the right. The purple axis (in the left image) is the time or ultrasound axis. The response from element #1 is indicated by the red arrows in the figure. The purpose of the fiducial is to provide a physical spatial reference point. The positional information from each element was recorded to verify that each element was wired in accordance with the element numbering produced by the UltraVision Phased-Array Calculator. The SN4 linear array was found to have 30 of the 32 elements operational at the time these data were taken. The SN4 matrix array had all of the array elements functioning at the time these data were taken although some of the array elements showed poor transmit performance. The elements will be discussed in the following section.

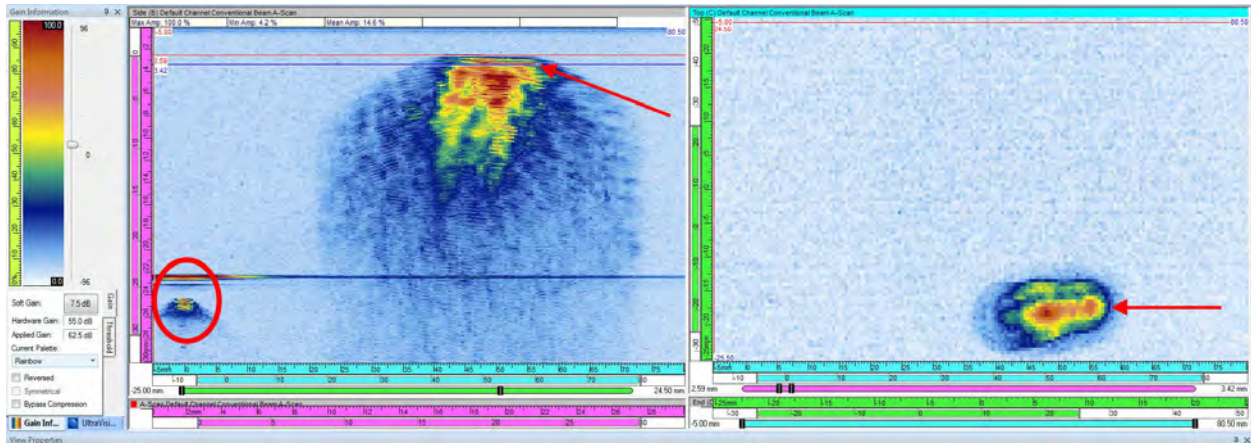


Figure 1.28. Raster Scan of Element #1 for the SN4 Linear Array Prototype Probe. Red arrows point to element 1 response; red circle indicates the fiducial response.

1.6.1.2 Evaluation of Transmit Uniformity per Element

The previously collected raster data sets used for the validation of the array pin connections were also used to evaluate the transmit uniformity for each element. In addition, data were acquired with all elements active simultaneously with a 0 ns delay. Each element was imaged both individually as well as in concert.

Figure 1.29 shows the UltraVision reconstruction of the raster scan of element #10 (as an example) from the SN4 linear array prototype probe using cutoff for the dynamic range. The raster scan side view (left) is along the primary axis (blue axis) and the time-gated C-scan (top) view is on the right. The purple axis (in the left image) is the time or ultrasound axis. The response from element #10 is indicated by the red arrows in the figure. Here it is shown that the element length in the active axis is 5.5 mm (0.21 in.) and 13 mm (0.51 in.) in the passive axis. This corresponds well with the 1.0×15 mm as-built size of the elements for the linear array. It is expected that dimensions of the sound field from each element will be somewhat larger than design dimensions due to divergence of the field occurring in the 4.5 mm span from the faceplate to the receiver. Similarly, element #33 of the matrix array is shown in Figure 1.30, also using no dynamic range cutoff.

All elements of the matrix array were functional at the time these measurements were made, although some of the elements were not functioning well enough to make element characterization measurements. These elements included 12, 13, 14, 45, and 53. The SNR in the raster scan data sets of these elements was so low that the -6 dB sizing could not be performed. The poor transmit performance on the matrix array is a likely cause for poor beam forming and steering performance.

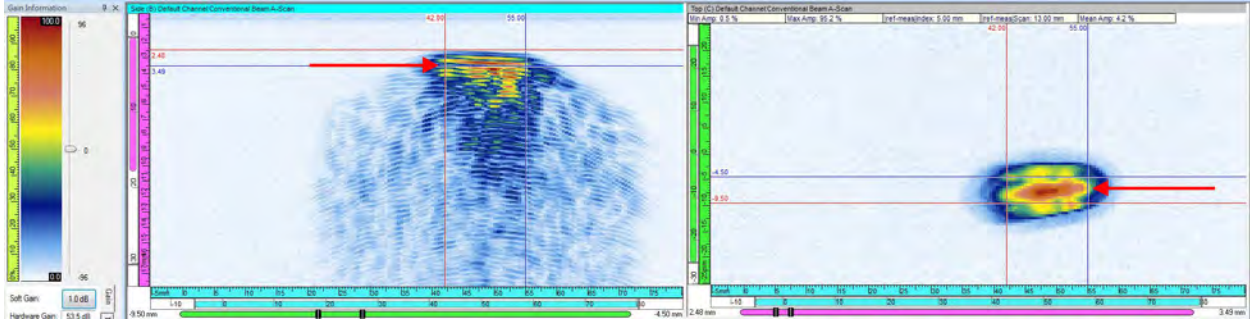


Figure 1.29. Raster Scan of Element #10 for the SN4 Linear Array Prototype Probe

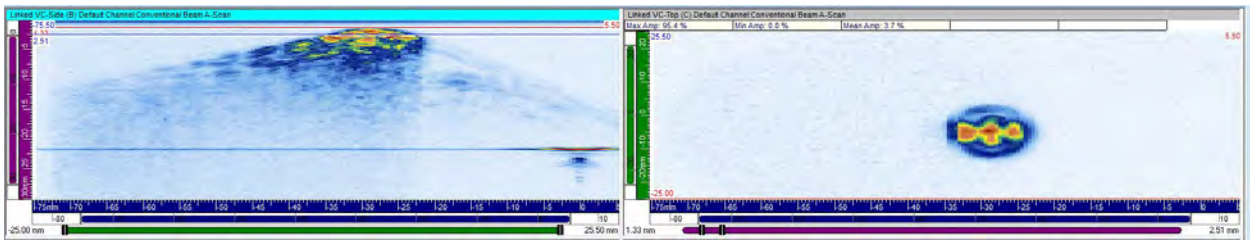


Figure 1.30. Raster Scan of Element #33 from the SN4 Matrix Array Prototype Probe

Besides the five poor performing elements of the matrix array, no dead zones were identified in this evaluation for the SN4 linear and matrix array probes. One limitation in this measurement is the raster scan resolution of 0.5×0.5 mm (0.02×0.02 in.), which reduces the ability to measure amplitude variations across the small element size of 1.0 mm (0.04 in.) in the active axis for both SN4 ETUs.

Table 1.7 provides the measured lengths and widths of the individual elements for the SN4 linear array probe at -6 dB points of the sound field maps. It should be noted that this exercise was not conducted to obtain accurate dimensions of the individual elements, but was aimed at evaluating the degree of spatial uniformity associated with effective excitation of each individual element. Because of divergence of the sound energy while pulsing the elements with no delays, the measured dimensions provided in these tables will indicate areas that are not being optimally excited, or areas where marginal bonding has occurred, precluding the element from coupling energy out of the probe. But these data should not be used to accurately measure the individual element dimensions. For this table, the length values correspond to the active X axis of the probe and the width values correspond to the passive Y axis of the probe. The average length and width at -6 dB are 4.8 mm (0.18 in.) and 11.1 mm (0.41 in.), respectively. These values can be loosely compared to the actual individual element dimensions of 1.0 mm (0.04 in.) length by 15 mm (0.59 in.) width.

Table 1.7. Individual Linear Array Element Sizing Results from Face Mapping Assessment at -6 dB

Element #	-6 dB sizing			
	Length (Primary Axis)		Width (Secondary Axis)	
	(mm)	(in.)	(mm)	(in.)
1	4.5	0.18	12.5	0.49
2	4.0	0.16	13.5	0.53
3	5.0	0.20	10.0	0.39
4	4.5	0.18	12.5	0.49
5	5.0	0.20	13.0	0.51
6	5.5	0.22	12.5	0.49
7	5.0	0.20	10.0	0.39
8		0.00		0.00
9	5.0	0.20	9.5	0.37
10	5.5	0.22	13.0	0.51
11	5.5	0.22	11.5	0.45
12	4.5	0.18	11.0	0.43
13		0.00		0.00
14	5.0	0.20	7.5	0.30
15	5.0	0.20	8.5	0.33
16	4.0	0.16	9.0	0.35
17	4.5	0.18	10.5	0.41
18	6.5	0.26	10.0	0.39
19	4.0	0.16	10.0	0.39
20	4.5	0.18	9.5	0.37
21	5.0	0.20	9.0	0.35
22	5.5	0.22	12.5	0.49
23	5.5	0.22	11.0	0.43
24	5.0	0.20	13.0	0.51
25	4.5	0.18	12.0	0.47
26	5.0	0.20	12.0	0.47
27	4.5	0.18	13.0	0.51
28	4.5	0.18	11.5	0.45
29	5.0	0.20	14.5	0.57
30	5.0	0.20	12.0	0.47
31	4.5	0.18	6.5	0.26
32	3.5	0.14	13.0	0.51

Table 1.8 provides this sizing information of the individual elements for the SN4 matrix array. For this table, the length values correspond to the active X axis of the probe and the width values correspond to the passive Y axis of the probe. The average length and width at -6 dB are 5.9 mm (0.23 in.) and 7.2 mm (0.28 in.), respectively. These values can be loosely compared to the actual individual element dimensions of 1.0 mm (0.04 in.) length by 7.4 mm (0.29 in.) width. The dashes in the table indicate dimensions that were not measured due to the poor/low transmission levels of the associated element.

Table 1.8. Individual Matrix Array Element Sizing Results from Face Mapping Assessment at -6 dB

Element #	-6 dB sizing			
	Length (Primary Axis)		Width (Secondary Axis)	
	(mm)	(in.)	(mm)	(in.)
1	5.0	0.20	7.5	0.30
2	8.5	0.33	8.0	0.31
3	11.0	0.43	7.0	0.28
4	1.5	0.06	11.0	0.43
5	5.5	0.22	5.5	0.22
6	10.0	0.39	8.0	0.31
7	5.0	0.20	7.0	0.28
8	4	0.16	7	0.28
9	2.5	0.10	7.0	0.28
10	10.0	0.39	11.0	0.43
11	3.0	0.12	4.5	0.18
12	-	-	-	-
13	-	-	-	-
14	-	-	-	-
15	4.5	0.18	5.5	0.22
16	7.0	0.28	6.5	0.26
17	7.0	0.28	7.0	0.28
18	5.5	0.22	6.5	0.26
19	7.0	0.28	7.0	0.28
20	4.5	0.18	6.0	0.24
21	7.5	0.30	7.5	0.30
22	5.0	0.20	10.0	0.39
23	6.5	0.26	6.5	0.26
24	7.0	0.28	7.5	0.30
25	7.5	0.30	6.5	0.26
26	6.5	0.26	7.5	0.30
27	4.0	0.16	7.0	0.28
28	5.5	0.22	7.0	0.28
29	5.5	0.22	7.5	0.30
30	4.5	0.18	6.0	0.24
31	5.0	0.20	6.5	0.26
32	4.5	0.18	6.5	0.26
33	5.5	0.22	6.5	0.26
34	6.0	0.24	10.0	0.39
35	5.5	0.22	7.5	0.30
36	6.5	0.26	7.0	0.28
37	5.5	0.22	7.5	0.30
38	5.0	0.20	7.5	0.30
39	6.5	0.26	7.5	0.30

Element #	-6 dB sizing			
	Length (Primary Axis)		Width (Secondary Axis)	
	(mm)	(in.)	(mm)	(in.)
40	5.5	0.22	8.0	0.31
41	11.0	0.43	7.5	0.30
42	5.0	0.20	7.5	0.30
43	3.5	0.14	7.0	0.28
44	5.0	0.20	6.5	0.26
45		0.00		0.00
46	6.0	0.24	7.5	0.30
47	5.5	0.22	7.0	0.28
48	6.5	0.26	7.0	0.28
49	8.0	0.31	7.5	0.30
50	7.0	0.28	7.0	0.28
51	7.0	0.28	7.5	0.30
52	7.0	0.28	7.5	0.30
53	-	-	-	-
54	5.0	0.20	7.0	0.28
55	5.5	0.22	7.0	0.28
56	6.5	0.26	7.0	0.28
57	5.0	0.20	7.0	0.28
58	6.0	0.24	7.5	0.30
59	6.0	0.24	7.5	0.30
60	4.5	0.18	8.0	0.31
61	5.0	0.20	7.0	0.28
62	6.0	0.24	6.5	0.26
63	6.5	0.26	6.5	0.26
64	5.5	0.22	7.0	0.28

1.6.1.3 Evaluation of Element-to-Element Cross Talk

A separate analysis performed on data acquired from both SN4 probes indicated the amount of signal leakage from element to element. The individual element raster scans captured energies received from neighboring elements and showed areas where energy was either mechanically transferred or individual elements were electrically connected within the array. The data sets from both arrays showed excellent isolation among elements, where the acoustic excitation of adjacent elements was not detected. An example of this can be seen in the C-scans of linear array element #8 in Figure 1.31 and matrix array element #57 in Figure 1.32. Ideally a probe would have -30 to -35 dB isolation between elements (Braatz et al. 2013). In this case, the measure of element isolation is not possible because of the lack of neighboring element excitation.

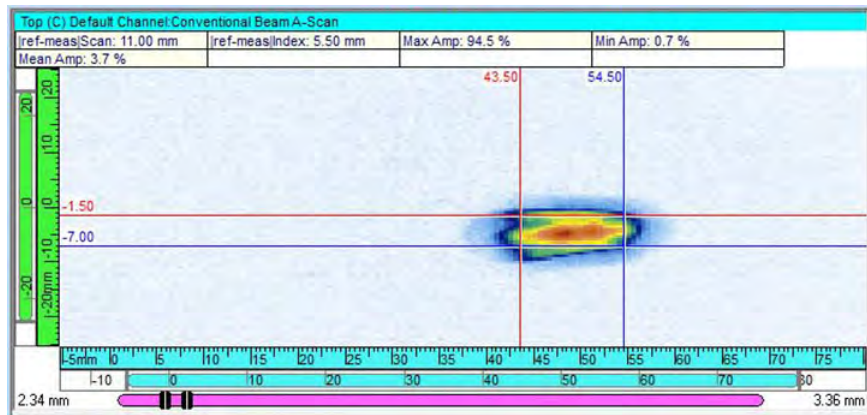


Figure 1.31. C-scan Linear Array of Element #12 Showing No Detection of Adjacent Element Excitation

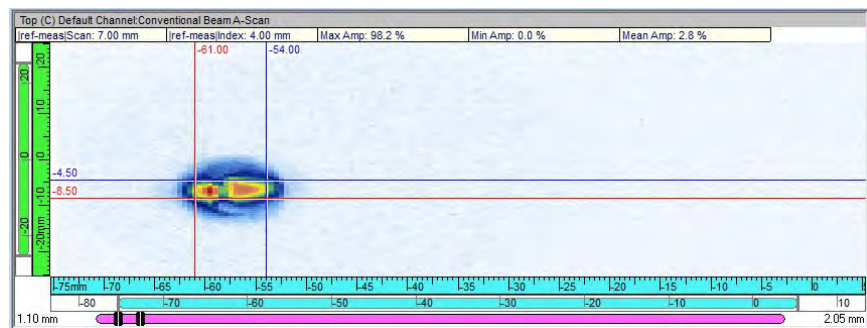


Figure 1.32. C-scan Matrix Array of Element #57 Showing No Detection of Adjacent Element Excitation

1.6.1.4 Individual Element Frequency Response Analysis, and Bandwidth Calculations

This subsection describes the subsequent analysis performed on facemap data collected for each element to determine frequency response and bandwidth information. The analysis was conducted by evaluating the first arrival peak response from each element after employing a standard excitation pulse, and capturing the transmitted waveform with a pinducer as described earlier. Data were analyzed in both the time and frequency domains for each element. An example of the analysis window is shown in Figure 1.33. In this figure, the C-scan, B-scan, and D-scan views of the element response are shown along with the RF waveform associated with the red reference cursors. A standard time-window was used to capture the first arrival portion of the RF-waveform response (sampling a minimum of 1½ cycles), and each individual FFT was then computed (shown bottom-left in Figure 1.33).

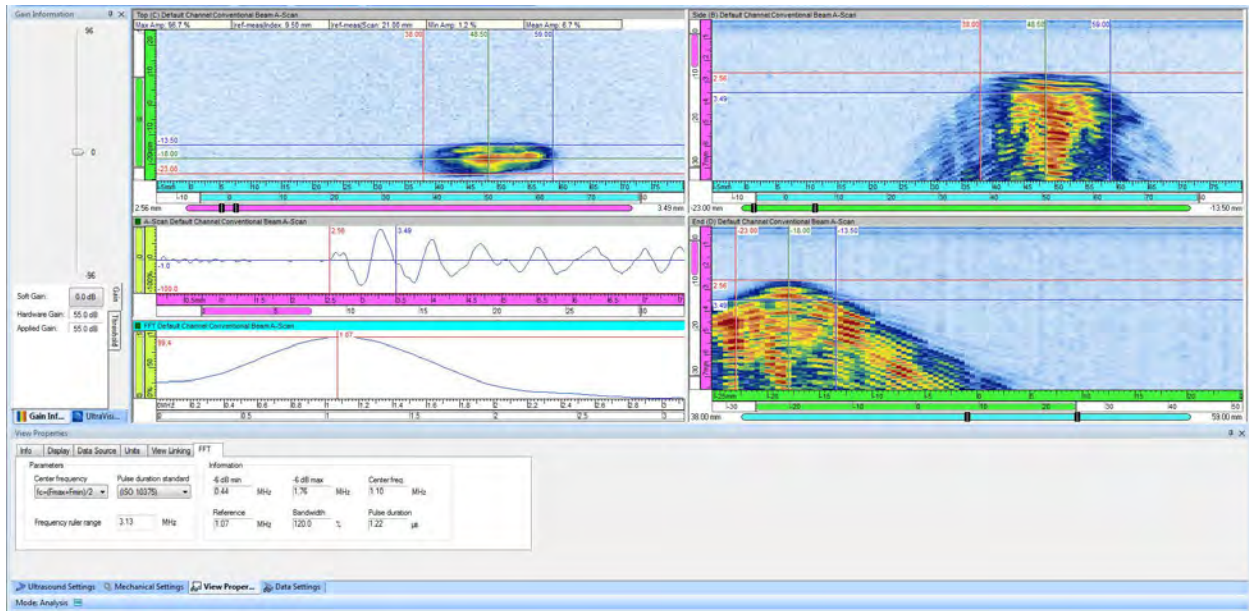


Figure 1.33. Linear Array Element #1 Analysis Window for Frequency Response and Bandwidth Evaluation

From the FFTs, peak, and center frequencies were documented and the 6 dB magnitude and frequency points (both upper and lower points) were recorded as per the guidance in ASTM E-1065. Bandwidth calculations were made and are presented in Table 1.9. The SN4 linear array element average center frequency, peak frequency, and bandwidth were 1.06 MHz, 1.09 MHz, and 132%, respectively. The frequency response values are slightly downshifted from the measured frequency response values of previously built SN1 and SN2 arrays using PZT-5A with a nickel faceplate. The same analysis was performed on the matrix array data, which is presented in Table 1.10. The SN4 matrix array element average center frequency, peak frequency, and bandwidth were 1.11 MHz, 1.12 MHz, and 125%, respectively.

Table 1.9. Element-by-Element Data and Calculations Resulting from the Frequency Response Analysis of Signal Responses from the SN4 Linear Array Prototype Probe, Captured from Immersion Testing in Water Using a Pinducer as the Receiver

Element #	Center Frequency (MHz)	Peak Frequency (MHz)	BW (%)
1	1.10	1.07	120
2	1.15	1.17	115
3	1.07	1.07	127
4	1.05	1.07	126
5	1.12	1.12	122
6	1.07	1.07	118
7	1.05	1.07	126
8	-	-	-
9	1.10	1.12	120
10	1.05	1.07	126
11	1.10	1.12	120
12	1.03	1.07	133
13	-	-	-
14	1.10	1.12	120
15	1.12	1.12	122
16	1.07	1.07	127
17	1.05	1.07	126
18	1.12	1.12	122
19	1.03	1.07	124
20	1.05	1.07	126
21	1.12	1.17	122
22	1.07	1.12	127
23	1.05	1.12	144
24	1.00	1.12	161
25	1.00	1.12	161
26	1.05	1.12	144
27	0.93	1.07	200
28	1.10	1.07	111
29	0.98	1.12	200
30	1.05	1.07	126
31	1.00	1.03	142
32	1.00	1.03	122

Table 1.10. Element-by-Element Data and Calculations Resulting from the Frequency Response Analysis of Signal Responses from the SN4 Matrix Array Prototype Probe, Captured from Immersion Testing in Water Using a Pinducer as the Receiver

Element #	Center Frequency (MHz)	Peak Frequency (MHz)	BW (%)
1	0.95	0.98	128
2	1.10	1.07	111
3	1.32	1.32	104
4	1.17	1.17	100
5	0.93	0.98	126
6	1.22	1.22	112
7	1.05	1.03	116
8	1.00	1.03	122
9	1.00	1.03	151
10	1.25	1.12	114
11	-	-	-
12	-	-	-
13	-	-	-
14	-	-	-
15	1.15	1.03	157
16	0.81	0.88	152
17	0.95	0.98	128
18	1.27	1.27	108
19	1.22	1.17	96
20	1.20	1.22	143
21	1.20	1.17	102
22	1.37	1.32	100
23	0.93	1.07	200
24	1.44	1.42	92
25	1.03	1.03	124
26	1.17	0.98	142
27	1.12	1.12	113
28	1.00	1.22	200
29	1.00	1.22	200
30	0.78	0.88	150
31	0.81	0.83	139
32	1.03	1.03	95
33	1.05	1.07	126
34	1.22	1.22	96
35	1.10	1.12	120
36	1.10	1.12	120

Element #	Center Frequency (MHz)	Peak Frequency (MHz)	BW (%)
37	1.10	1.12	120
38	1.12	1.12	113
39	1.15	1.12	115
40	1.07	1.07	118
41	1.00	1.27	200
42	1.05	1.07	116
43	0.98	0.98	120
44	0.95	0.98	128
45	-	-	-
46	1.25	1.27	114
47	1.25	1.27	122
48	1.17	1.22	133
49	1.25	1.27	122
50	1.27	1.27	115
51	1.17	1.22	133
52	1.00	1.03	122
53	-	-	-
54	1.20	1.22	127
55	1.12	1.12	122
56	1.15	1.17	115
57	1.15	1.12	115
58	1.25	1.22	106
59	1.20	1.17	110
60	1.05	1.07	116
61	1.07	1.07	118
62	1.12	1.12	122
63	1.20	1.22	118
64	1.10	1.12	120

1.6.2 Post-Fabrication Testing Using Elements in Concert (in Water)

This subsection describes post-fabrication, performance testing, and functional validation of the SN4 arrays while using the transmitting elements in concert. This evaluation will assess the probe's ability to form the sound field at specified depths and azimuthal angles in water. These evaluations were performed in similar manner to the setup used in Section 1.6.1. Unlike the individual element assessment, the receiver pinducer was not located near the faceplate of the array. Instead, the pinducer was held at a specified distance from the array for each assessment. Proper formation of the sound field at specified depths within the working distance of the array design is critical to probe performance. The performance results in these evaluations were used to determine viability of further testing.

1.6.2.1 Evaluation of Selected Depth Focus Points

The UltraVision 3.6R5 software suite was used to generate specific delay laws for the SN4 linear and matrix arrays, such that target depth focuses of 50.8 and 76.2 mm (2.0 and 3.0 in.) at 0° (azimuthal) could be achieved. The nanosecond delays are precisely timed so that the contribution from each individual element can constructively interfere with the other elements, producing a sound beam maximum at a particular depth. The reception pinducer was positioned at the depth of the focal plane and raster scanned. The raster scans were spatially encoded with a resolution of 0.5 mm (0.02 in.) in the scan direction for a scan length of 85 mm (3.34 in.) and 0.5 mm (0.02 in.) resolution in the index axis for a length of 60 mm (2.36 in.). Figures 1.34 and 1.35 show the focused beam at 0° and 76.2 mm focal depth for both the linear and matrix arrays, respectively. In these figures, the top left image shows the C-scan (top) view clipped at -6 dB and the lower left image shows the A-scan. The right half of the image shows the orthogonal side views (B-scan and D-scan). Table 1.11 provides the dimensional data associated with the active and passive sound field dimensions for the FY14 22-element linear probe, and both SN4 probes as a function of focal depth. The spot sizes of the previous 22-element linear array are included for reference to previous performance of linear array designs.

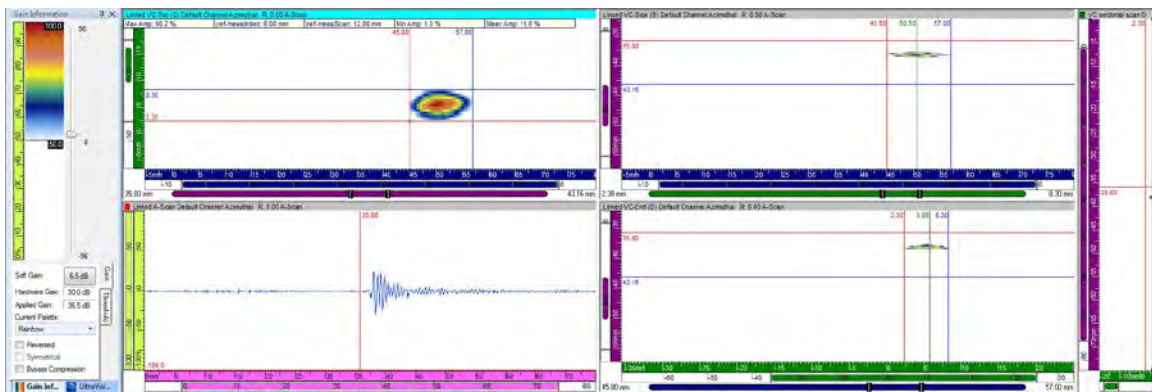


Figure 1.34. 0° Depth Focus at 76.2 mm (3 in.) for the SN4 Linear Array Prototype Probe. The top left C-scan shows the sound field clipped at -6 dB.

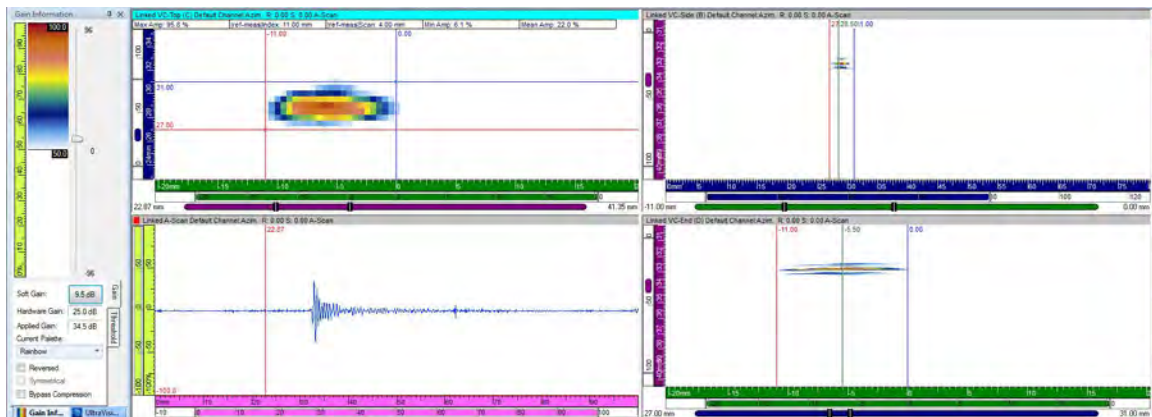


Figure 1.35. 0° Depth Focus at 76.2 mm (3 in.) for the SN4 Matrix Array Prototype Probe. The top left C-scan shows the sound field clipped at -6 dB.

Table 1.11. Passive and Active (length and width) Sound Field Dimensions as a Function of the Focal Depth, at -6 dB Points, for the SN2 22-Element Linear Probe and both SN4 Prototype Probes

Probe	Target Depth Focus (mm)	Target Depth Focus (in.)	-6 dB			
			Length (passive) (mm)	Length (passive) (in.)	Width (active) (mm)	Width (active) (in.)
SN2	50.8	2.0	13.1	0.51	4.5	0.18
	76.2	3.0	12.6	0.49	4.0	0.16
SN4 Linear	50.8	2.0	11.0	0.43	6.0	0.23
	76.2	3.0	12.0	0.47	6.0	0.23
SN4 Matrix	50.8	2.0	8.0	0.31	5.0	0.19
	76.2	3.0	11.0	0.43	4.0	0.15

From an analysis of Table 1.11, it is seen that probe SN2 sound field values in the length direction are larger at both focal depths than the sound fields produced by the SN4 linear and matrix probes. The smaller sound field dimensions are necessary for improving detection and resolution capabilities, but this must also be balanced with the requirement for getting sufficient acoustic energy at the target depth in sodium.

1.6.2.2 Evaluation of Selected Angles

Similar to the evaluation of depth focusing capabilities of the SN4 arrays, the angle evaluation shows beam formation at a specified depth and azimuthal angle. The UltraVision 3.6R5 software suite was used to generate specific delay laws for each of the elements such that angles of 5, 10, 15, and 20 degrees azimuthal at target depths of 50.8 mm (2 in.) and 76.2 mm (3 in.) were formed. The nanosecond delays are precisely timed so that the contribution from each individual element can constructively interfere with the other elements producing a sound beam maximum at the particular angle and depth. The reception pinducer was positioned at the depth of the focal plane and raster scanned. The raster scans were spatially encoded with a resolution of 0.5 mm (0.02 in.) in the scan direction for a scan length of 85 mm (3.34 in.) and 0.5 mm (0.02 in.) resolution in the index axis for a length of 60 mm (2.4 in.). Figures 1.36 and 1.37 illustrate the 20° azimuthal beam focused at 76.2 mm (3 in.) generated by the SN4 linear and matrix arrays. These figures show the C-scan (top) view of the sound field in the upper left and verify that the array is capable of forming an acceptable spot size at 76.2 mm depth while steering in water. The sound fields produced at this depth and angle do not exhibit symmetry in either axis. Further steering of the array, beyond 20°, will introduce the presence of side lobes and probe performance would begin to abate. Dimensions of the steered sound fields for both SN4 arrays are provided in Table 1.12.

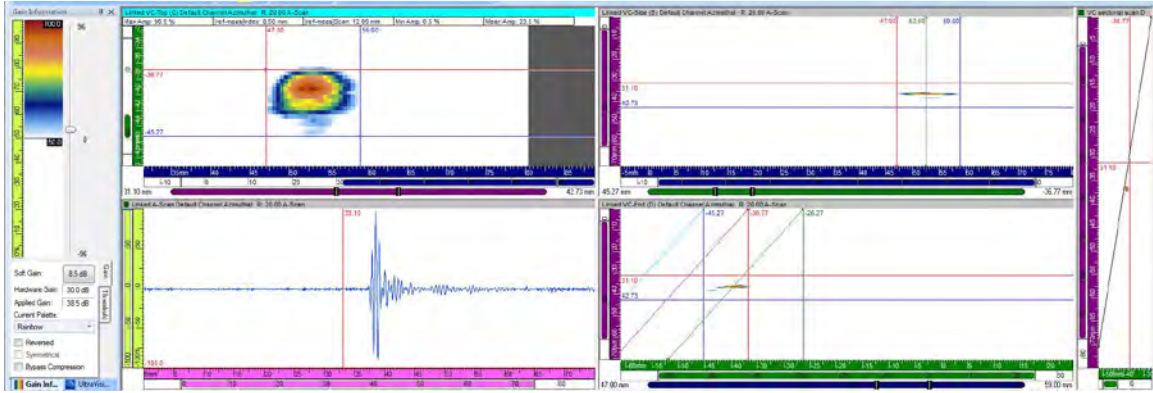


Figure 1.36. Linear Array Sound Field for 20° Azimuthal at a Depth of 76.2 mm (3 in.) Clipped to -6 dB

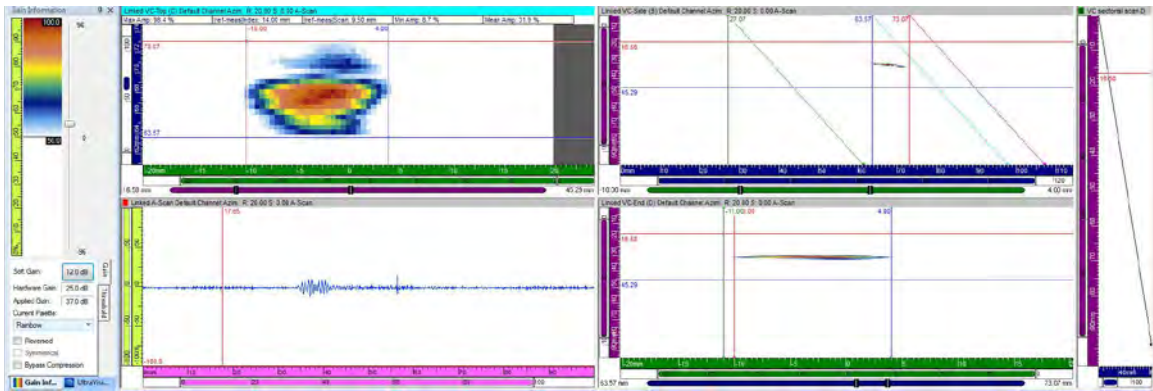


Figure 1.37. Matrix Array Sound Field for 20° Azimuthal at a Depth of 76.2 mm (3 in.) Clipped to -6 dB

The analysis of the spot size dimensions produced by the SN4 arrays confirmed that both designs perform well when steering the beam off-axis. The two elements that are not functioning in the linear array are likely contributors to increase the dimension of the sound field in the primary active direction. In this same manner, the six weaker elements of the matrix array also are likely contributing to probe steering performance and beam formation.

Table 1.12. Sound Field Dimensions for Linear and Matrix Arrays at 50.8 and 76.2 mm Focal Depth at -6 dB

Array	Target Depth Focus (mm)	Target Depth Focus (in.)	Azimuthal Angle	-6 dB			
				Length (passive) (mm)	Length (passive) (in.)	Width (active) (mm)	Width (active) (in.)
Linear	50.8	2.0	5	12.0	0.47	6.5	0.25
Linear	50.8	2	20	9.0	0.35	8.5	0.33
Linear	76.2	3	5	12.5	0.49	6.5	0.25
Linear	76.2	3	20	12.0	0.47	8.5	0.33
Matrix	50.8	2	5	8.0	0.31	4.5	0.17
Matrix	50.8	2	20	10.5	0.41	9.0	0.35
Matrix	76.2	3	5	12.0	0.47	5.0	0.19
Matrix	76.2	3	20	14.0	0.55	9.5	0.37

1.6.3 Sound Field Dimensional Characterization Analysis for SN4 Prototype Probes

This subsection describes post-fabrication testing and analysis of sound field mapping data obtained in water for the SN4 prototype probes. From a review of Subsections 1.6.2.1 and 1.6.2.2, and the data provided in Tables 1.11 and 1.12, it is clear that the sound field dimensions for the focal “spot” size of the prototype array meets acceptance criteria for depth focusing without azimuthal steering. The measured focal spot sizes agree well with the simulated spot sizes presented in Section 1.4. In contrast, the focal spot sizes produced when electronic steering is invoked show some deviation from the predicted spot sizes. These results suggest some level of performance degradation when steering the beam off axis.

1.6.4 Spatial Resolution and SNR Analysis for SN4 Prototype Probes

This subsection describes post-fabrication testing of the SN4 prototype probes, focused on the acquisition of ultrasonic data describing the spatial resolution performance for these ETUs. Spatial resolution data and testing procedures using raster scanning of the probe and employing flat reflectors with various spacing to evaluate array resolution performance in water are presented. Sound field dimensional analysis is presented and a comparison of the spatial resolution performance of the SN4 probes will be discussed.

A simple resolution target was built from a 3/4 in. thick Plexiglas plate. A set of 0.5 in. deep threaded holes were tapped into the plate to allow for the placement of six pairs of 1.5 in. hex socket-head cap screws, placed at different distances from one another. All screws were 28.57 mm (1.125 in.) above the Plexiglas back wall. Each pair of screws was separated 25.4 mm (1.0 in.) apart from the next pair. The pair with the widest center-to-center separation had a distance of 25.4 mm (1.0 in.). The next closest pair was 19.05 mm (0.75 in.), and in descending distance order, subsequent pairs were spaced at 12.7 mm (0.5 in.), 10.16 mm (0.4 in.), 7.62 mm (0.3 in.), and 6.35 mm (0.25 in.), respectively. The screw heads were filled with epoxy and surfaced to provide a flat reflector with a nominal diameter of 5.72 mm (0.225 in.). A digital photograph of the target is provided in Figure 1.38.

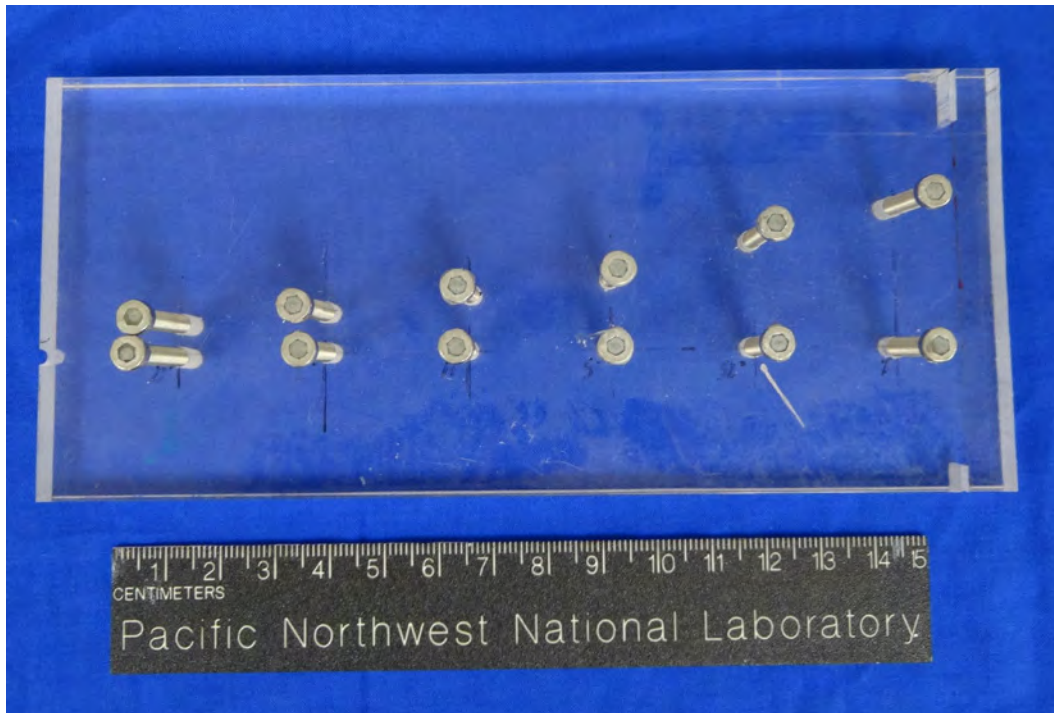


Figure 1.38. Photograph of the Resolution Target Used to Assess Imaging Resolution Characteristics

The water path was set at 76.2 mm (3.0 in.) from the target plane with the appropriate focal laws in place for optimal imaging of the screw caps. The depth of focus provided an ample signal response off the Plexiglas plate for a constant background signal response. The SN4 linear array and matrix array probes were scanned in a raster pattern over the resolution target at a standoff distance of 76.2 mm (3 in.) in water. The raster scans used a 0.5×0.5 mm (0.02×0.02 in.) resolution scan pattern. Data sets were collected with each transducer in a skew 0° and $90/270^\circ$ orientation. The PA-UT images were evaluated, and a dimensional analysis was conducted to determine the resolving capability of the probe. The SNR was also computed from the resultant images. Figure 1.39 illustrates the PA-UT image, including a time-gated C-scan view (x-y axis, top-down composite view of the screw-cap reflectors) for the SN4 linear array prototype probe. Scanner limitations prevented the collection of data across all the pin sets in a single scan, and consequently only the 12.7 mm (0.5 in.), 10.16 mm (0.4 in.), 7.62 mm (0.3 in.), and 6.35 mm (0.25 in.) pin sets are presented here.

From a review of the data acquired from the resolution target standard, the SN4 probes are not capable of resolving the two individual screw-cap reflectors at a center-to-center separation distance of 6.35 mm (0.25 in.). However, both of these reflectors are essentially touching at the edges, so one would anticipate this result as is evident by the smearing of the two pin responses. Both the linear and matrix ETUs were able to distinguish/resolve the 7.62 mm (0.3 in.) pin sets in the skew $90/270^\circ$ orientation but not in the skew 0° orientation due to the oval-shaped sound field. Again, these results were anticipated based on the orientation of the sound field to the reflectors. Further analysis was performed to determine that the measured SNR from the linear array was 14.8 and 15.0 dB for skew 0° and 270° , respectively.

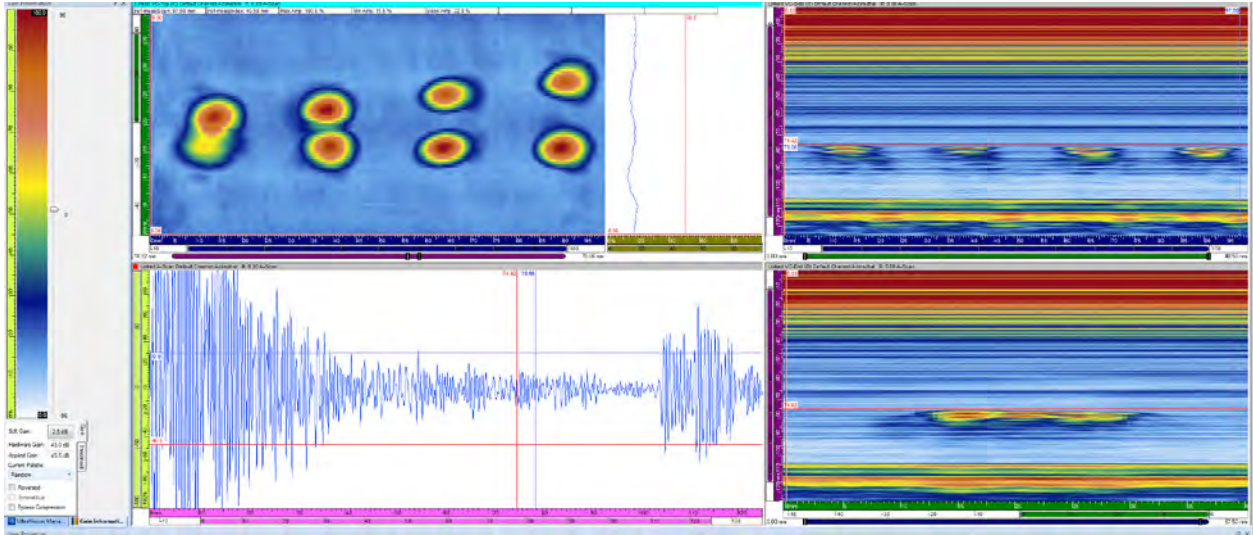


Figure 1.39. PA-UT Image of the Resolution Target Using the SN4 Linear Array Probe in Water at a Focal Distance of 76.2 mm (3.0 in.) and a Probe Skew of 270°

For reference, data collected at the same distance with the SN4 matrix array probe is shown in Figure 1.40. In this data, all pin sets were detected and only the 6.35 mm (0.25 in.) pin set was not resolved. The SN4 matrix array probe performed well when resolving the pin tops in water. The SNR was measured to be 7.4 and 13.3 dB for probe skew 0° and 90°, respectively.

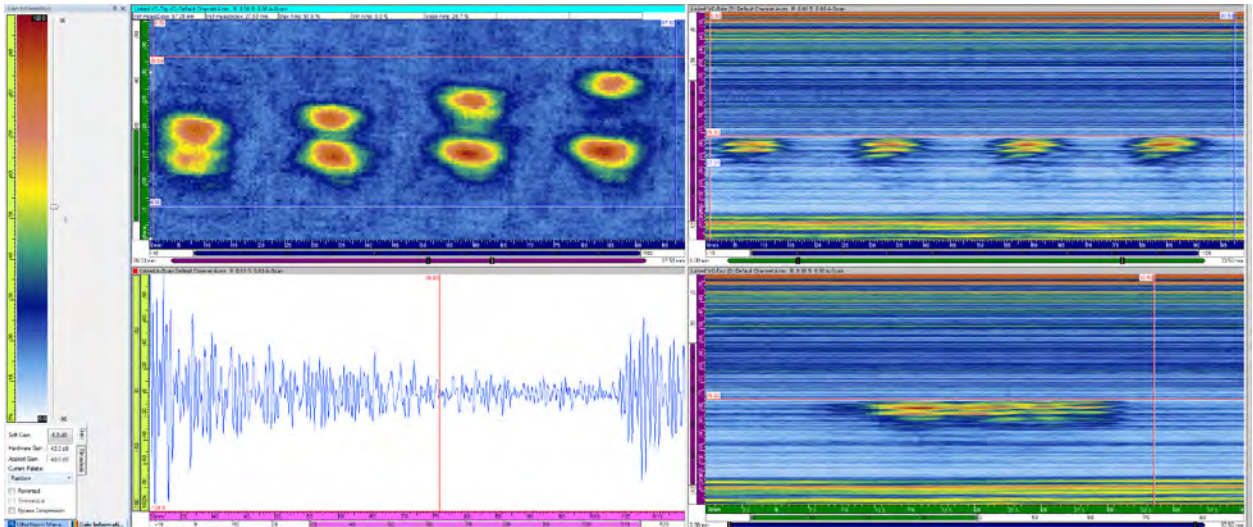


Figure 1.40. PA-UT Image of the Resolution Target Using the SN4 Matrix Array Probe in Water at a Focal Distance of 76.2 mm (3.0 in.) and a Probe Skew of 90°

Table 1.13 provides the as-built dimensions of the resolution target, as well as the ultrasonically measured dimensions recorded using the SN2 linear array from FY14/FY15 and both SN4 ETUs. The measured dimensions were quite accurate relative to the true state. As can be seen from the data in Table 1.13, as the probe approaches its resolution limit, the dimensional measurement accuracy begins to decrease. The oval shape of the sound field will greatly reduce a probe's ability to resolve in the axis where this sound field is largest. This is evident in the C-scan images of symmetrical targets, such as pin tops, where the

reconstructed image of the target is blurred. Later discussion of post-processing techniques will address the effort to combine data sets that are collected with the transducer in two orthogonal orientations in an effort to reduce this blurring effect.

Table 1.13. True-State Dimensions of the Resolution Target Reflectors and Ultrasonically Measured Separation Dimensions from the PA-UT Data Obtained from SN2 and SN4 Probes

	Spacing Center-to-Center (mm)			
As-built spacing	12.7	10.16	7.62	6.35
SN2	12.63	9.67	7.21	8.24
SN4 linear skew 0	11.5	9.5	*	*
SN4 linear skew 270	12.0	9.5	7.0	*
SN4 matrix skew 0	12.0	*	*	*
SN4 matrix skew 90	12.5	10.0	7.0	*

*Pins in set were detected but not distinguished/resolved from one another.

The resolution assessment of the SN4 linear and matrix array probes in water continued by collecting data on the new stainless steel (SS) PNNL resolution target, shown in Figure 1.41. A design schematic is shown in Figure 1.46 of Section 1.8. This target features the lettering of “PNNL” machined out at various depths as described in the design schematic. The lettering starts at 1.58 mm (0.63 in.) machined depth and increases in 1.58 mm (0.63 in.) increments up to 6.35 mm (0.25 in.) depth. In addition to the lettering on the target, nine notches of varying width and depth were machined into the bottom half of the target. All notches are 9.52 mm (0.375 in.) in length. The notches have a width of 3.17 mm (0.125 in.), 2.03 mm (0.08 in.), or 1.01 mm (0.04 in.). The depth of the notches also varies between 2.03 mm (0.08 in.), 1.01 mm (0.04 in.) and 0.5 mm (0.02 in.).

The raster scan data sets were collected over a scan distance of 80 mm (3.15 in.) and an index distance of 85 mm (3.34 in.) for the SN4 linear array probe. The data sets collected with the matrix array probe spanned a distance of 64 mm (2.51 in.) in the scan axis and 66 mm (2.59 in.) in the index axis. The resolution in both scan and index axes was 0.5 mm (0.02 in.) for all data sets.

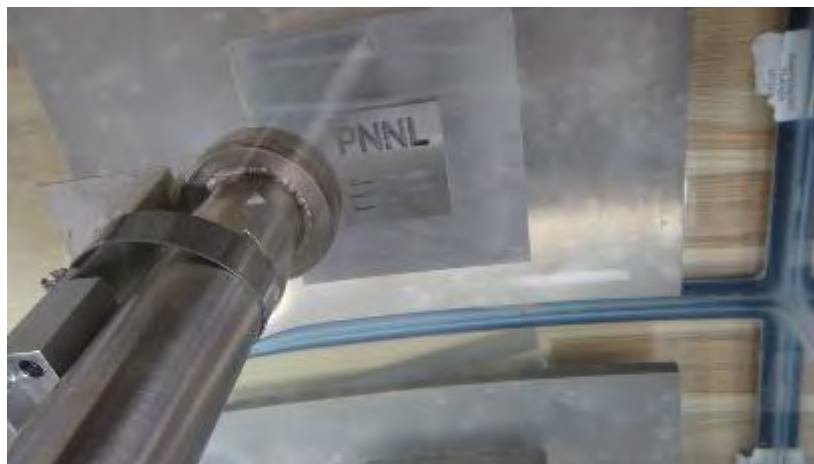


Figure 1.41. Image of the SN4 Matrix Array Probe Being Raster Scanned Across the PNNL Resolution Target at a Distance of 76.2 mm (3.0 in.)

The SN4 linear and matrix array probes were raster scanned over the target at distance of 76.2 mm (3.0 in.) in both 0° and 90° probe skew orientations. Collecting data in orthogonal probe skew orientations allows the narrow and wide dimensions of the oval-shaped sound field to resolve the features of the target. This is important because the orientation of the beam is crucial to resolving the separation between the letters of the target. This can be clearly seen when comparing the C-scan images in the upper left of both Figures 1.42 and 1.43. In Figure 1.42 the linear array probe skew was set to 0°, and in this case the beam orientation is such that the letters and columns of notches can be distinguished from one another across the scan axis (blue axis). Also in this figure, the lettering is blurred in the index direction (green axis) and the rows of notches are not distinguished from one another. This blurring and axis-dependent resolving capability is directly tied to the asymmetry of the spot size and consequently the array orientation used when collecting data. For additional clarity, a not-to-scale representation of the oval sound field is also shown in the C-scan region of this image.

Figure 1.43 shows a C-scan image of the SS PNNL target in the upper left where the linear array was used in the 90° skew configuration. These data show a poor resolving power in the scan axis (blue axis) where the PNNL lettering is not distinguished individually and the columns of notches are blurred together. Alternatively, an adequate resolving capability in the index axis (green axis) is shown by the lack of blurring of the lettering in the index axis and the ability to resolve the rows of notches from one another. As in Figure 1.42, a not-to-scale representation of the asymmetric sound field is included in Figure 1.43 for clarity.

This exercise was also conducted using the SN4 matrix array and the results are shown in Figures 1.44 and 1.45. As seen in the figures, these data are consistent with that collected using the SN4 linear array where features of the target are distinguished more clearly in the axis where the sound field spot size dimension is minimal.

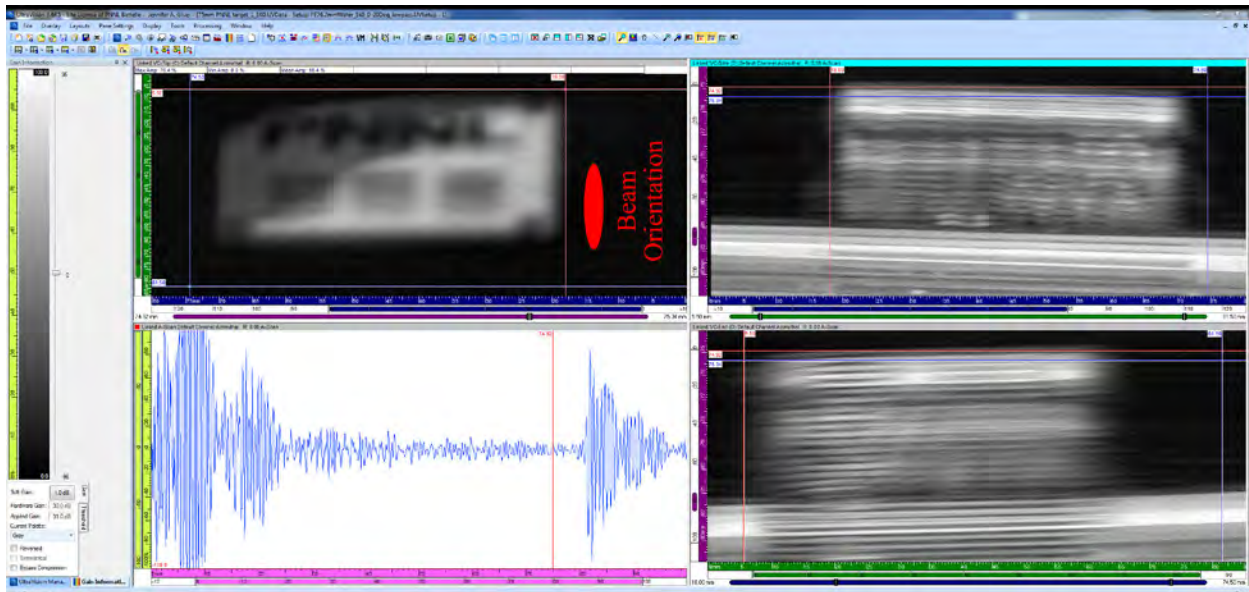


Figure 1.42. PA-UT Image of the PNNL Resolution Target Using the SN4 Linear Array Probe in Water at a Focal Distance of 76.2 mm (3.0 in.) and a Probe Skew of 0°

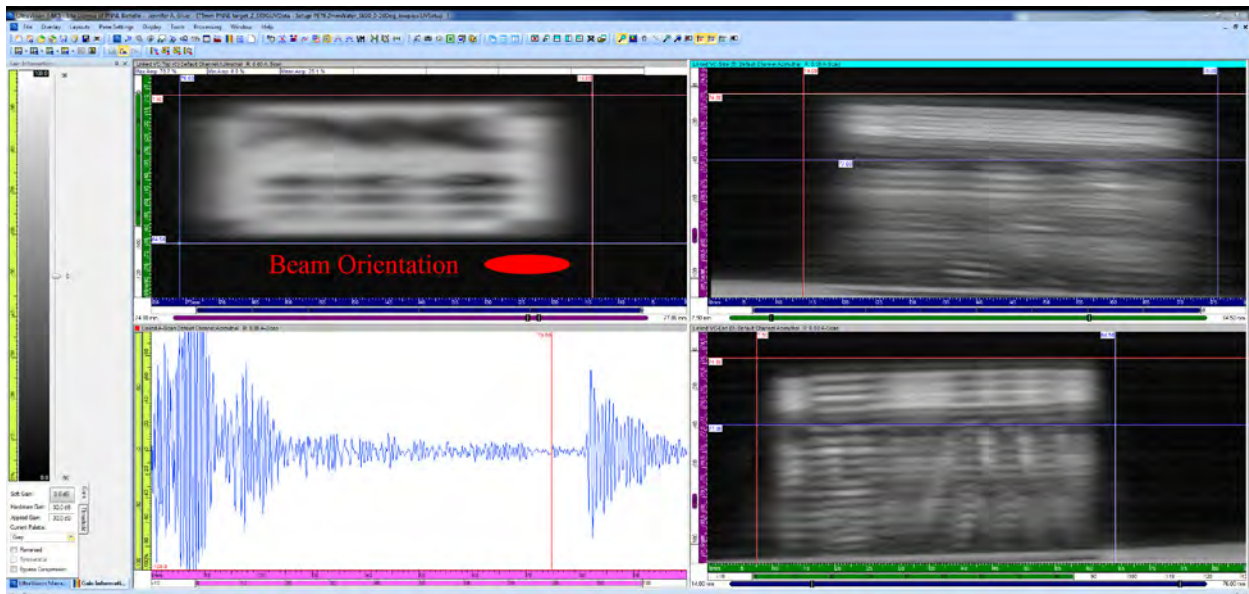


Figure 1.43. PA-UT Image of the PNNL Resolution Target Using the SN4 Linear Array Probe in Water at a Focal Distance of 76.2 mm (3.0 in.) and a Probe Skew of 90°

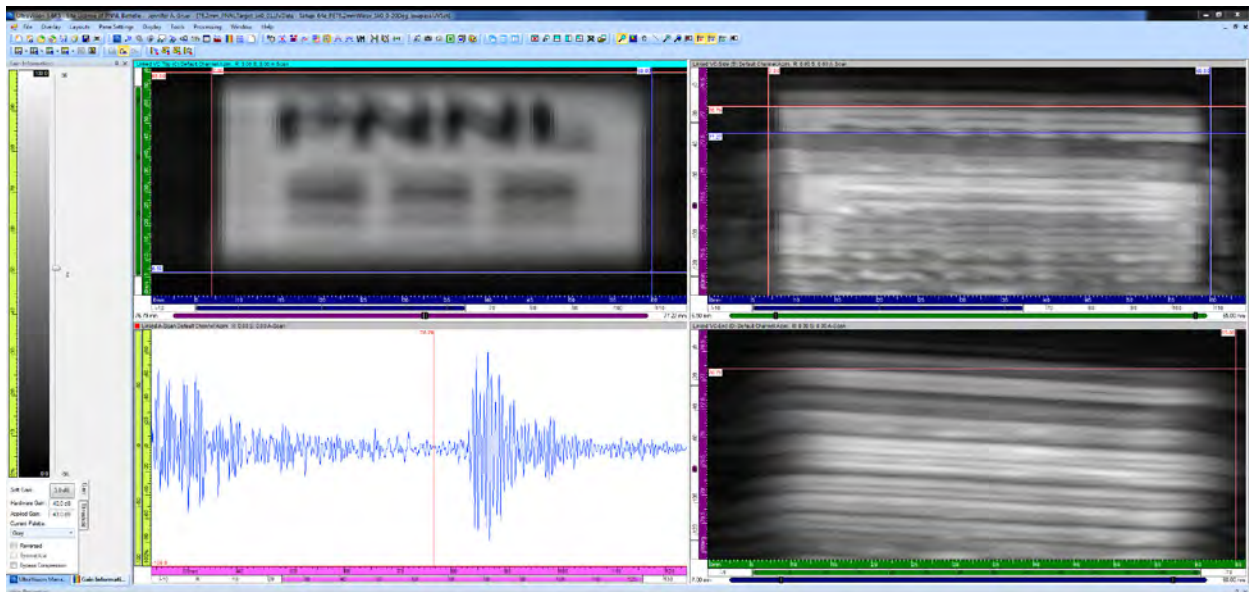


Figure 1.44. PA-UT Image of the PNNL Resolution Target Using the SN4 Matrix Array Probe in Water at a Focal Distance of 76.2 mm (3.0 in.) and a Probe Skew of 0°

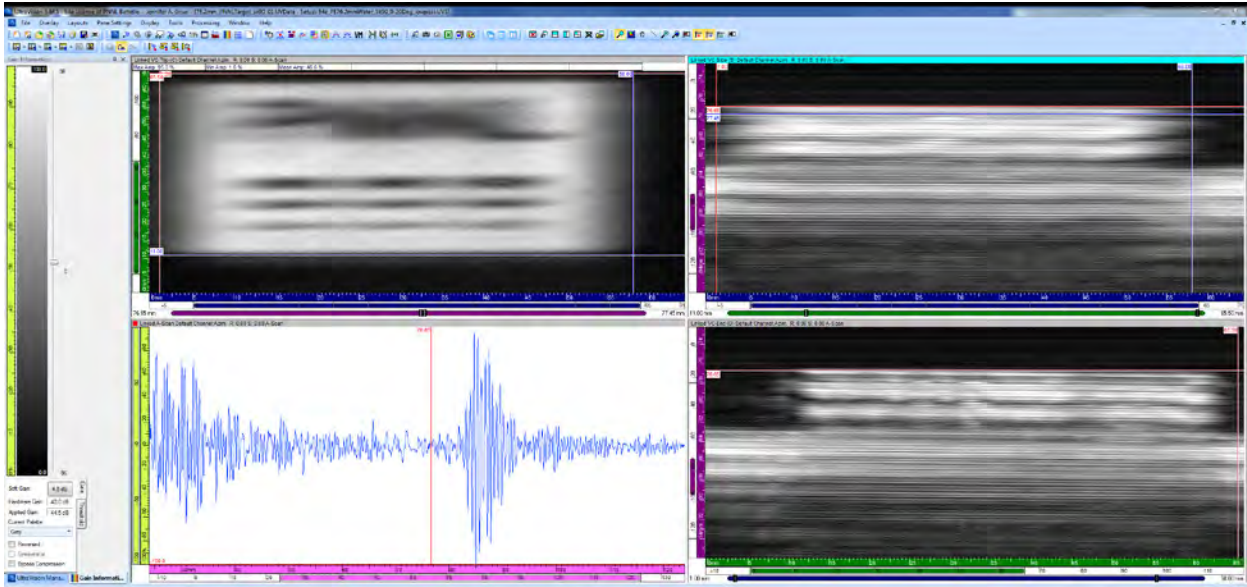


Figure 1.45. PA-UT Image of the PNNL Resolution Target Using the SN4 matrix Array Probe in Water at a Focal Distance of 76.2 mm (3.0 in.) and a Probe Skew of 90°

The data collected on the SS PNNL target is a perfect candidate for the exploratory data analysis and post-processing efforts outlined in Section 1.8 of this report. One of the goals of this analysis in late FY16 and early FY17 will be to develop a data processing approach to combine the orthogonal data sets collected with each probe and reconstruct the data such that the improved resolving power from each probe skew orientation can be represented in a single data set. Clearly these efforts must first be focused on data collected in water and then, after the methods are well understood, they can be applied to data sets collected in sodium.

1.7 Primary Inspection Parameters for 3D Imaging Assessment

This section of the report defines the primary inspection parameters and critical attributes that provide the criteria for assessing the 3D image performance, functionality, and effectiveness of the SN4 PA-UT prototypes. The effort reported here is focused on analyses of data and performance metrics obtained from imaging work conducted with both the SN4 linear array and the SN4 matrix array prototype ETUs in water and sodium.

In FY16, both the SN4 probes were tested in sodium at 260°C. The primary inspection parameters and critical attributes for evaluating the 3D image quality of the SN4 probes in sodium included:

1. Inspection time (duration)
2. Number of scanning repetitions
3. Data sampling frequency
4. Sensor-to-target distance
5. Spatial scanning increment size
6. Sodium temperature
7. Wetting of the probe face

8. Thermal cycling
9. Target size and orientation
10. Signal-to-noise ratio
11. Ability to resolve targets in sodium

With the analyses of data obtained from these performance characterization tests, PNNL was able to quantify key performance parameters that were compared and contrasted between the two different SN4 probe designs for their capabilities to detect and characterize reflectors in water and sodium. Summary highlights of data and imaging results from water and in-sodium tests are provided in Sections 1.8 and 1.9, respectively, and the conclusions obtained from the evaluation of these probes are discussed in Section 1.10.

1.8 Imaging Assessment in Water for SN4 Prototype Probes and Post Processing Method for Noise Reduction in UT Data

This section describes the imaging tests and data obtained from the SN4 prototype probes in water (at room temperature) to provide a baseline for determination of whether or not the probe was mature enough to be tested in sodium. The scanning configuration for the water testing employed three resolution targets. The primary target used in FY13, FY14, and FY15 has been described previously in Braatz et al. (2013). The second target was described in Section 1.6.4. The third and newest target was fabricated in FY16 and included a set of machined letters that spell out “PNNL” and various resolution slots of different widths and depths. The design schematic defining the machining specifications for this target is provided in Figure 1.46. A digital photograph of this target is provided in Figure 1.47.

The probes were configured for x-y axes raster scanning in an immersion tank for data acquisition. During scanning, it was noted that the matrix array probe resulted in generally lower signal amplitudes in comparison to the linear array probe in water. However, it was still decided to move forward with both SN4 probe designs with in-sodium tests in FY16. The results provided in Section 1.6.4 show ultrasonic images resulting from the testing of the SN4 PA-UT probes in water, using both resolution targets. It can be seen that the SNR in water is suitable for detection and resolution of relevant target features, providing the technical basis for conducting immersion tests in sodium as the next stage of evaluation. Data from the 64-element matrix array probe do indicate a slightly higher inherent level of ringing and acoustic noise within the probe, and some of these noise sources can be attributed to a combination of reverberations within the probe housing and shaft, as well as minor grounding issues coupled with motor noise due to the scanning motor electronics.

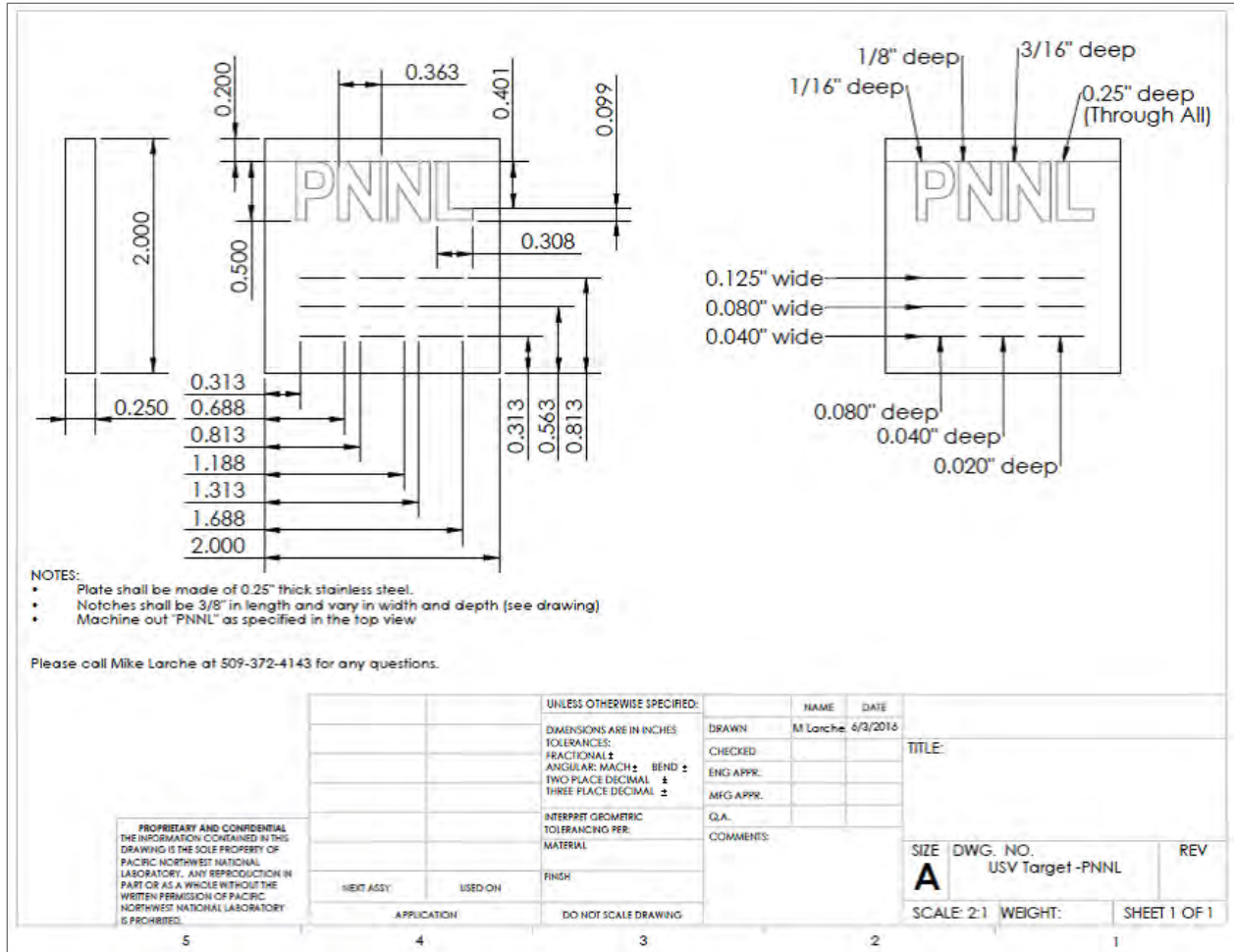


Figure 1.46. Design Drawing for the FY16 PNNL Resolution Target



Figure 1.47. Photo of FY16 PNNL Resolution Target

During the FY15 campaign, the implementation of a simple A-scan noise subtraction algorithm was introduced in order to clean up the images and reduce noise bands from various sources. This approach, while simple to implement, provided some level of improvement toward reducing noise in the data. Subsequent discussions with PNNL experts in computational engineering with experience in noise reduction techniques for medical ultrasonic data led to the pursuit of more advanced techniques for post-processing of the UT data in FY16. Figure 1.48 shows the improvements to some FY15 A-scan data from using this algorithm.

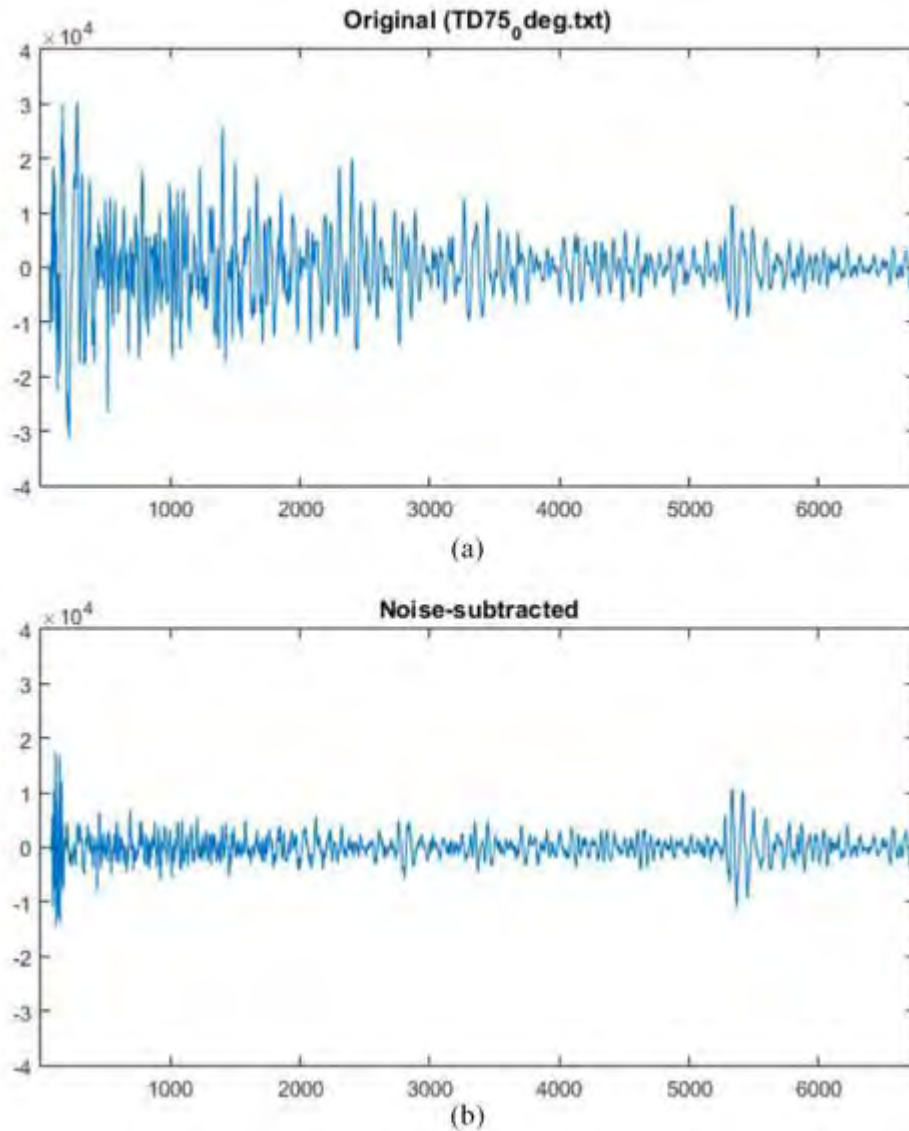


Figure 1.48. FY15 Post-Processed Data Illustrating (a) Raw RF Waveform (A-scan); (b) Processed RF Waveform after Subtraction

Early in FY16, prior to the acquisition of new FY16 data in water or sodium, PNNL continued investigating noise reduction methods by applying frequency domain filtering of the data using MatLab signal processing tools. PNNL initiated continued development and evaluation of noise reduction and image enhancement using data obtained from FY15 efforts. A variety of filtering techniques were studied.

A low-pass filter to reduce the noise bands emanating from within the probe housing and creating interfering low-level signals was applied and assessed. Signals were analyzed in the time and frequency domains and data were re-processed to determine the viability and level of improvement in the resultant ultrasonic images. Figures 1.49 through 1.52 provide illustrations of early FY16 efforts to reduce noise and improve image results from PA-UT in-sodium data obtained at 260°C in FY15.

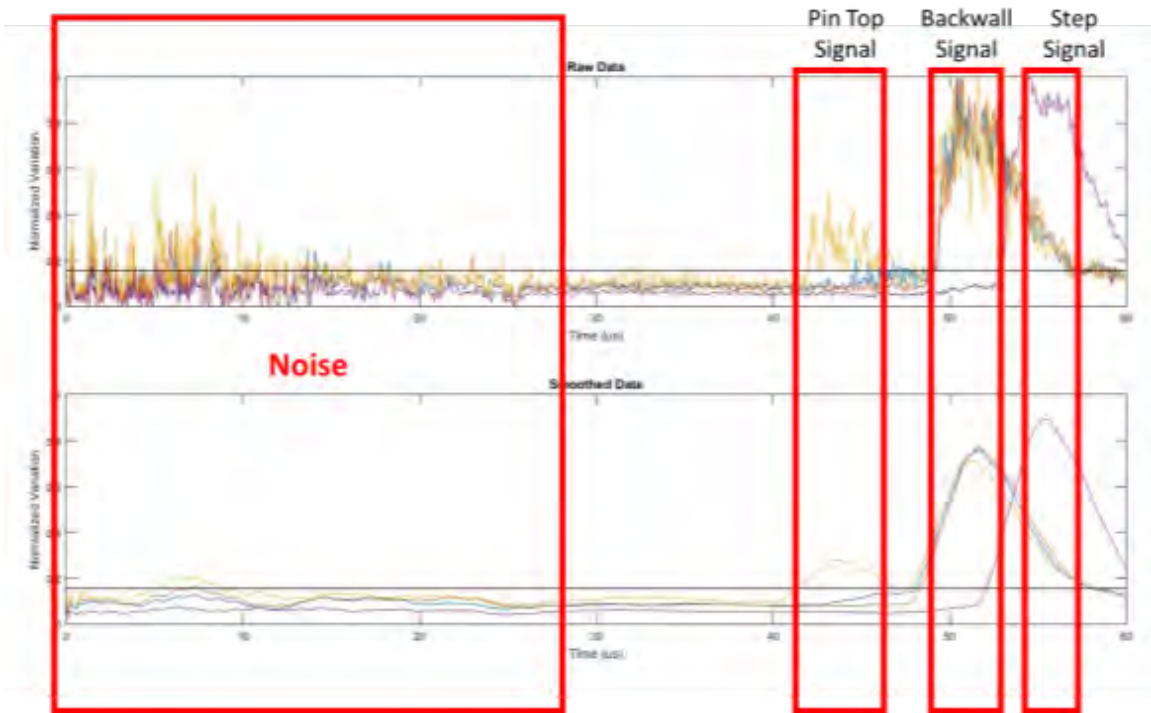


Figure 1.49. Evaluation and Categorization of Various Ultrasonic Signals from Data Acquired in FY 15, for In-sodium Tests at 260°C from Target Reflectors

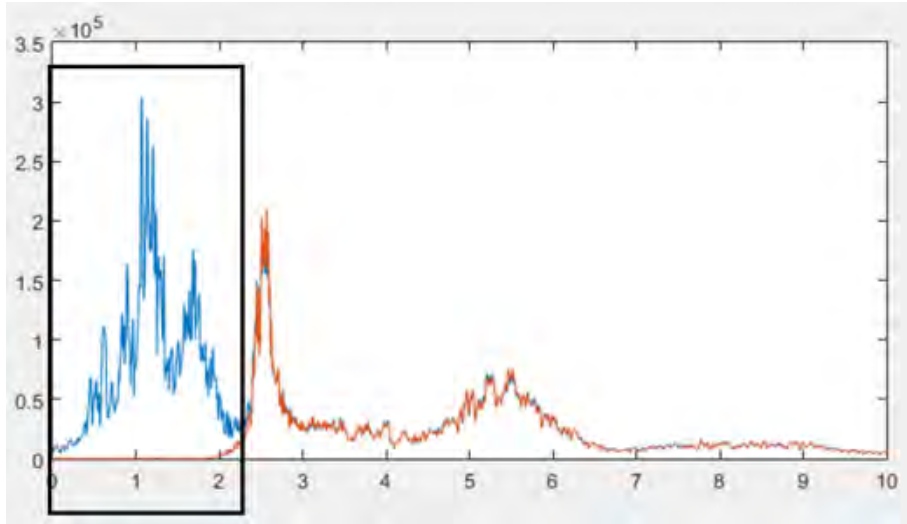


Figure 1.50. Illustration Showing the Mean Frequency Response (x axis in MHz) and Filtered FFT Results of FY 15 Ultrasonic Data. Boxed area indicates the application of a low-pass filter eliminating noise components above approximately 2.3 MHz.

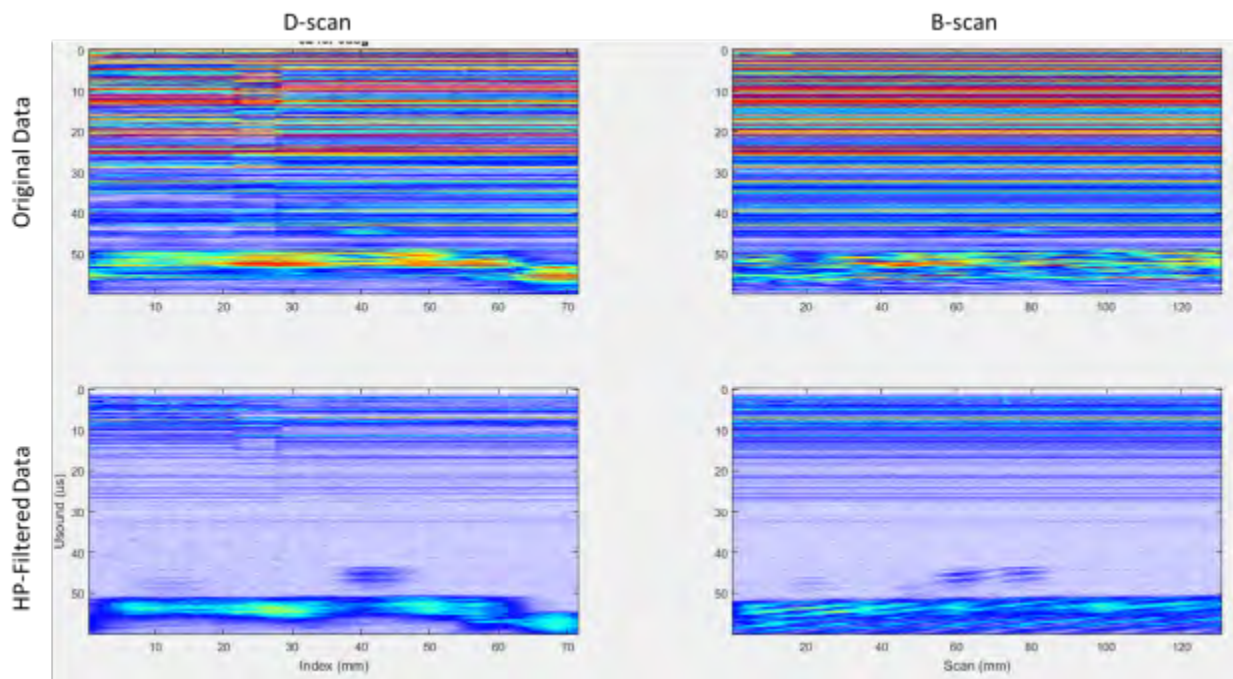


Figure 1.51. B-scan and D-scan Image Views of Specific Targets in Sodium from FY 15 Data. Top row shows original data with noise bands; bottom row shows post-processed data using the high-pass filtering approach.

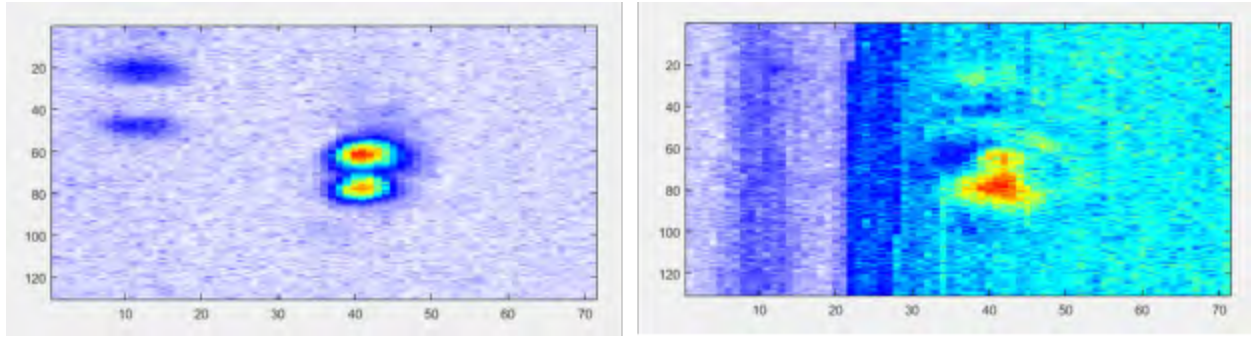


Figure 1.52. *Right:* Raw PA-UT Data with No Processing. *Left:* Time-Gated and Frequency Filtered Data (post-processed).

Late in FY16, PNNL began investigating a more advanced and rigorous signal processing approach to improve the ultrasonic images obtained with the SN4 PA-UT probes. The image reconstruction approach is known as Analytic Signal Magnitude processing, and has been employed successfully in medical ultrasonic imaging and other venues for improving ultrasonic image details and enhancing detection and discrimination capabilities from ultrasonic data.

For every measured ultrasonic waveform, $f(t)$, with “out-of-phase” component, defined by the Hilbert transform

$$H[f](t) = 1/\pi \int_{-\infty}^{\infty} f(s)/(t-s)ds,$$

we may compute the magnitude of the analytic signal, given by

$$e(t) = \sqrt{f(t)^2 - bH[f](t)^2},$$

which quantifies the arrival of energy, carried by the acoustic wave, at the sensor element (Gammell 1981a; Gammell 1981b). A plot of $f(t)$ and $e(t)$ as functions of time shows that $e(t)$ “envelopes” $f(t)$ and is therefore sometimes also referred to as the signal envelope. Being smoother than $f(t)$, it is frequently more useful for identification of features in ultrasonically interrogated samples, for instance those studied in NDE, or in medical ultrasonics (Gammell 1981a; Gammell 1981b). Figure 1.53 illustrates some results using this signal processing methodology from a target detection trial in water using the SN4 32×1 linear array with the primary target described in Section 1.9.2 and detailed technically in Braatz et al. (2013), Diaz et al. (2014a), and Diaz et al. (2015b).

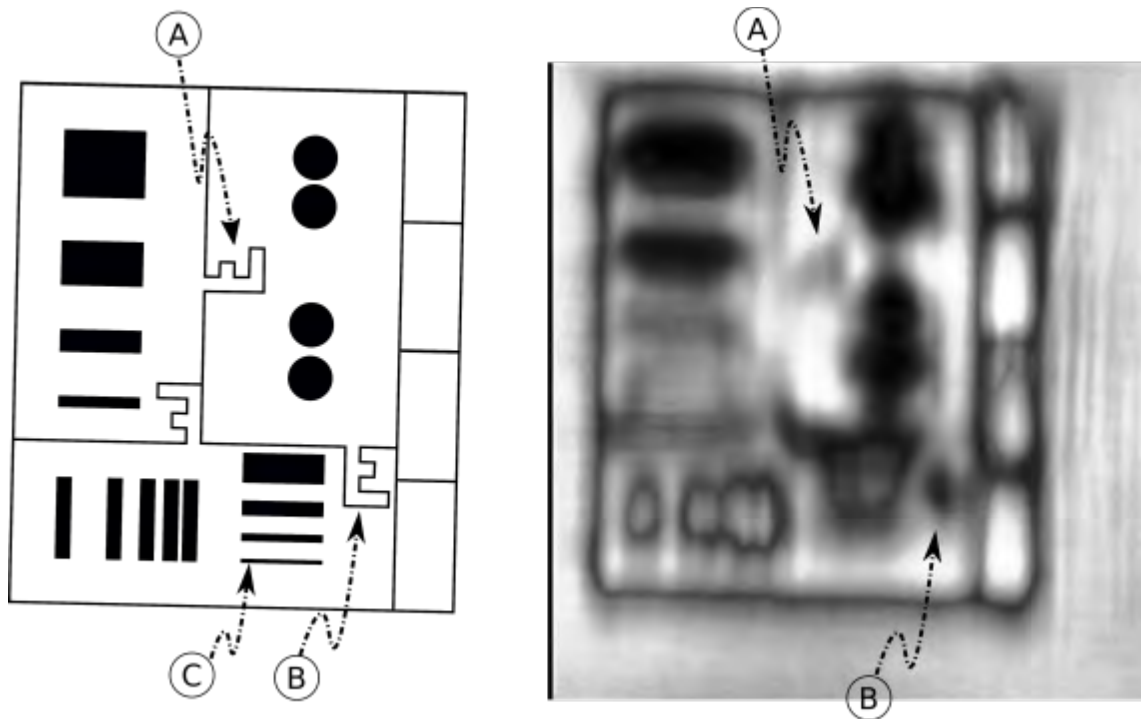


Figure 1.53. Stainless Steel Target Drawing (*left*) and Ultrasonic Image (*right*) Reconstructed Using Analytic Signal Magnitude Processing

Letters indicate correspondence between the drawing and image features in the case of special interest zones “A” and “B,” where evidence of the letter “F” has been machined into the target, while zone “C” denotes a notch that is not evident in the ultrasonic image. All other specimen features appear in the ultrasonic image although they are “blurred” due to convolution with the point-spread function of the array. It is likely that the image resolution could be significantly improved by employing deconvolution.

This approach employs ultrasonic waveforms obtained using the SN4 32×1 linear PA-UT probe at 75 mm focal distance from the target in water, and stored for later post-processing analysis. The resulting 3D data set consisted of 3125-point waveforms, corresponding to (x,y) positions on an 80×85 point spatial grid encompassing the scanned target sample.

Analysis consisted of computing the envelope, $e(t)$, of each 32×1 linear PA-UT-point signal, $f(t)$, and then projecting each waveform to a single point on the 80×85 point grid by taking its maximum value. The result of performing this analysis of data acquired by scanning the SS target sample while immersed in water is shown on the right-hand side of Figure 1.53. To the left of the figure is shown a top-down machinist’s drawing of the actual target.

In general, the analytic-signal magnitude image seems to capture most of the features shown in the machinist’s drawing. These include features that should be difficult to detect, including two of the “F” features indicated by circled letters “A” and “B” (although these are observed to have different degrees of resolution). However, not all of the features are detected, including the third “F” and one of the smaller notches indicated by the circled “C.”

This image reconstruction approach has shown promise for applicability with PA-UT data obtained from targets in water. Some of these reconstruction challenges might be further reduced or eliminated if a good

estimate of the point-spread function (PSF) of the array were known. Several attempts were made to estimate this function based on scans from other samples and also by extracting sub-segments of the image shown in Figure 1.53. Unfortunately, none of these appear to be suitable for estimation of the PSF. Future work could attempt to produce specimens that would permit direct measurement of the PSF as well as exploration of deconvolution routines of increasing sophistication; that is, simple Fourier, Wiener, or Richardson–Lucy deconvolution. It is anticipated that late in FY16 and early in FY17, work can continue to address ultrasonic image reconstruction methods and signal processing algorithms using FY15 and FY16 ultrasonic data for improved imaging, detection, and discrimination capabilities in sodium.

1.9 Imaging Assessments in Sodium for SN4 Prototype Probes

This section describes the sodium wetting challenges, the solution to mitigate those issues, and imaging tests and data obtained from the SN4 prototype probes in sodium. The scanning configuration for the in-sodium tests is identical to that described in the performance demonstration protocol provided in Diaz et al. (2015b).

1.9.1 Probe Face, Sodium Preparations, and Scanning Configuration for In-Sodium Scanning

This subsection describes the issues of transducer wetting, toward achieving effective transmission of ultrasonic energy through the faceplate of the PA-UT probe, and into the sodium for imaging purposes. In addition, this section addresses preparation issues for the probe face, the sodium bath, and the raster scanning system used for data acquisition. Over the past few years, sodium wetting of the probe has become a challenging issue to overcome. In FY14, PNNL developed a process to consistently mitigate wetting problems. During the first test of the SN2 probe in sodium in July 2014, no ultrasonic energy was transmitted into the sodium. Effective wetting was not being accomplished. Wetting of the ultrasonic probe is a function of material oxidation and gas adsorption at the interface of the probe faceplate and the liquid sodium (Addison 1984). Effective wetting of the probe face is a key factor in providing a suitable environment for effective ultrasonic transmission of energy into the medium and impacts the resultant measurement accuracy as well.

The sodium wetting issue is defined by a combination of two primary factors in sodium. The first is associated with the polish and surface finish of the probe faceplate. While from a visual standpoint the faceplate may appear suitably polished for optimal wetting, there is no proof that the wetting is effective from an ultrasonic standpoint. In FY10 through FY13, the differences in surface preparation of the various probes were noteworthy. It must be understood that the maximum displacement for a PZT-5A element is only about 350×10^{-12} m/v. This simply means that the displacement between the surface of the Ni faceplate and the sodium is only a few microns, and any thin layer of contamination can preclude the energy from passing through. Recent work at PNNL has focused on addressing critical issues of temperature, corrosion, thermal expansion, and wetting phenomena for improving ultrasonic transmission and reception of energy in sodium. Assessing the Curie temperature and physical constants of various piezo-elements as they relate to ultrasonic performance characteristics has been an important focus area of research in previous years. In addition, damage to the probe from thermal shock has been a critical focus of the earlier work at PNNL (Braatz et al. 2013; Diaz et al. 2014a; Watkins et al. 2012). The potential for fracture of the piezo-element because of high thermal gradients or transients, and significant thermal expansion mismatches, played a key role in the probe design process.

The second wetting issue is associated with time in sodium and, more importantly, contaminants in the sodium; in particular, the oxide levels. There is nothing in the literature denoting a necessary time duration required at 260°C for a polished oxide-free surface, only information for unpolished surfaces full of oxide, so no clear guidance was available on this matter. PNNL research indicated that clearly wetting was not an off-on condition; that a surface does not go from non-wetted immediately to full-wetted, but that wetting is a progressive phenomenon, described like a wave-front. It is a time-temperature dependent operation, and is also dependent on the oxide thickness in which wetting starts, progresses, and then eventually becomes fully wetted over time. Effective wetting no doubt requires longer time on an unpolished oxide surface, and subsequently occurs more quickly on a polished surface. PNNL established a rule allowing at least 30 minutes at 260°C for wetting to appear, and for a stable signal response to be achieved. In addition, the literature mentions that for Ni, the mono-oxide of Ni (NiO) is the usually expected species and is expected to dissolve, but that at high solubility levels of O₂ in sodium, the ternary oxides of Ni have been seen, NaNiO₂ and Na₂NiO₂. It says some ternary oxides can be more stable, and particularly more stable when high O₂ levels are present. It does say that the Ni ternary oxides are expected to dissolve, but this still may be O₂-level-dependent (Addison 1984). From trials performed at PNNL in FY13 and FY14, it has been shown that excessive levels of O₂ (>3 ppm) are sufficient to preclude effective wetting on the PA-UT probe faces. In order to address these issues, PNNL developed a process for effective surface preparation and polishing of the Ni faceplate of the probe prior to in-sodium testing. This process has been well documented in Diaz et al. (2014b) and Diaz et al. (2015b).

Modifications to the sodium containment were made early in FY15. Heating of the sodium bath has been modified to incorporate a custom heater block and temperature controller. In addition, two custom-made sodium test vessels were fabricated. The entire system (heater block, temperature controller, and reaction test vessel) were evaluated and made fully operational in the spring of FY15. In FY14 the cabling for the ultrasonic probe and the scanner platform were inserted into the glovebox through a very small pass-through port. This port was modified to allow for a larger volume of cables as required by the FY15 data acquisition system and probe configuration. Large quantities of fresh sodium were procured for FY16 testing and all sodium went through a filtration process prior to use in tests.

Finally, in FY15, PNNL completed the design, fabrication, and testing of an upgraded USV scanner and controller platform for in-sodium tests. This platform was designed to provide an x-y axes raster scanning capability for PA-UT probes in sodium. In large part, it was determined in FY14 that polar (rotational) scanning of a PA-UT probe from a fixed point was insufficient for obtaining suitable amounts of specular energy and the required level of redundancy from targets immersed in sodium. In FY15 and FY16, PNNL decided to invoke a raster scanning capability to translate the PA-UT probe directly over the target region of interest, and simultaneously examine the target over a range of inspection angles. Not only does this configuration provide richer ultrasonic data because of multiple points of insonification over the area of interest, but the data are visualized and presented in a much improved image that is easier to interpret. The photographs provided in Figure 1.54 show the portable, rack-mounted scanning controller and 3-axis (x-, y-, and z-axes) scanner platform for use in both laboratory and sodium glovebox applications. This scanning platform provides mechanical scanning accuracy in the x- and y-axes of 0.025 mm.

This scanning platform was transported to the laboratory facility where the sodium glovebox resides, and was configured for operation just outside the glovebox. Cabling from the instrument control rack was tethered through the port, and connected to the scanner platform that was already positioned inside the glovebox over the sodium containment vessel. The vessel is pre-configured with the target placed at the bottom, and centered in the containment vessel. After pre-polishing of the probe face, the probe was covered and sealed, and then inserted through the port. These distances require long cable lengths that do affect signal amplitude because of attenuation. Once the probe and cables are routed inside the glovebox, the port is sealed and the argon atmosphere is re-established. A final polishing is conducted on the probe

face as per the protocol defined in Diaz et al. (2015b). Photographs of the data acquisition system, sodium glove-box, and sodium containment vessel are provided in Figures 1.55 through 1.57.

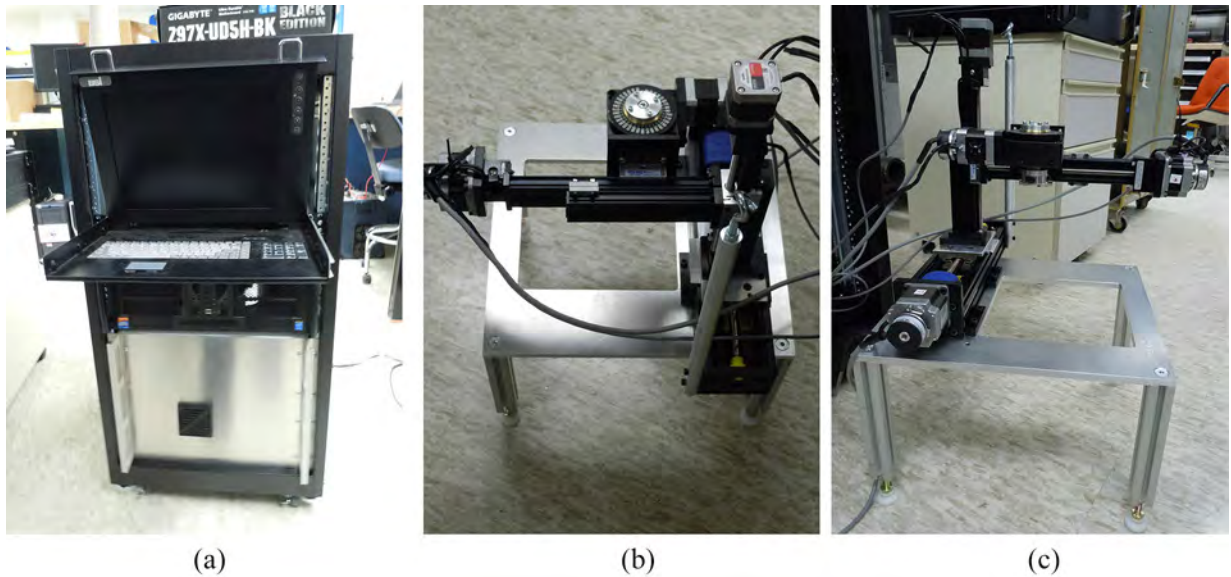


Figure 1.54. *Left:* Rack Mounted Scanning Controller Instrumentation and Motor Drivers. *Middle:* Top View of 3-Axis Raster Scan Platform. *Right:* Side View of 3-Axis Raster Scan Platform.

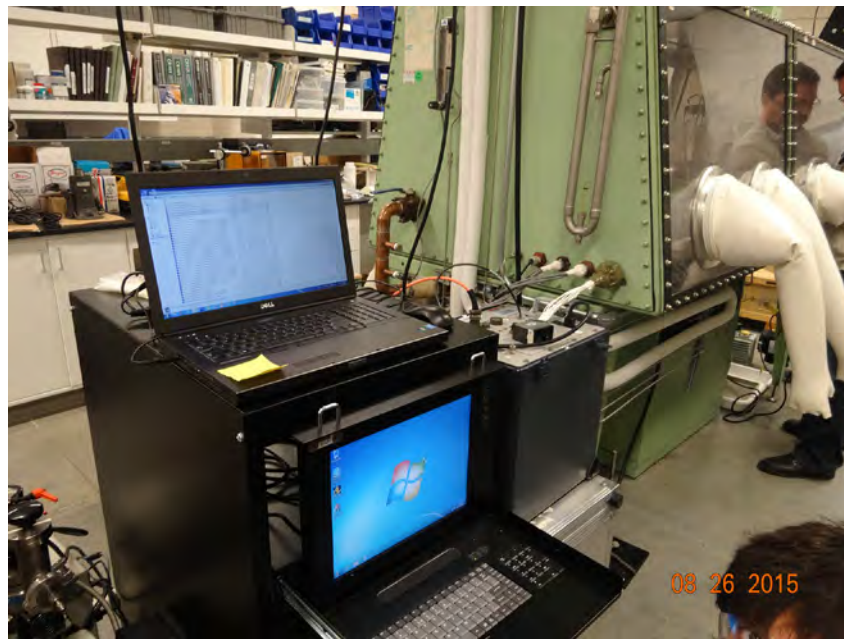


Figure 1.55. Rack-Mounted Scanning Controller System, Configured for Use Near the Sodium Glovebox



Figure 1.56. Scanning Platform, Configured over the Sodium Containment Vessel within the Sodium Glovebox

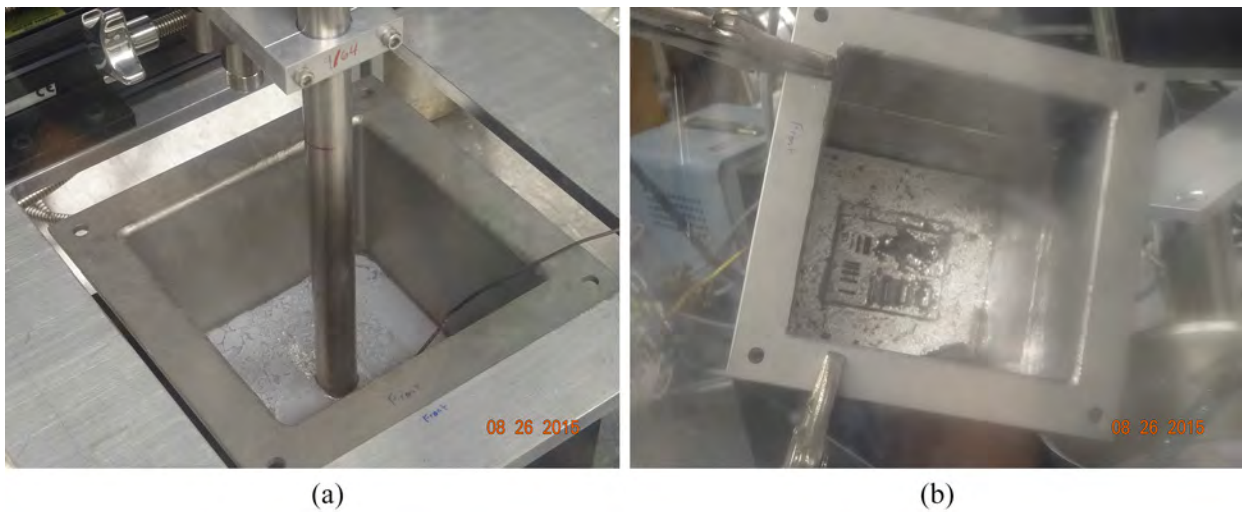


Figure 1.57. (a) SN2 Probe after Scanning has been Completed, Just Prior to Removal from Sodium Containment Vessel; (b) Target after Sodium has been Emptied from Containment Vessel

1.9.2 In-Sodium Testing Results

The ultrasonic images generated from in-sodium PA-UT scans using the SN4 probes and provided here were created using the UltraVision 3 software. These datasets have not been post-processed using any advanced noise reduction algorithms. The evaluation of these advanced processing approaches is described in detail in Section 1.8; however, more work is required to effectively implement one or more of these image reconstruction techniques to the in-sodium data. All data discussed here were acquired at 260°C. In this subsection, we primarily focus our discussion on the results from the SN4 32×1 linear array prototype probe being raster scanned over the entire target volumes at various focal depths (standoff between the probe and the base of the target). The primary target used for in-sodium tests has been described in great detail in Braatz et al. (2013), Diaz et al. (2014a), and Diaz et al. (2015b). However, since this target was initially fabricated, one of the vertical pin reflector features was removed. The photograph provided in Figure 1.58 shows the target and identifies the pin that was subsequently removed.

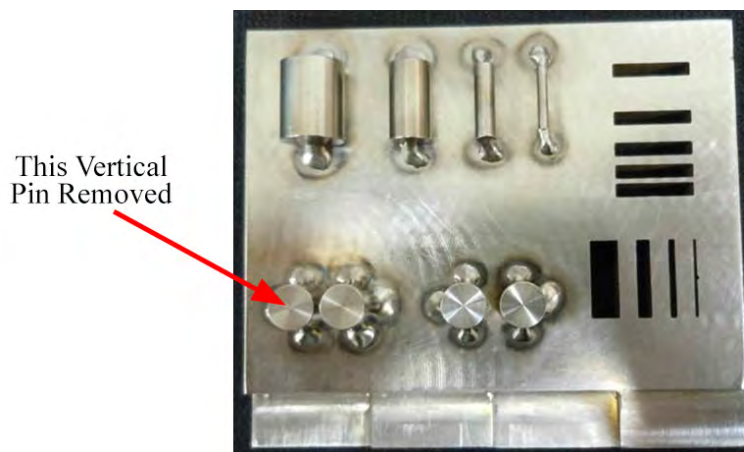


Figure 1.58. Stainless Steel Imaging Reflector Target Used for Performance Demonstration in Sodium at PNNL

Prior to presenting the in-sodium data imaging, detection, and feature characterization results, it is necessary to discuss the criteria for defining how two closely spaced reflectors are resolved from the ultrasonic data. For the data analysis conducted in FY16 and described here, it must be noted that a rectangular PA-UT probe is not a point source; however, at the focal point, the PA-UT probe focuses the sound field as a point source would be represented by the Airy Pattern (point source diffraction pattern) as shown in Figure 1.59.

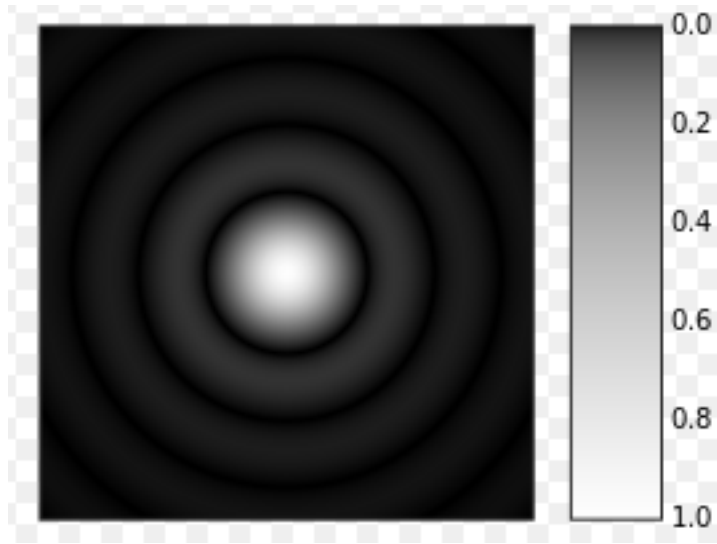
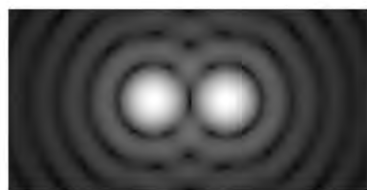
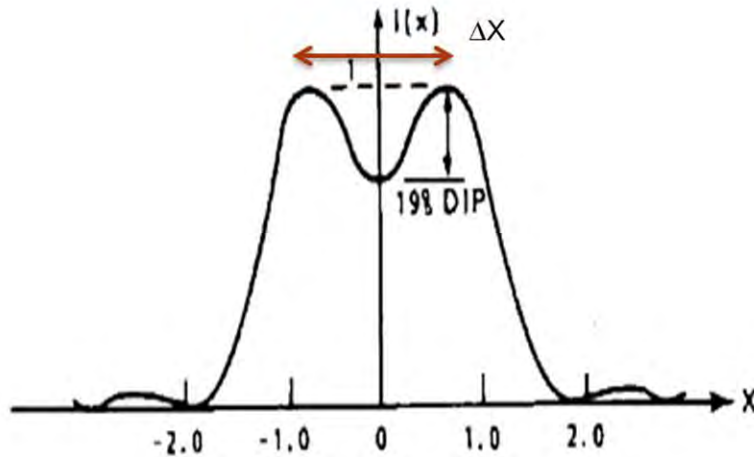
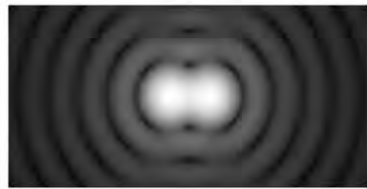


Figure 1.59. Illustration of the Point Source Diffraction Pattern (Airy Pattern)

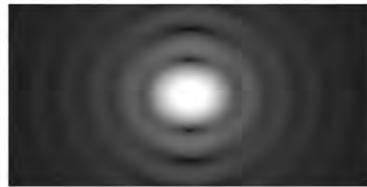
Therefore, PNNL decided to use a 19% amplitude dip as a guideline/reference for the criteria used to determine when two closely spaced reflectors can be effectively resolved and discriminated. The Rayleigh criterion defines the minimum resolvable detail—the imaging process is said to be diffraction-limited when the first diffraction minimum of the image of one source point coincides with the maximum of another. Two point sources are resolved when the center of the Airy disk (maximum) from 1 point source falls on the first zero or minimum of the Airy disk of the second point source. Image intensities show a 19% dip (Busse et al. 1984; Wikipedia 2015a, b). This is best illustrated in Figure 1.60.



(a) Resolved



(b) Resolved at Rayleigh Criterion



(c) Not resolved

Figure 1.60. Illustration of the Rayleigh Resolution Criterion Defining Spatial Resolution for Two Closely Spaced Reflectors. Top: Graphical Depiction of 19% Amplitude Dip. Bottom: Visual Depiction of Airy Disk Pattern for Various Scenarios of Two Closely Spaced Reflectors.

For a point source or focused circular probe the Rayleigh resolution (ΔX) is defined as:

$$\Delta X = 1.22(\lambda f/a)$$

where λ = wavelength, f = focal length, and a = probe aperture. This criterion was used during the analysis to determine resolution performance from the ultrasonic data.

Mechanical scanning parameters for the data presented in this section are described here. In the scan axis (y-axis), the step size resolution was 0.5 mm over a scan length of 75 mm. In the index axis (x-axis), the steps size resolution was 0.5 mm over a scan width of 75 mm. True-depth focusing was employed at two different depths—50.8 mm, and 76.2 mm. At both standoff heights from the target, scans were obtained, using incident angles of 0° to $+20^\circ$ in 5° increments.

As with most pulse-echo ultrasonic imaging approaches, the data may be presented in a number of ways. The 32×1 linear array SN4 probe was raster scanned over the top of the reflector targets, and covered the entire region in both x- and y-axes. In addition, multiple incident angles were applied, and the various target features were insonified by multiple (redundant) incident wavefronts, captured and then analyzed both individually and in a merged fashion. In pulse-echo mode, one can apply time-gated windows to the data and employ various approaches for detection of target features. If, for instance, the analyst applies a gate (time-window) that is focused on the back surface of the target, then areas that do not indicate the presence of a specular response (reflected echo) will be of much lower amplitude than areas reflecting energy back to the probe from the back surface of the target. In this way, a “shadowing” effect can be used to illustrate the detection of anomalies or target features. This technique is only useful for detection if a back surface reference reflector is available. In this case, the back surface of the target is available for this purpose. Figure 1.61 illustrates the imaging results from data acquired in FY15 using the SN2 probe after applying this type of time-window gate. A photo of the target is placed next to the image so the reader can correlate the lower amplitude responses (shadows) with the target features that were detected.

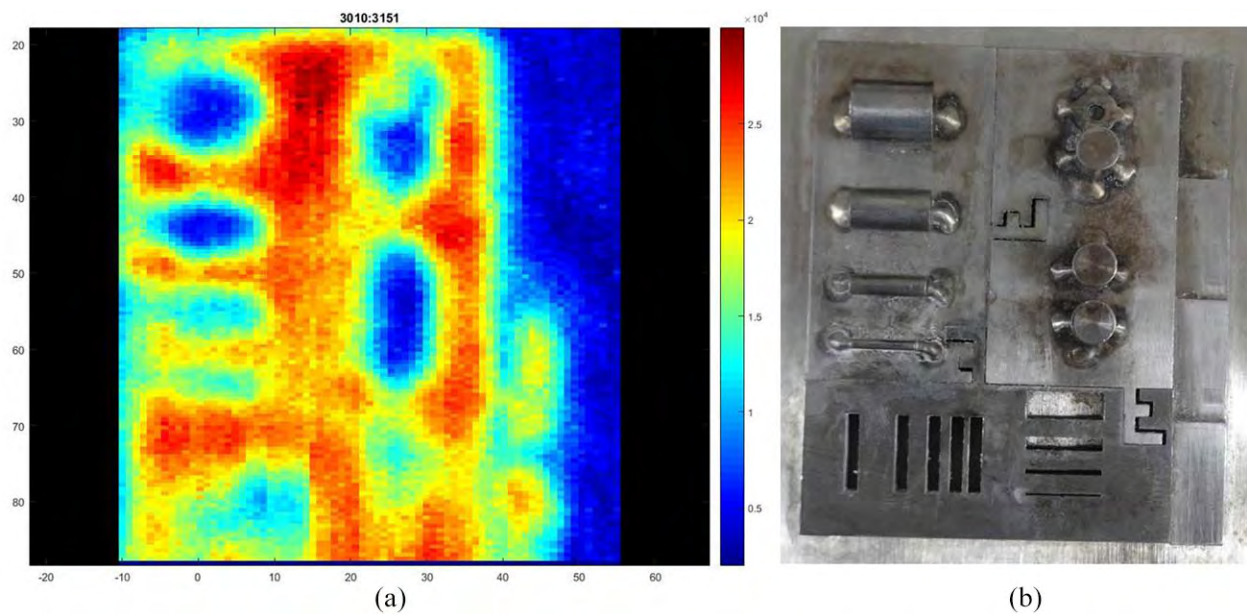


Figure 1.61. Processed Ultrasonic Image (C-scan view) Showing the Shadowing Effect, or Lack-of-Backwall Echo Response (a) Corresponding to the Various Features on the Target (b) for FY15 data.

These data were obtained at a 75 mm standoff height in sodium at 260°C. While some degree of system noise and probe noise contributed to a non-optimal SNR in these tests, the raster scan data acquisition modality provided good imaging and detection results at a 75 mm focal distance from the target. A post-processing noise subtraction algorithm was applied to the raw ultrasonic data to improve image quality in FY15. This example image showing a lack of backwall or shadowing as the probe is translated directly over the target was acquired at 0° incidence. From this image, all of the horizontal pins and the three vertical pins are detected via analysis of a back-surface gate. Even the larger slots and the first two step reflectors on the lower right-hand side of the target are detected. The target was not precisely leveled and, therefore, gating of the ultrasonic data was challenging. In contrast, the FY16 data (provided in Figure 1.48 and taken at the same focal distance in sodium) are shown without any signal processing or noise reduction algorithms being used.

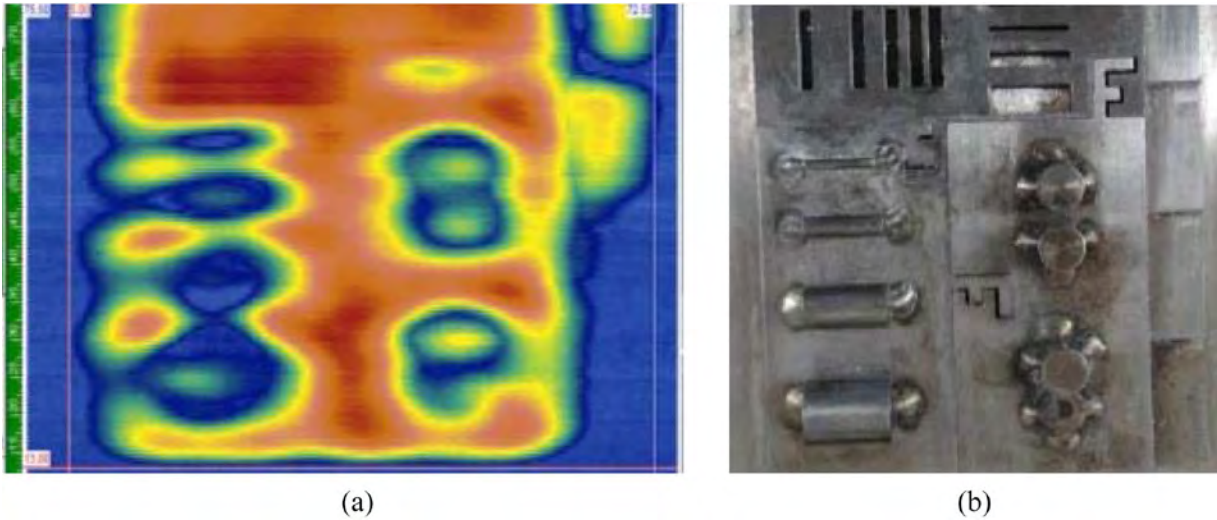


Figure 1.62. Unprocessed (Raw) Ultrasonic Image (C-scan view) Showing the Shadowing Effect, or Lack-of-Backwall Echo Response (a) Corresponding to the Various Features on the Target (b) for FY16 data.

A comparative analysis of the data between the FY15 and FY16 probes indicates some significant improvements in signal strength, SNR, image resolution capabilities, and the ability to characterize target features. Additional images/views were obtained that show reflected energy from the various target features, allowing for calculation of feature dimensions and also resolution capability. By employing various time gates and spatially isolating reflected echoes in various views (B-scans, C-scans, and D-scans), it is possible to highlight and discriminate specific target features (from noise), compute SNR, and dimensionally characterize the features where possible. For reference to raster scanning in the x-y plane over the target, an A-scan is a time-domain waveform representation of data obtained at a single x-y coordinate point, and is represented by a time-series (signal response voltage as a function of time). Time values for these waveforms can be directly correlated with sound field propagation depth into the material (along the z-axis). A C-scan is a composite view of peak amplitude data in the x-y plane, at any given coordinate in z (depth). A B-scan is a composite view of peak amplitude data in the y-z plane, while a D-scan is simply an orthogonal B-scan, illustrating peak amplitude data in the x-z plane. Ultrasonic images (B-, C-, and D-scan views) illustrating both lack of signal (shadowing) and reflected energy from the three vertical pins and four horizontal pins are provided in Figures 1.63 and 1.64. Depending on the particular view, some reflectors have been gated out. Some of the views show that the target may not have been leveled appropriately; however, while the target mockup was configured to be level with the bottom of the sodium containment vessel, the actual probe shaft was slightly bent due to weld fabrication inconsistencies with the probe shaft. This slight “bend” in the shaft created a slight tilt of the probe as it was secured in the raster scanning fixture.

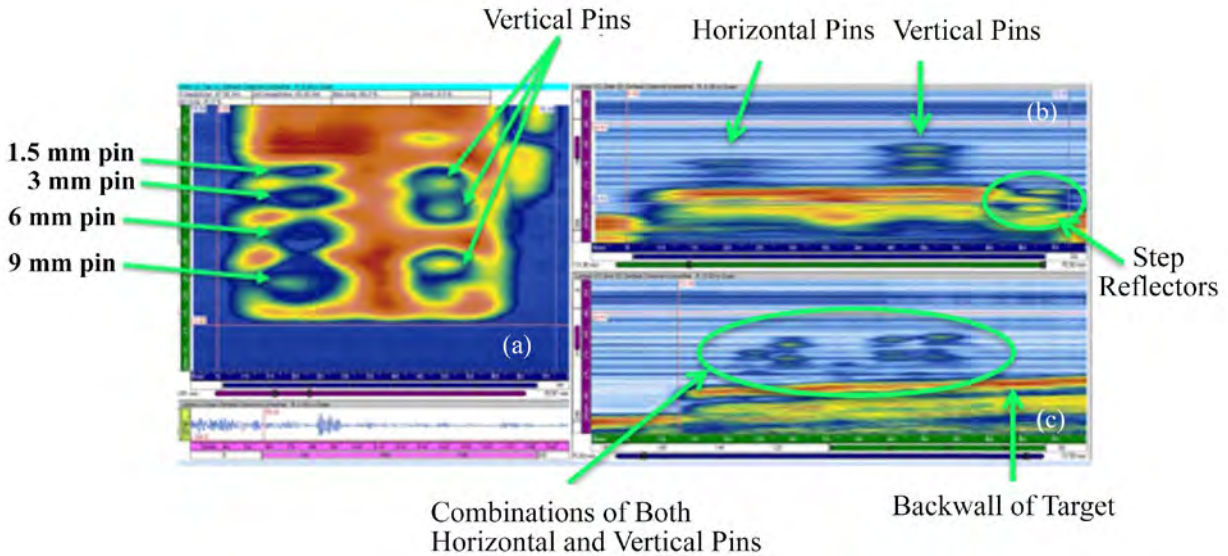


Figure 1.63. (a) C-scan View Showing the Lack of Backwall Shadowing Effect from all Three Vertical and all Four Horizontal Pins; (b) B-scan View and (c) D-scan View Showing Reflected Energy Signal Responses from All Horizontal and Vertical Pins.

Figure 1.64 provides various composite ultrasonic image views illustrating the detection of all pins both (horizontal and vertical orientations), including the step discontinuities on the side of the target.

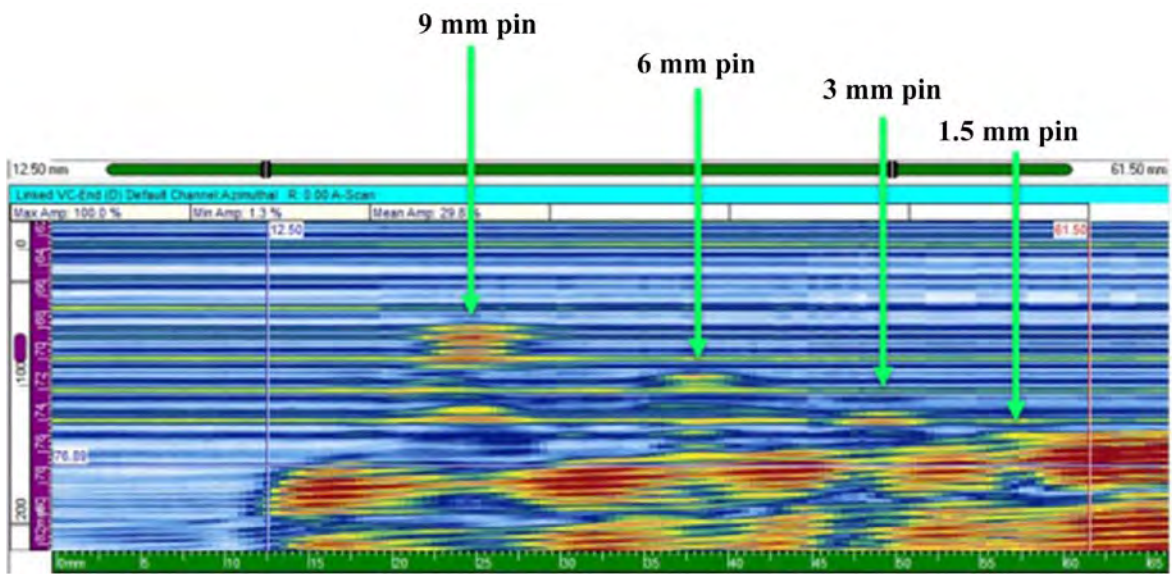


Figure 1.64. D-scan View Illustrating the Four Horizontal Pins of Different Diameters

While reverberations, noise, and ringing are evident, it is clear that the various target reflectors are detectable above the noise. In addition, these are raw ultrasonic data files without any signal processing or noise suppression algorithms having been applied. The processed data (anticipated to be completed in late FY16 or early FY17) should be much cleaner, where noise bands have been reduced or eliminated, signal responses from target features are more readily apparent, and the SNR is at least 10 dB (factor of 3.16) higher than what is currently seen in the raw data.

Other C-scan views illustrate a “top” view over the target, and can better isolate the vertical pins to help determine if they can be resolved and if their diameters can be accurately characterized. The images in Figure 1.65 provide additional C-scan views used in the analysis. These images can be “clipped” to only view the amplitudes that are -3 dB or -6 dB down from the peak amplitude within the window, in order to assess resolution performance, and to conduct sizing and characterization of various reflectors.

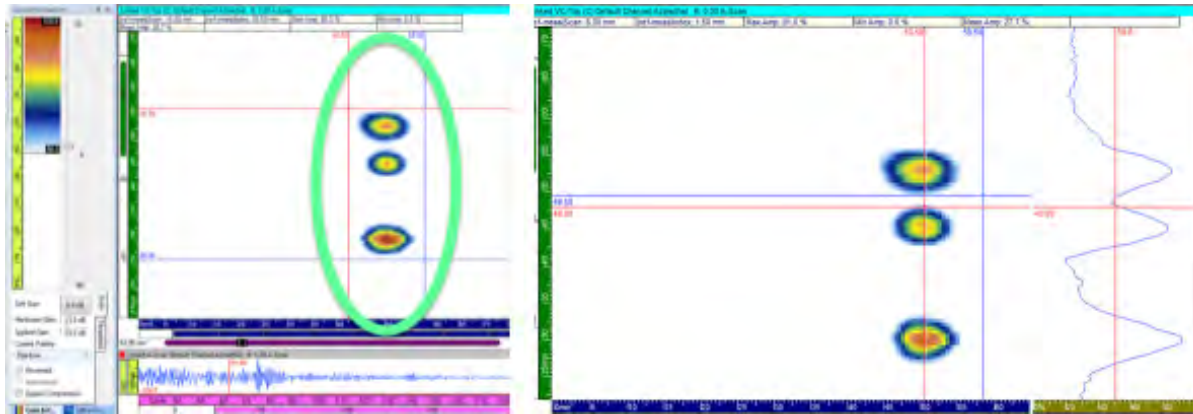


Figure 1.65. C-scan (top-down) Views. All three vertical pins are shown inside the green ellipse (*left*). Resolution is obtained using the Rayleigh resolution criterion (*right*).

These types of ultrasonic views are generated by applying different time-gates and spatial windowing to better isolate pin responses for acquiring resolution, sizing, and characterization results. From Figure 1.65, it is easy to note that the two closely spaced vertical pins are readily resolved in sodium at 260°C . In this same manner, B-scan and D-scan (side-views) can be evaluated to determine depth extent. The images in Figures 1.66 and 1.67 illustrate D-scan ultrasonic images that have been gated to isolate all three of the vertical pins.

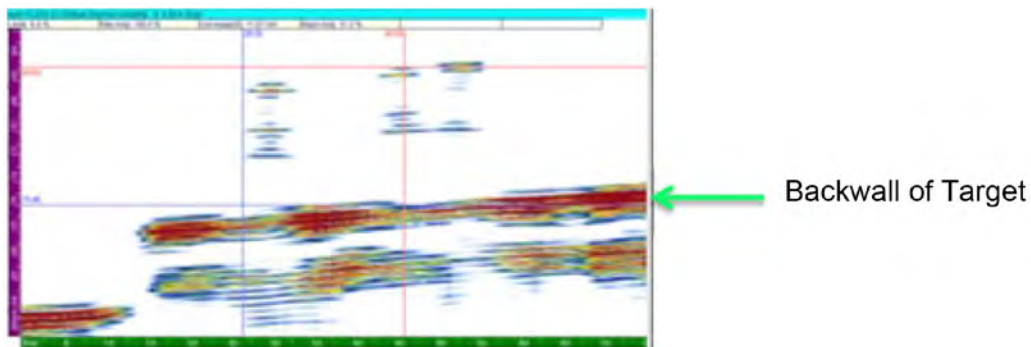


Figure 1.66. D-scan (end-view) Depicting Signal Responses from all Three Vertical Pins

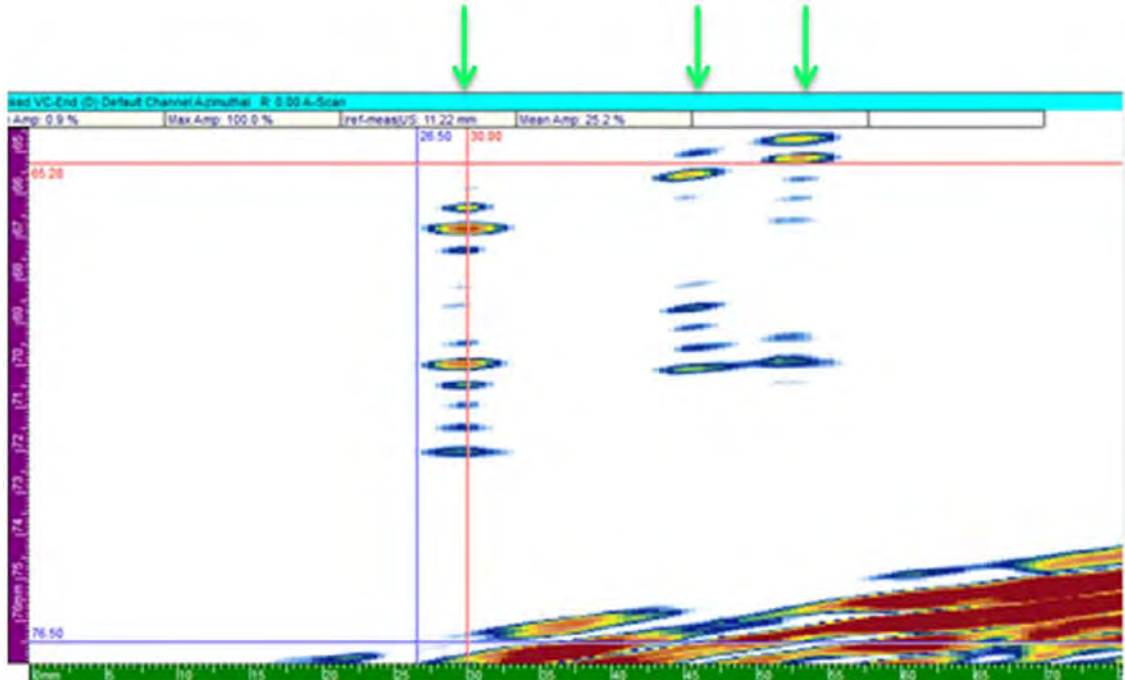


Figure 1.67. D-scan (end-view) Depicting Magnified Signal Responses from all Three Vertical Pins, Identified by Green Arrows

The horizontal pins can be further isolated to focus solely on the signal responses from individual pins. As an example, the 9 mm (largest diameter) horizontal pin is isolated in Figure 1.68. From this perspective, using the target backwall as a fiducial marker, the horizontal pin diameters can be measured. The D-scan image provided in Figure 1.68 illustrates this.

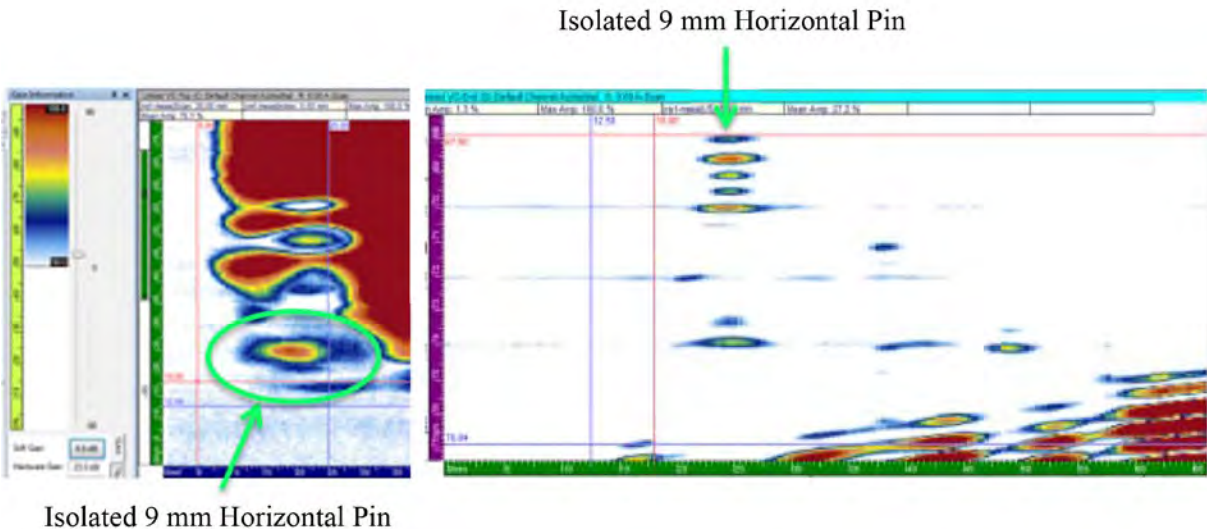


Figure 1.68. C-scan (top-view) (*left*); D-scan (end-view) (*right*), Depicting Signal Responses from 9 mm Diameter Horizontal Pin

The target also has a set of four step reflectors that provide flat reflector geometries that are at different depths from the back wall depth. The ultrasonic images in Figure 1.69 clearly show that all four steps are detected in sodium. In addition, three of the four were sized from the data. The fourth step was too difficult to size due to the slant in the data attributed to the non-leveled probe. This was discussed earlier due to a fabrication issue that introduced a slight bend (warping) in the probe shaft after welding a strain-relief “Y” channel into the top of the shaft.

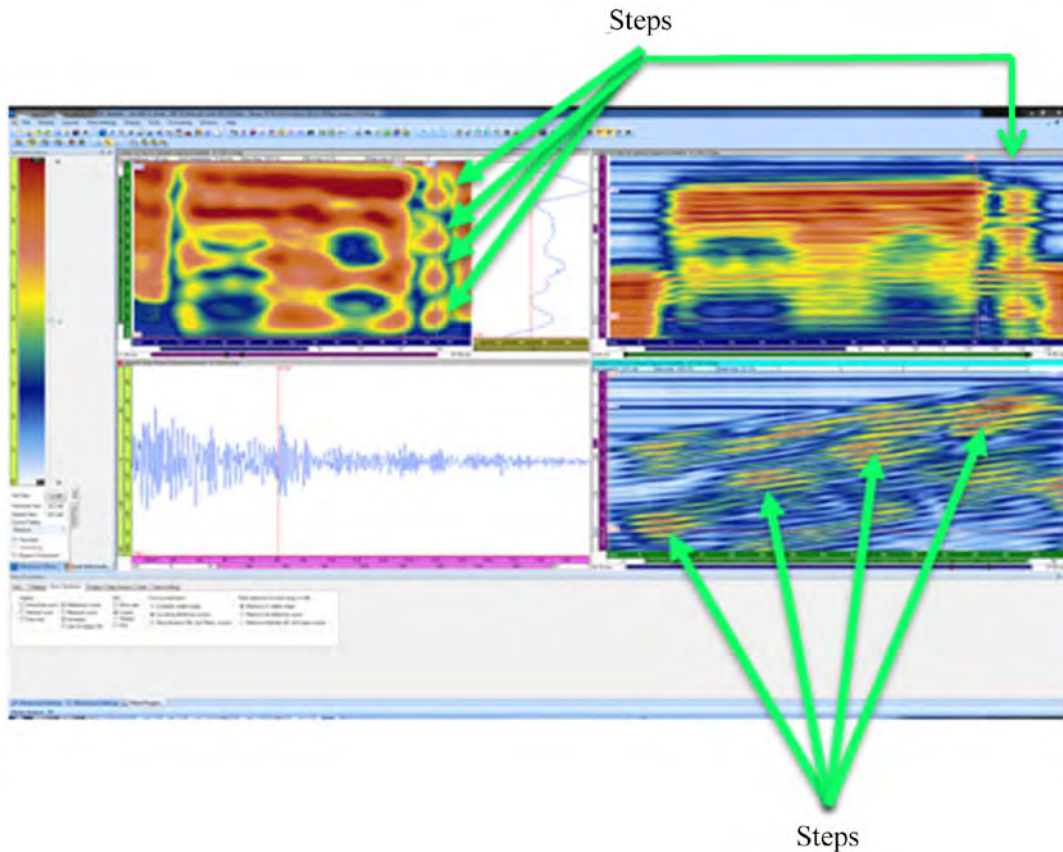


Figure 1.69. A- (lower left), B- (upper right), C- (upper left), and D-scan (lower right) Views Illustrating the Detection and Localization of the Four Step Reflectors on the Target in Sodium, at 260°C from Raw Unprocessed Ultrasonic Data

From a review of the SN4 linear array PA-UT data provided here, the backwall signal response (or lack thereof, illustrating shadowing effects) is a useful technique for initial detection of reflectors. This information, coupled with specular reflected energy from target features, allows for the detection, localization, and potential characterization (sizing) of these reflectors in sodium. The tops of all three vertical pins are easily detected, and the anticipated dropout or “shadowing” of the ultrasonic field from the pins is also detected. The SNR for the specular reflected energy from the tops of the vertical pins was measured to be 11.6 dB in FY15 and 13.3 dB in FY16, which corresponds to a nearly 2 dB increase in signal-to-noise between the two probes (SN2 and SN4). The two closely spaced vertical pins (identified as vertical pin #1 and vertical pin #2) were the focus of the resolution and sizing assessment. These pins were easily resolved as well. All four horizontal pins were detected by the SN4 32×1 linear array probe, and the three largest horizontal pins were accurately sized. The SNR for the specular reflected energy from the top of the largest (9 mm diameter) horizontal pin was approximately 10 dB, which corresponds

to a factor of 3.16:1 in voltage ratio of signal-to-noise. For the second largest pin, the SNR was approximately 7.5 dB, which corresponds to a voltage ratio factor of 2.4:1.

For comparative analysis, Table 1.14 provides the sizing results for the two vertical pins (both diameter and height) and also the two larger horizontal pins (height only) for data obtained in FY15 using the SN2 probe. Sizing of those vertical and horizontal pin reflectors that could be suitably resolved was conducted at -3 dB and -6 dB points in FY15, and at -6 dB only during FY16.

Table 1.14. Vertical and Horizontal Pin Sizing Results for FY15

Pin Description	Pin Orientation	True-State Dimension (mm)	-3 dB Measured Diameter (mm)	-6 dB Measured Diameter (mm)	-6 dB Measured Height (mm)	SNR (dB)
Pin #1	Vertical	6 diameter; 11 height	4.75	8.25	9.9	11.6
Pin #2	Vertical	6 diameter; 11 height	4.5	7.75	9.9	--
Pin #3	Vertical	6 diameter; 11 height	--	--	--	--
Largest	Horizontal	9 height/diameter	--	--	8.7	10.0
Second Largest	Horizontal	6 height/diameter	--	--	5.6	7.5
Third Largest	Horizontal	3 height/diameter	--	--	--	--
Fourth Largest	Horizontal	1.5 height/diameter	--	--	--	--

While pin #3 was detected in FY15, it was not able to be sized from the data. Also, the two smaller horizontal pins of diameter 3 mm and 1.5 mm, respectively, were not detected in FY15. In FY16, the best detection and sizing results in sodium were obtained from the SN4 32x1 linear array ETU probe. In order to compare the results of FY15 and FY16 data to better understand the performance improvements between these probes, the FY16 sizing data are provided in Table 1.15.

Table 1.15. Vertical and Horizontal Pin Sizing Results for FY16 Unprocessed (Raw) UT Data

Pin Description	Pin Orientation	True-State Dimension (mm)	-6 dB Measured Diameter (mm)	-6 dB Measured Height (mm)	SNR (dB)
Pin #1	Vertical	6 diameter; 11 height	6.0	11.1	12.9
Pin #2	Vertical	6 diameter; 11 height	5.0	11.0	13.3
Pin #3	Vertical	6 diameter; 11 height	6.0	11.2	10.7
Largest	Horizontal	9 height/diameter		8.92	9.7
Second Largest	Horizontal	6 height/diameter		5.10	9.1
Third Largest	Horizontal	3 height/diameter		2.55	4.6
Fourth Largest	Horizontal	1.5 height/diameter	Detected, Not Measured		--

In FY15, only two of the four step reflectors were detected but neither could be characterized from the data. In FY16, all four of the step reflectors on the “right” side of the target (see Figure 1.61 or Figure 1.62) were detected, while leveling issues due to the warped probe shaft had some impact on detection and sizing capabilities, even the smallest step reflector was accurately sized from the sodium

data. Additionally, portions of both sets of orthogonal notches (see lower portion of the target in Figure 1.61) were detected, but none of these notches could be accurately sized. Sound field dimensions coupled with leveling issues precluded the ability to resolve and characterize these notches. More importantly, it was not known if the notch crevasses were completely wetted at the time of the scanning, which likely contributed to a lack of SNR on these notch reflectors. Table 1.16 provides the sizing and SNR data for the step reflectors.

Table 1.16. FY16 –6 dB Sizing and SNR Data for Target Step Reflectors in Sodium at 260°C

Step	Depth of Step Below Backwall (mm)	Measured Depth of Step (mm)	Maximum Amplitude (% Screen Height)	Mean Noise (dB)	SNR (dB)
1	1.0	1.03	96.8	23.1	12
2	2.0	2.06	98.9	22	13
3	3.0	3.28	96.8	20.1	14
4	5.0	5.19	98.2	16.3	16

1.10 Discussion and Conclusions

This TLR provides a summary of the work conducted at PNNL in FY16 on the under-sodium viewing project, including a performance evaluation of the SN4 linear and matrix-array PA-UT ETU probes. This evaluation established the foundation for determining the viability of conducting in-sodium tests with the SN4 probes in FY16. In addition, this TLR provides the results from a performance demonstration test using the SN4 32×1 linear array ETU probe for target detection trials in sodium at 260°C. The activities conducted during this assessment focused on evaluating the performance characteristics and employing the primary inspection parameters described in Sections 1.3, 1.5, and 1.7 for in-sodium target detection trials.

During FY16, PNNL designed, fabricated, and tested two PA-UT ETU probes, a 32×1 element linear array, and a 64-element, matrix array 32×2, PA-UT ETU probe. PNNL completed a set of performance evaluation tests to quantify the probe’s capabilities for target detection and characterization. A set of pre-fabrication pulse-echo tests on individual array elements (in water) were conducted, followed by a set of post-fabrication pulse-echo testing on individual array elements, also in water. This included measurements to validate the array pin connections, the transmit uniformity for each element, the cross talk (to assess inter-element coupling between neighboring elements), and an evaluation of selected depth focus points and angles (to assess how effectively the probe can skew the sound field off its 0° primary axis). PNNL then conducted an assessment of temperature resistance and thermal cycling effects (in hot oil). A number of laboratory measurements and performance characterization scans were also conducted to quantify a set of critical attributes used as metrics for assessing and comparing probe performance and capabilities of both SN4 probes to the SN2 probe tested and demonstrated in FY15. Key efforts included the acquisition of:

1. Individual voltage responses from each element after employing a standard excitation pulse, and received with a broadband pinducer for receiving signal responses
2. Center and peak frequency responses from the FFTs of individual elements
3. –6 dB BWs of each element
4. Sound field dimensions (focal spot size) at –6 dB and –12 dB points at a nominal distance from the face of the probe in water using a pinducer receiving probe

5. Spatial resolution testing using raster scanning of the probe and employing flat reflectors with various spacings to evaluate array resolution performance in water
6. Evaluation of signal-to-noise ratio from both pre-fabrication testing of the individual elements and post-fabrication tests.

With the analyses of data obtained from these performance characterization tests, PNNL was able to quantify key performance parameters that were compared and contrasted between the two SN4 ETU probes. In addition, insights into the comparative evaluation between the SN4 linear array and the SN2 probe were generated. In particular, sound field dimensions (spot size), resolution capabilities, SNR, frequency response, and BW characteristics constitute the suite of critical attributes used to evaluate these probes. In this discussion, where applicable, the reader is referred to Diaz et al. (2014b) for pertinent characterization and performance information associated with the SN2 probe in FY14 and FY15 respectively.

From a review of the data provided in Sections 1.5 and 1.6, it is clear that the various stages of fabrication and the materials and quality of the processes employed for construction of the elements, backing, soldering, and bonding can all have critical impact on probe performance. Prior to fabrication of the housed SN4 probe arrays, it was shown that the 32×1 linear array probe had inherently lower noise levels and a slightly improved SNR for the individual elements over that of the $32 \times 1 (\times 2)$ matrix array probe; on the order of 2–6 dB. During this portion of the assessment, all elements for both SN4 probe designs were found to be functional and operating properly. After fabrication and housing, as each element was being validated for connectivity, it was found that 64 of 64 elements were confirmed to be operational for the SN4 matrix array probe (with 6 specific elements operating at lower efficiency) and 30 of 32 elements were confirmed operational for the SN4 linear array probe. In addition, some elements had a reduced level of efficient performance from an energy transmission perspective, while the general noise and reverberation levels appeared to be better controlled than in FY15. While some noise bands and prominent reverberations still exist in both of these probes, these sources are not yet well understood, but likely include grounding issues, electrical impedance matching issues with wires, line soldering joints, probe noise, and motor/system noise. The insertion of the Zetec cabling provided some improvement to the general noise level and to signal fidelity in FY16.

An assessment of the transmit uniformity on an element-by-element basis was conducted, and these measurements established a foundation for assessing areas of the arrays that were not emitting energy in an efficient manner, or where areas were marginally bonded. The SN4 arrays did not exhibit significant areas of complete dis-bonding where no ultrasonic energy was being emitted, but there were areas on both arrays where sound transmission was not as strong as in other areas. These less efficient areas or zones did not have a significant effect on the overall performance of the probe, in comparison to the SN1 and SN3 probes developed in past years. While the overall activity of all elements (64 of 64 for the SN4 matrix array probe and 30 of 32 for the SN4 linear array probe) were demonstrated, and there was no evidence of dis-bonding over the aperture of the SN4 arrays, it was noted that there were elements that emitted significantly more acoustic energy than others across both arrays. Unless fabrication processes can be refined further to reduce machining tolerances and soldering effectiveness, these types of variations are expected.

Laboratory measurements provided valuable dimensional data associated with the sound fields for both SN4 probes, and an assessment of the element-to-element cross talk showed that inter-element ultrasonic leakage was more effectively isolated for these probes over that of the FY15 SN2 probe. The SN4 probes exhibited much improved element-to-element isolation, and from a measurement perspective, the cross talk between individual elements in both the 64-element matrix array probe and the linear array probe

were not detectable. This means that the elements were truly isolated more effectively than in previous probe designs. Both probes showed suitable capabilities for demonstrating effectiveness at generating sound fields with the appropriate focal depths and dimensions, and both probes illustrated the capability to skew its primary sound field lobe over the designed range of angles (-20° to $+20^\circ$). This ability to effectively control off-axis beam steering is critical for a PA-UT probe.

During FY16, data were acquired to conduct an assessment of the amplitude and frequency response, BW, SNR, and element sensitivity for both probes. Individual voltage responses from each element after employing a standard excitation pulse were captured with a pinducer for later analysis. The most obvious difference of significance between the two probes was in the signal amplitudes and general SNRs. While the operational frequencies were generally identical, the SN4 linear array prototype probe generated higher sonic intensities (signal amplitudes) than the SN4 matrix array probe. The source of this difference is not fully understood, but in theory, larger piezo-elements will generate higher amplitude signal voltages over smaller piezo-elements. The 32-element linear SN4 array was comprised of individual elements each with an area of 15 mm^2 . The individual element size of the 64-element matrix SN4 array was essentially half this size, 7.4 mm^2 , with twice the number of elements and since the matrix array probe was operated in pulse-echo mode, the total transmission area for this probe is nearly identical to that of the 32-element linear array. Because both probes operated in pulse-echo mode, the entire aperture of the probe is employed for generating the sound field at any given focal distance, and is used to compute the effective piezo-element area responsible for transmission of ultrasonic energy. In the case of the SN4 matrix array, only a fraction of a millimeter of PZT material had been removed to isolate the two arrays, so the total probe aperture employed for transmission of ultrasonic energy is nearly identical for both probes. This translates to an effective total piezo-element area of 480 mm^2 . This is compared to an effective total piezo-element area for the SN2 probe of 330 mm^2 . The SN4 probes have an active transmission area that is over 45% larger than the active piezo-element energy transmission area of the SN2 probe for actively generating ultrasonic energy.

From an analysis of the sound fields of both probes, it is clear that the sound field dimensions for the focal “spot” size of the two SN4 probes are slightly different from that of the SN2 probe, as was anticipated, based on simulation and modeling results described earlier. However, between the two SN4 probes evaluated in FY16, the sound field dimensions are nearly identical for both the linear and matrix array ETUs. The data showed that both SN4 probes have sound fields that are slightly improved (smaller, tighter sound field) over that of the SN2 probe in both passive and active element dimensions (length and width, respectively). With regard to resolution performance in water, the SN4 probes should (in theory) be capable of resolving all of the reflectors provided by the resolution target described in Section 1.6.4. However, the data show that the SN4 probes are capable of resolving the reflectors that are separated by a center-to-center distance of 7.62 mm (0.3 in.); however, the reflectors that are separated by a center-to-center distance of 6.35 mm (0.25 in.) were not resolved. This was anticipated because these reflectors are essentially touching on their edges. The SN4 linear and matrix array probes performed nearly identically with regard to detection and resolution capabilities in water. Throughout testing, much effort was put forth to try to reduce noise by systematically isolating and measuring various points in the system to identify areas that were contributing to the noise in the signals. In addition, low-pass filtering was applied throughout the data acquisition effort. A low-pass filter of 5 MHz was applied to condition the signals in an effort to reduce noise and improve SNR. Finally, in evaluating the SNR from the water data obtained in this study, the SNR for the SN4 linear array probe was measured to be 15 dB and the SNR for matrix array probe was 13 dB. In water the SN4 probes demonstrated equivalent post-fabrication SNR levels to that of the SN2 probe.

While many key performance parameters and critical attributes exist to quantify the performance of a PA-UT probe, the primary characteristics are those that best describe the capability of a probe to

effectively detect, resolve, and characterize the reflectors or anomalies required for identification during an examination. In light of the results in FY15 with the SN3 probe, PNNL continued efforts in late FY15 to pursue in-sodium testing of the SN2 probe to demonstrate that the next critical challenge is to overcome the wetting issue of the probe in sodium. It is believed that this issue, coupled with an inability to raster scan the probe over the target area, was the primary sources of the poor SNR and poor imaging performance of the SN2 probe in FY14. The best data obtained in FY15 performance demonstration tests came from 0° incident sound fields and shallow angled data between -4° and +4°. In contrast, in FY16, even better image data were obtained from the SN4 linear array in sodium using 0° to +20° at 76.2 mm focal depth.

During the latter portion of FY15, PNNL assessed the SN2 probe in sodium. With regard to inspection time (duration), sodium temperature, and thermal cycling, this probe provided the required level of robustness to withstand any negative effects that could potentially impact probe performance. In FY14 the SN2 probe was tested in water after the in-sodium target detection trials were completed, and this probe demonstrated normal functionality and operability, verifying that no damage was incurred during in-sodium testing from temperature, thermal cycling, or the duration of testing in the glovebox in FY14. In FY15, the SN2 probe spent an additional 5+ hours of time in sodium at 260°C. This probe now has 12+ hours of performance, immersed in sodium at 260°C, with no measurable decline in functionality or performance. This is a key positive result of USV developments at PNNL. In addition, and for the first time, the SN2 probe was provided the opportunity to function at its designed focal distance and operate in a raster scan modality, increasing the effectiveness of insonification through direct translation of the probe over the entire target area. The imaging, detection, resolution, and characterization results from the target were drastically improved over what was previously achieved in any earlier year. That being said, results from FY16 using the SN4 linear array probe have surpassed that of the SN2 probe in FY15 across the board, with improved SNR, enhanced signal fidelity, and a superior capability for detection and characterization of targets in sodium at 260°C.

In FY15 wetting of the sodium became much less of a factor because of lessons learned and enhanced processes and protocols for maintaining effective wetting of the Ni faceplate in sodium. From a review of the data obtained in sodium (Diaz et al. 2015a), it is clear that the SN2 probe showed an improved ability to detect all three vertical and two of the horizontal pins. Additionally, the probe showed the capability to resolve and accurately characterize the two closely spaced vertical pins (pin #1 and pin #2) of the target, and also the two largest horizontal pins. Sizing of the pin spacing was more accurate and the SNR was greatly improved from any results in previous years. In FY14, this very same probe was not capable of detecting the pin tops because no specular reflected energy was received from the top of the pins. In FY15, the SNR from direct reflected energy off the pin tops was nearly 12 dB. This corresponds to an increase of nearly 4 times the signal sensitivity over the performance from last year. The metrics of SNR and signal dropout (shadowing) indicate an improved ability of the probe to detect the zones where the pins reside, and to capture a backwall signal with higher amplitude signal responses. The two closely spaced vertical pins are separated by a distance of 1.23 mm (edge-to-edge). In FY16, detection and sizing results were even further enhanced. The longitudinal wave mode speed of sound in liquid sodium at 260°C is 2460 m/s. Using the average center frequency of the SN4 linear array probe (1.06 MHz), the wavelength in sodium for the SN4 probe is given by the equation:

$$\lambda = c / f$$

where λ = wavelength, c = speed of sound, and f = frequency.

Thus, the wavelength in sodium for the SN4 probe is computed as 2.3 mm. In theory, PA-UT imaging should be able to resolve (at best), $\lambda / 2$, which in the case of the SN4 linear array probe is 1.15 mm. The

edge-to-edge spacing between vertical pin #1 and pin #2 is less than a wavelength. From a review of the sodium data, the measured pin separation from ultrasonic images captured at 260°C was 1.5 mm at the -6 dB point. So, the SN4 linear array probe was capable of measuring the edge-to-edge distance between the two vertical pins to within 0.22 mm of the true-state separation. The fact that the SN4 probe was capable of resolving two reflectors spaced less than 1λ apart (in sodium at temperature) is an outstanding result. In addition, the data show that the probe was capable of measuring the heights of the pins (the vertical pins and the three larger horizontal pins) to within 2% or less of their true state for vertical pins and within 17% for the horizontal pins. Sizing of the vertical pin diameters was significantly more accurate than sizing for the horizontal pins. This was anticipated, as the horizontal pins are essentially line reflectors, where the vertical pin tops provide a greater cross-sectional area from which to obtain specular reflected energy. In addition, all four step reflectors were detected and accurately sized. This was not the case in FY15, using the SN2 probe. Most surprising was the fact that the comparative assessment between the FY15 SN2 probe and the FY16 SN4 linear array probe was conducted using FY15 data where noise reduction algorithms had been implemented. The FY16 data were comprised of raw UT data where no noise reduction or image reconstruction had been implemented. Preliminary implementation of advanced approaches for enhanced resolution and improved SNR have indicated that significant performance improvements to the FY16 data are anticipated in late FY16 and early FY17. PNNL anticipates generating a summary of technical efforts focused on newly generated detection and sizing results from the use of advanced image reconstruction and signal processing algorithms in the coming months.

PNNL assessed both probes using identical data acquisition and operational parameters. With the analyses of data obtained from these target-detection tests, PNNL was able to identify specific performance improvements between the two ETU probes, and also identify areas where more work needs to be done, if the linear array SN4 design is deemed worthy of future evolution. In particular, major improvements in detection capability, resolution capability, SNR, and environmental robustness were identified with the SN4 linear array probe in FY16. PNNL has concluded that the primary drivers inhibiting the achievement of suitable detection and resolution capabilities in sodium are:

- Control of noise sources, including grounding noise, internal probe noise, cable/connector noise, and system/motor noise
- A capability to steer and control this well-focused beam within reasonable limits
- The ability to raster scan the probe over the entire target area to increase reflected energy redundancy and enhance imaging reconstruction and interpretation.

The last two bullets (limitations) were addressed by PNNL in FY15 and FY16, and the remaining bullet will be the focus of work in FY17 with a focus on implementing advanced image reconstruction methods and signal processing algorithms for improvement of SNR. In FY16, the primary challenge was to increase sound field propagation and image resolution in sodium by designing an array that provides a tighter, more symmetric and more focused sound field (spot size and depth of field). The pulse-echo design may likely be the most advantageous design for this application as has been demonstrated in both FY15 and FY16. A larger aperture 1D pulse-echo linear array design improved resolution and sensitivity, while increasing signal strength due to larger element sizes. In addition, this design provided a suitable ability to control/steer the sound field, focus suitable amounts of energy while continuing to improve sound field focal dimensions. The FY16 effort was successful at reducing noise sources using custom designed cables from international phased array experts in Canada. FY17 efforts will employ FY16 data and demonstrate image enhancements and improved detection/resolution capabilities from post-processing of raw ultrasonic data using advanced signal processing approaches.

2.0 References

Addison CC. 1984. *The Chemistry of the Liquid Alkali Metals*. John Wiley & Sons Ltd, New York.

ASTM E1065/E1065M-14, *Standard Practice for Evaluating Characteristics of Ultrasonic Search Units*. ASTM International, West Conshohocken, Pennsylvania, 2014. DOI 10.1520/E1065-08.

ASTM E2491-13, *Standard Guide for Evaluating Performance Characteristics of Phased-Array Ultrasonic Testing Instruments and Systems*. ASTM International, West Conshohocken, Pennsylvania, 2013.

Braatz BG, CL Aardahl, DL Baldwin, AD Cinson, JL Fernandes, AM Jones, PE Keller, MR Larche, R Mathews, CA Mullen, AF Pardini, GJ Posakony, ML Watkins, HT Chien, WP Lawrence, DM Engel and SH Sheen. 2013. *FY2013 Joint Technical Report on Progress in Development of Ultrasonic Under-Sodium Viewing Technology to Enable Inspection Systems for In-Service Inspection and Repair of Liquid Metal Fast Reactors*. PNNL-22872, Pacific Northwest National Laboratory, Richland, Washington.

Busse LJ, HD Collins and SR Doctor. 1984. *Review and Discussion of the Development of Synthetic Aperture Focusing Technique for Ultrasonic Testing, SAFT UT*. NUREG/CR-3625, PNL-4957, U.S. Nuclear Regulatory Commission, Washington, D.C.

Diaz AA, DL Baldwin, CE Chamberlin, AD Cinson, MK Edwards, TS Hartman, AM Jones, MR Larche, R Mathews, CA Mullen, AF Pardini, GJ Posakony, MS Prowant, HT Chien, DM Engel, WP Lawrence and SH Sheen. 2014a. *FY 2014 Joint Technical Report on Progress in Development of Ultrasonic Under-Sodium Viewing Technology to Enable Inspection Systems for In-Service Inspection and Repair of Liquid Metal Fast Reactors*. PNNL-23671, Pacific Northwest National Laboratory, Richland, Washington.

Diaz AA, DL Baldwin, CE Chamberlin, MK Edwards, MR Larche, R Mathews, KJ Neill and MS Prowant. 2015a. *FY15 Status of Immersion Phased Array Ultrasonic Probe Development and Performance Demonstration Results for Under Sodium Viewing*. PNNL-24704, Pacific Northwest National Laboratory, Richland, Washington.

Diaz AA, DL Baldwin, AD Cinson, AM Jones, MR Larche, RA Mathews, CA Mullen, AF Pardini, GJ Posakony, MS Prowant, TS Hartman and MK Edwards. 2014b. *M3AR-14PN2301022 Technical Letter Report - Identify and Quantify the Mechanistic Sources of Sensor Performance Variation Between Individual Sensors SN1 and SN2*. PNNL-23531, Pacific Northwest National Laboratory, Richland, Washington.

Diaz AA, MR Larche, R Mathews, KJ Neill, DL Baldwin, MS Prowant, MK Edwards and CE Chamberlin. 2015b. *Protocol for Performance Demonstration of Immersion Phased Array Ultrasonic Probes for Target Detection Trials in Liquid Sodium*. PNNL-24625, Pacific Northwest National Laboratory, Richland, Washington.

Gammell PM. 1981a. "The Analytic Signal Magnitude for Improved Ultrasonic Signatures." In *Proceedings of the DARPA/AFWAL Review of Progress in Quantitative NDE, October 1979–January 1981*, pp. 563-566. August 1981, La Jolla, California. Paper 84.

Gammell PM. 1981b. "Improved Ultrasonic Detection Using the Analytic Signal Magnitude." *Ultrasonics* 12:73-76.

Watkins ML, BG Braatz, AM Jones, DL Baldwin, GJ Posakony, PE Keller, AD Cinson, MS Prowant, KM Denslow, HT Chien, WP Lawrence, SH Sheen and K Wang. 2012. *Joint Technical Report on Progress in Development of Ultrasonic Under-Sodium Viewing Technology to Enable Inspection Systems for In-Service Inspection and Repair of Liquid Metal Fast Reactors*. PNNL-21853, Pacific Northwest National Laboratory, Richland, Washington.

Wikipedia. 2015a. *Airy Disk*. Accessed September 20, 2015. Available at https://en.wikipedia.org/wiki/Airy_disk.

Wikipedia. 2015b. *Angular Resolution*. Accessed September 20, 2015. Available at https://en.wikipedia.org/wiki/Angular_resolution.

Wooh S-C and Y Shi. 1999. "Three-Dimensional Beam Directivity of Phase-Steered Ultrasonic." *Journal of the Acoustical Society of America* 105(6):3275-3282.

Wooh SC and Y Shi. 1998. "Influence of Phased Array Element Size on Beam Steering Behaviour." *Ultrasonics* 36:737-749.

Wooh SC, Y Shi and L Azar. 2000. "Beam Focusing Behaviour of Linear Phased Arrays." *NDT & E International* 33:189-198.



Pacific Northwest
NATIONAL LABORATORY

*Proudly Operated by **Battelle** Since 1965*

902 Battelle Boulevard
P.O. Box 999
Richland, WA 99352
1-888-375-PNNL (7665)

U.S. DEPARTMENT OF
ENERGY

www.pnnl.gov